Factors Affecting Heat Transfer from Firebrands and Firebrand Piles and the Ignition of Building Materials

Elias Bearinger

Thesis submitted to the faculty of the Virginia Polytechnic Institute and State University in partial fulfillment of the requirements for the degree of

Master of Science
In
Mechanical Engineering

Brian Y Lattimer
Thomas E Diller
Thomas A Coates

May 28th, 2021
Blacksburg, Virginia

Keywords: Firebrands, Wildfires, Heat Transfer, Ignition

Factors Affecting Heat Transfer from Firebrands and Firebrand Piles and the Ignition of Building Materials

Elias Bearinger

ABSTRACT

Firebrands, small pieces of burning vegetation or debris generated by fires, are one of the primary ways wildfires ignite structures. Due to their small size, firebrands can be carried several kilometers by high winds before landing on combustible surfaces such as decks or roofs and potentially igniting homes. Until recently, little has been known about the heat transfer capabilities of firebrands to the surfaces on which they land. Understanding the heat transfer from firebrands is an essential step in engineering for greater fire resilience.

In the first phase of this research, heat transfer from individual firebrands to horizontal surfaces was investigated using oak firebrands made from commercially available lumber. The firebrand shape, wind speed, and wind direction were varied to see how these variables affect the heat transfer. A method of inverse heat transfer analysis based on infrared thermographs was used to measure distributed heat fluxes from firebrands to the surfaces through time. This measurement technique provided spatial resolutions of < 0.5 mm, approximately 10 times higher than previous experiments in this field. Results showed that localized heat transfer was significantly higher than had previously been reported, reaching as high as 80 kW/m^2 in some cases. It was also found that wind speed, wind direction, and firebrand shape all affected the heat transfer from individual firebrands.

Firebrands have also been shown to accumulate in piles on decks or roofs creating complex systems that have different ignition capabilities than individual firebrands. Potentially many factors could influence the heat transfer from firebrand piles including wood moisture content, wood type (hardwood or softwood), wood density, wood state (live, dead, or artificial), wind speed, pile mass, firebrand diameter, and firebrand length. The second phase of this research used the same method of high-resolution heat transfer measurement to assess which of these factors significantly impacted the heat transfer from firebrand piles. Design of experiments was used to develop the test matrices and a rigorous statistical framework was employed to evaluate results at the $\alpha = 0.05$ level. It was found that wind speed, firebrand length, and an interaction between firebrand length and diameter were important. Additionally, it was found that there was a difference between the heat transfer from piles made with artificial and real firebrands. Pile mass did not appear to significantly impact the heat flux from firebrand piles.

The last phase of this research developed a simple engineering model to predict the ignition of common building materials by firebrand piles. The model used time-varying heat transfer data from firebrand pile tests and material properties developed by testing on select building materials in a cone calorimeter. The model predicted the surface temperature rise of the material due to an exposure heat flux with ignition being predicted when the surface temperature exceeded the ignition temperature of the material. The model was used to predict ignition for a number of pile/fuel combinations and experiments were run to validate the predictions. It was found that the model did an excellent job in predicting ignition for materials which did not melt.

Factors Affecting Heat Transfer from Firebrands and Firebrand Piles and the Ignition of Building Materials

Elias Bearinger

GENERAL AUDIENCE ABSTRACT

Uncontrolled wildfires burning close to human civilizations result in hundreds of deaths, the destruction of thousands of structures, and billions of dollars in economic damages each year. One of the primary ways wildfires ignite structures is through firebrands: small pieces of burning vegetation or debris generated by the fire. These firebrands can be carried great distance by strong winds, eventually landing on decks or roofs and potentially igniting homes. Until recently, little has been known about the heat transfer from firebrands to the surfaces on which they land. Understanding firebrand heat transfer will allow building materials to be selected that are resistant to ignition by firebrands and reduce the number of structures destroyed by wildfires.

In the first phase of this research, heat transfer from individual firebrands was investigated. The firebrand shape, wind speed, and wind direction were varied to see how these variables affect the heat transfer. A high-resolution measurement technique was used, allowing heat transfer to be measured with approximately 10 times higher resolution than previous experiments. Results showed that localized heat transfer was significantly higher than had previously been reported and indicated that wind speed, wind direction, and firebrand shape all affected the heat transfer from individual firebrands.

Firebrands have also been shown to accumulate in piles on decks or roofs creating complex systems that have different ignition capabilities than individual firebrands. Potentially many factors could influence the heat transfer from firebrand piles including wood moisture content, wood type (hardwood or softwood), wood density, wood state (live, dead, or artificial), wind speed, pile mass, firebrand diameter, and firebrand length. It was found that wind speed, firebrand length, and an interaction between firebrand length and diameter were important. Additionally, it was found that there was a difference between the heat transfer from piles made with artificial and real firebrands.

The last phase of this research developed a simple engineering model to predict the ignition of common building materials by firebrand piles. The model used time-varying heat transfer data, and material properties developed by experimental testing. The model was used to predict ignition of select building materials with different firebrand piles, and experiments were run to validate the predictions. It was found that the model did an excellent job in predicting ignition for materials which did not melt.

ACKNOWLEDGEMENTS

I would like to use this as an opportunity to acknowledge and credit all those who have helped me along the way in completing this master's degree. I have been incredibly fortunate to have been surrounded by so many outstanding people.

First and foremost, I would like to thank my advisor, Dr. Brian Lattimer, for his guidance in the research presented here, his extraordinary kindness and understanding during the COVID-19 pandemic, and his support of a collaborative, balanced research environment. I have learned a tremendous amount from Dr. Lattimer's expertise in field of fire research and without his help, none of this would have been possible.

A significant debt of gratitude is also owed to Dr. Jonathan Hodges, Lead Engineer at our industry partner Jensen Hughes. Despite managing a rigorous industry workload, Dr. Hodges always found time to assist in troubleshooting and answering my questions. Dr. Hodges' acumen for modeling and complex data analysis drastically improved the quality of our results. Dr. Hodges has truly gone above and beyond to provide outstanding partnership and guidance for this project.

I would also like to thank the members of my thesis committee, Dr. Thomas Diller and Dr. Adam Coates. Dr. Coates has repeatedly offered advice and tutelage in all aspects of our research related to forestry. His insights have provided a cross-discipline dimension that has profoundly increased the completeness of this work. Dr. Diller's support was instrumental in the development of our wind tunnel testing facility. Dr. Diller and Dr. Coates have been exceptionally accommodating of my defense date, setting aside a significant amount of time in busy week for both to attend my defense.

I would also like to thank to my lifelong friends the Passinos for their unwavering support and love during this endeavor. Their friendship has helped in every aspect of my life and I truly would not be where I am today without them. In particular, Emma Passino has provided amazing companionship and encouragement. I am also forever grateful to my friend Kathryn for her friendship and generosity. Kathryn's extraordinary kindness and general cheerfulness helped me endure social isolation during the COVID-19 pandemic and the tribulations of graduate school.

Finally, I would like to extend my unending gratitude to my family. My mom, Dianne, has been ceaselessly nurturing, going above and beyond to be understanding and helpful during this time. My dad, David, has provided tremendous support through my degree, particularly during my job search. His advice and support have continually uplifted me. Lastly my sister, Zoe, continues to be a source of inspiration and amazement. Her companionship and love have meant more to me than anything else. I am truly blessed to have these incredible people in my life.

Table of Contents

ABSTRACT v
GENERAL AUDIENCE ABSTRACT iii
ACKNOWLEDGEMENTS iv
1. INTRODUCTION 1
1.2 Research Objectives 1
1.3 Organization 2
2. LOCALIZED HEAT TRANSFER FROM FIREBRANDS TO SURFACES 3
ABSTRACT 3
2.1. INTRODUCTION 3
2.2. EXPERIMENTAL METHODS 4
2.2.1 Test Apparatus 4
2.2.2 Heat Transfer Measurement 6
2.3 Firebrands 8
2.2.4 Test Procedure and Matrix 9
2.3. RESULTS 10
2.3.1 No Wind 10
2.3.2 Parallel Wind 12
2.3.3 Perpendicular Wind 13
2.3.4 Firebrand Temperature 15
2.3.5 Wind Speed Effects 15
2.3.6 Repeatability 16
2.4. DISCUSSION 17
2.5. CONCLUSION 18
2.6. ACKNOWLEDGEMENTS 18
REFERENCES 18
3. STATISTICAL ASSESSMENT OF PARAMETERS AFFECTING FIREBRAND PILE HEAT TRANSFER TO SURFACES 22
ABSTRACT 22
3.1. INTRODUCTION 22
3.2. EXPERIMENTAL METHODS 24
3.2.1. Experimental Setup 24
3.2.2. Design of Experiments 29
3.2.3. Analysis 34

3.3. RESULTS 36
3.3.1. Data Overview 37
3.3.2. Moisture Content Study 38
3.3.3. Wood Type Study 39
3.3.4. Density Study 40
3.3.5. Wood State Study 41
3.3.6. Full Factorial Study 43
3.4. DISCUSSION 44
3.5. CONCLUSION 46
REFERENCES 47
4. PREDICTING IGNTION FROM EXPOSURE TO FIREBRAND PILES 51
ABSTRACT 51
4.1. INTRODUCTION 51
4.2. METHODS 52
4.2.1. Ignition Model 52
4.2.2. Material Properties 54
4.2.3. Experimental Setup 57
4.2.4. Heat Flux Tests 61
4.2.5. Ignition Tests 62
4.3. RESULTS 63
4.3.1. Material Properties 63
4.3.2. Pile Heat Fluxes 65
4.3.3. Ignition Prediction 66
4.3.4. Ignition Experiments 68
4.4. DISCUSSION 69
4.5. CONCLUSION 71
REFERENCES 72
5. CONCLUSION 76
6. FUTURE WORK 76

List of Figures

Figure 1. Test stand to characterize localized heat transfer from firebrands.....5
Figure 2. Verification for quantifying localized heat transfer using the IHT measurement. 8
Figure 3. Oak firebrand geometries.....9
Figure 4. Peak heat flux with time for different types of firebrands with no wind. 11
Figure 5. Heat flux distributions at time of highest peak heat flux for different types of firebrands with no wind.....12
Figure 6. Peak heat flux with time for different firebrands, long side parallel to 1.0 m/s of wind. 12
Figure 7. Heat flux distributions at time of highest peak flux for different types of firebrands with long side parallel to 1.0 m/s of wind. 13
Figure 8. Peak heat flux with time for different types of firebrands with long side perpendicular to 1.0 m/s of wind. 14
Figure 9. Heat flux distributions at time of highest peak flux for different types of firebrands with long side perpendicular to 1.0 m/s of wind.....14
Figure 10. Firebrand temperature distribution at the time of peak temperature for no wind (top row) and firebrand perpendicular to wind at 1.0 m/s (bottom row).....15
Figure 11. Effect of wind speed on the peak heat flux with time for the cuboid L=38mm, one notch firebrand with the long side perpendicular to the wind. 16
Figure 12. Repeatability of peak heat flux with time (cuboid, L = 38 mm, no notch). 16
Figure 13. Test apparatus used to evaluate heat transfer from firebrand piles under various conditions. Note image insert contains close view of measurement area. 25
Figure 14. Galvanized steel wire cage used to constrain firebrand piles (shown in red).....26
Figure 15. 6.6 mm × 6.75 mm grids (shown in red) lying totally within the bounds of the 50 mm circular pile (shown in white).....35
Figure 16. Grid heat flux values through time for example test. Vertical red line indicates the 120 s mark. 37
Figure 17. Histogram of 120s averages for each of twenty-nine grids within a test. 75th percentile heat flux value is shown in red. 38
Figure 18. Interval plot showing the 95% CI for each group in the moisture content study.....39
Figure 19. Interval plot showing the 95% CI for each group in the wood type study. 40
Figure 20. Interval plot showing the 95% CI for each group in the density study. 41
Figure 21. Interval plot showing the 95% CI for each group in the wood state study.....43
Figure 22. Pareto chart (a) and normal plot (b) for the full factorial tests with all terms included 43
Figure 23. Pareto chart (a) and normal plot (b) for the full factorial tests with ABCD, ACD, and BCD terms removed.....44
Figure 24. The parabolic heat flux used to validate the numeric integration technique. 53
Figure 25. Comparison of the exact solution and numeric estimation of the surface temperature rise for parabolic exposure flux. 54
Figure 26. Cone calorimeter testing apparatus 55
Figure 27. Experimental setup used to measure exposure flux from firebrand piles.....57
Figure 28. Steel wire cage used to constrain the firebrand piles (shown in red).....58
Figure 29. Energy balance conducted on each pixel to resolve distributed heat flux measurements.....59
Figure 30. 6.6 mm × 6.75 mm grids (shown in red) lying totally within the bounds of the 50 m circular pile (shown in white).....60

Figure 31. Heat flux data from all 29 grids from a single test plotted through time 61
Figure 32. Setup used to test ignition of fuel samples by firebrand piles 63
Figure 33. 1/tig versus exposure flux for piloted ignition of building materials.....64
Figure 34. 1/tig versus exposure flux for spontaneous ignition of building materials. 64
Figure 35. 75th percentile 120s average grid heat flux values 66
Figure 36. Probability of ignition.....70
Figure 37. Comparison of time to ignition using experimental data (True), time-varying heat flux data and spontaneous ignition material properties (tig), and q120s'' (tig, 120s).....71

List of Tables

Table 1. Firebrand test matrix and mass data.....10
Table 2. Summary of heat fluxes measured in this work at different resolutions.....17
Table 3. Experiments used to evaluate the effect of eight factors on heat transfer from firebrand piles 30
Table 4. Test matrix used to assess the effect of starting moisture content on the heat transfer from firebrand piles.....31
Table 5. Test matrix used to assess the effect of firebrand wood type on the heat transfer from firebrand piles. 31
Table 6. Test matrix used to assess the effect of firebrand wood density on the heat transfer from firebrand piles. 32
Table 7. Test matrix used to assess the effect of firebrand wood mode on the heat transfer from firebrand piles. 33
Table 8. Full-factorial test matrix used to assess the effect of unburned firebrand length and diameter, pile mass, and wind speed on the heat transfer from firebrand piles.....34
Table 9. Summary of the statistical analysis of the effect of starting moisture content of unburned firebrands on the heat transfer from firebrand piles. 38
Table 10. Summary of the statistical analysis of the effect of firebrand wood type on the heat transfer from firebrand piles. 40
Table 11. Summary of the statistical analysis of the effect of unburned firebrand dry density on the heat transfer from firebrand piles. 41
Table 12. Summary of the statistical analysis of the effect of wood mode on the heat transfer from firebrand piles.....42
Table 13. Fisher's individual tests for difference of means.....42
Table 14. Firebrand pile test matrix 62
Table 15. Thermal properties of common materials 65
Table 16. Probability of ignition of each test on common materials 67
Table 17. Times to ignition based on piloted results.....67
Table 18. Times to ignition based on spontaneous results 68
Table 19. Ignition testing results.....68

1. INTRODUCTION

Every year wildfires are responsible for hundreds of deaths and the destruction of thousands of structures around the world. Driven by changing climates, forest management practices, and the continued expansion of human civilizations into wildland environments, the toll from wildfires is expected to keep growing. One of the primary ways in which wildfires ignite structures is through firebrands, which are small pieces of burning vegetation and debris lofted by the fire winds. Firebrands are particularly dangerous due to their ability to travel several kilometers from the fire location before landing on combustible materials and causing ignition. Both individual firebrands and firebrand piles have been shown to ignite building assemblies, but until recently little has been known about the heat transfer capabilities of firebrands to the surfaces on which they land. Understanding the heat transfer capabilities of firebrands allows building materials to be selected which will resist firebrand ignition, an essential step in engineering for greater fire resilience.

1.2 Research Objectives

The objective of this work was to use high-resolution heat flux measurement techniques to understand heat transfer from both individual and piles of firebrands and use this data to develop an engineering model for predicting ignition of building materials. The overall research objectives of this work were as follows:

1. Determine the impact of individual firebrand shape and contact on the heat transfer to a horizontal surface with different wind speeds and wind directions,
2. Identify the most important parameters that have a statistically significant effect on the heat transfer from firebrand piles, and
3. Develop and validate a model to predict ignition of building materials exposed to a firebrand pile

The first objective of this research investigated how wind speed, wind direction, and firebrand shape influenced the heat transfer from individual firebrands to horizontal surfaces. Smoldering oak firebrands of different shapes were tested in wind speeds ranging from 0 to 2.1 m/s with wind applied both parallel and perpendicular to the length of the firebrand. Distributed heat transfer measurements were taken through time using infrared thermographs and inverse heat transfer analysis. This technique afforded spatial resolutions of < 0.5 mm, allowing highly localized heat transfer to be resolved.

The second objective of the research was to use the same measurement technique and focused on which factors affect the heat transfer from firebrand piles. The nascent field of firebrand pile research has investigated a variety of different firebrand pile configurations without consensus regarding which factors are important in influencing the heat transfer. Phase two of this work employed design of experiments to statistically determine which factors had a significant impact on the heat transfer. The factors investigated all related to the characteristics of the firebrand pile itself and included wood moisture content, wood type (hardwood or softwood), wood density, wood state (live, dead, or artificial), wind speed, pile mass, firebrand diameter, and firebrand length.

The third and final objective of this research developed an engineering model to predict ignition of solid combustible materials by firebrand piles. The model calculates the surface temperature rise of the material due to an exposure heat flux with ignition being predicted when the surface temperature exceeded the ignition temperature of the material. Material properties for nylon, pressure treated southern yellow pine deck board, and composite deck board made from plastic and wood fibers were experimentally determined. This data along with heat fluxes measured from firebrand piles was used to predict ignition for several pile/fuel combinations. Experiments were run to validate these predictions.

1.3 Organization

This work is comprised of three main chapters, each corresponding to a separate paper written during the course of this research project. The papers provide the findings for the three research objectives described in the previous section.

Chapter 2 contains the paper "Localized Heat Transfer from Firebrands to Surfaces" which was authored by Elias Bearinger, Jonathan Hodges, Fengchang Yang, Christian Rippe, and Brian Lattimer. This paper was published in Fire Safety Journal through the 13th International Association for Fire Safety Science (IAFSS) Conference where it was selected for the Sheldon Tieszen Award. Elias Bearinger completed all experimental work for this paper as well as writing portions of the text and presenting the paper as the IAFSS conference. Dr. Hodges, Dr. Yang, and Dr. Rippe completed the bulk of the data analysis, while Dr. Lattimer wrote portions of the text.

Chapter 3 contains the paper "Statistical Assessment of Parameters Affecting Firebrand Pile Heat Transfer to Surfaces", authored by Elias Bearinger, Brian Lattimer, Jonathan Hodges, Christian Rippe, and Anil Kapahi. This paper has been submitted to Frontiers of Mechanical Engineering journal which is hosting a special issue on fire engineering. The experimental and writing portions of this paper were completed entirely by Elias Bearinger, while data analysis was conducted by Elias Bearinger, Dr. Lattimer, and Dr. Hodges. Dr. Lattimer, Dr. Hodges, Dr. Rippe, and Dr. Kapahi all provided contributions to the development of the experimental framework as well as guidance and edits to the paper.

Chapter 4 contains the last paper: "Predicting Ignition from Exposure to Firebrand Piles", authored by Elias Bearinger, Brian Lattimer, and Jonathan Hodges, which will be submitted to a relevant journal in the coming months. Elias Bearinger conducted all experimental work supporting this publication as well as writing the paper. Elias Bearinger and Dr. Lattimer both contributed to the model development and data analysis. Dr. Hodges provided input on experimental and data analysis design as well as reviewing data.

2. LOCALIZED HEAT TRANSFER FROM FIREBRANDS TO SURFACES

Elias D. Bearinger[a], Jonathan L. Hodges[b], Fengchang Yang[b], Christian M. Rippe[b] and Brian Y. Lattimer[a*]
[a]Virginia Tech, Mechanical Engineering, 635 Prices Fork Rd, Blacksburg, VA, USA, lattimer@vt.edu
[b]Jensen Hughes, 2020 Kraft Dr, Suite 3020, Blacksburg, VA, USA

ABSTRACT
Firebrands are known to cause spot fires and structure ignition far from the fire front, but there is a limited understanding of the heat transfer from firebrands to surfaces. In this work, high resolution heat flux distributions were measured for single firebrands with different geometries using IR thermography and inverse heat transfer analysis. Localized heat fluxes from a single firebrand were measured to be 25 – 80 kW/m^2, which is 2-3.5 times higher than previous work with heat flux gauges and energy balance methods that spatially average the heat transfer from the firebrand. Firebrand geometry, wind speed, and wind speed orientation relative to the firebrand affect the heat flux magnitude and duration of the exposure.

2.1. INTRODUCTION

Wildland fires continue to threaten urban communities due to overgrown vegetation and the increasing number of structures built in the wildland area. In these wildland fires, firebrands are lofted far from the fire front where they ignite vegetation and structures starting spot fires. As a result, significant research has focused on understanding the generation, transport, and ignition processes due to firebrands as described in several reviews [1]–[4]. One area cited in these reviews as needing more attention is a better fundamental understanding of how firebrands ignite combustible materials and vegetation. This requires quantifying conditions for firebrands to ignite fuels, firebrand temperature, and heat transfer from the firebrand to the surface.

Early work to understand the ignition of combustible materials and vegetation by firebrands focused on determining the conditions for firebrands to cause different fuels to ignite. Several researchers have investigated the mass of firebrands required to ignition building construction materials [5], [6], [7], [8] and insulations [9], including the effects of wind. Piles of 2.0-7.0 g of firebrands were required for ignition with wind required to cause flaming ignition. This is similar to what is required to cause smoldering wood to transition to flaming [10]. Other researchers have conducted experiments on the ignition of vegetation beds from cylindrical firebrands [11], [12] and disk shaped firebrands [13], with a lower mass of cylindrical shaped firebrands causing ignition due to more surface contact by the firebrands falling down into the fuel bed. Simulations on the effect of contact resistance between firebrands and a wood surface has also shown that decreasing contact resistance increases the temperature rise of wood [14]. These studies indicate that the likelihood of ignition increases with an increase in the firebrand pile size, fuel type, and geometry of the fuel surface. Also, they highlight the complexity of the heat transfer between the firebrands and the fuel surfaces including surface contact effects.

In order to generate realistic firebrands in the laboratory environment, the shape and size of the firebrands must be considered. Filkov et al. [15] collected firebrands during prescribed burns in the New Jersey Pine Barrens. It was found that the majority of firebrands were bark fragments,

with less than 30% of the collected samples being pieces of twigs or branches. To measure the cross-sectional area, the bark firebrands were modeled as rectangles, while firebrands made of twig or branch segments were modeled as cylinders. 80% of the measured firebrands had cross-sectional areas between 50 and 200 mm^2. Manzello et al. [16] burned Korean pine trees in a laboratory environment, using water pans to collect the firebrands. All of the firebrands collected were cylindrical in shape, with an average diameter and length of 5.0 and 34 mm, respectively. These results were similar to burning experiments using Douglas fir trees. These results show that firebrands with both rectangular and cylindrical shapes are important.

Limited measurements have been conducted on the heat transfer from firebrands to a surface. Manzello et al. [6] used an energy balance and the firebrand temperature to estimate the average heat transfer across the firebrand to the surface. For a single glowing cylindrical firebrand, the average heat flux over the firebrand was predicted to be 23 kW/m^2 with 1.3 m/s of wind and 34 kW/m^2 with 2.4 m/s of wind. Water cooled heat flux gauges and thin skin calorimeters with 12 mm diameter sensing surfaces were used to measure heat flux levels from single and piles of firebrands [7]. For single cylindrical firebrands (6.35 – 12.7 mm diameter, 25.4 mm long, 0.1 – 0.6 g mass), the heat fluxes were measured to be 7 – 25 kW/m^2 with no wind. A technique to measure spatial heat transfer from firebrands is being developed using a Nd:YAG laser, a quartz platform, and CMOS camera, but no firebrand measurements have been made [17].

The focus of this paper is to provide high resolution measurements of the heat transfer from a firebrand to a horizontal surface to capture the spatial variation below and around the firebrand. Ignition is a local phenomenon that will depend on the highest heat transfer levels from the firebrand. Since the contact between the firebrand and surface may be variable and the air flow around the firebrand may change its temperature non-uniformly, spatial distributions in the heat transfer from the firebrand to the surface are needed to quantify the highest heat transfer levels to assess ignition potential. In this work, the inverse heat transfer method using IR thermography of a stainless steel plate [18], [19] was used to quantify high resolution heat flux distributions from a single firebrand placed on a horizontal surface. The effects of firebrand geometry, firebrand contact with the surface, wind speed, and firebrand orientation with the wind on the heat flux to the surface were quantified. Localized heat flux measurements were spatially averaged to compare with other measurements in the literature.

2.2. EXPERIMENTAL METHODS

A series of experiments were performed to quantify the spatial and temporal variation in heat flux from a single firebrand to a surface. An inverse heat transfer method using IR thermographs was used to quantify the heat flux from the firebrand to the surface at a resolution of 0.4 mm. A description of the apparatus, firebrands, and inverse heat transfer method is provided below along with the test matrix performed in this study.

2.2.1 Test Apparatus

The experimental setup to quantify the heat transfer from a single firebrand to a surface is shown in Figure 1. The setup consisted of a thin 304SS stainless steel plate painted black, an IR camera to measure temperature of the underside of the plate (Camera 1), an IR camera to measure the firebrand temperature (Camera 2), and a blower to provide wind. Firebrands were placed on a 0.8 mm thick 304SS plate painted black on both sides with four coats of Rust-Oleum™ high-heat black paint with a measured emissivity of $\varepsilon = 0.97$ [20]. The stainless steel plate was square with

each side being 0.61 m long and was supported in each corner by a wooden stand. The wooden stand was 0.92 m tall and sufficiently stable that the plate did not move during the testing.

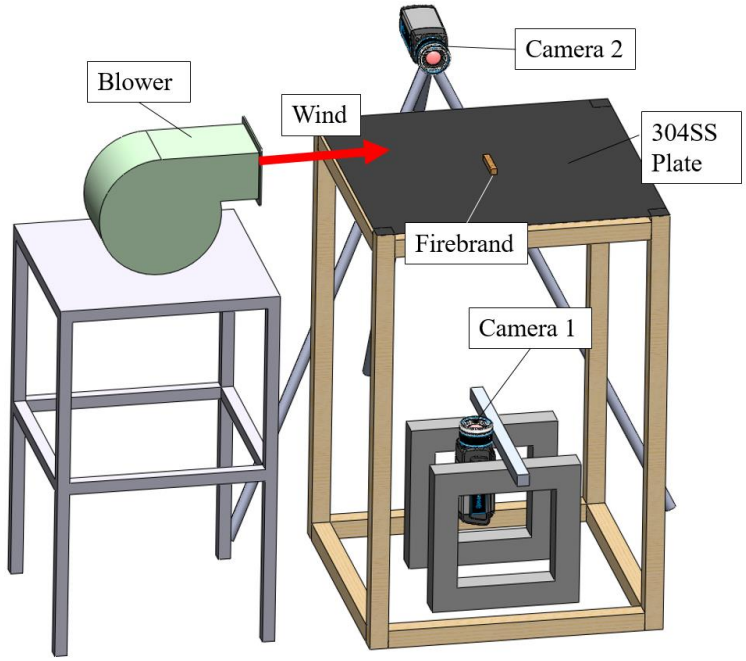

Figure 1. Test stand to characterize localized heat transfer from firebrands.

Two FLIR A655sc infrared cameras operating in the 7-14 μm wavelength range were used to measure surface temperatures. The cameras had a 640 × 480 pixel resolution and used a 24.6 mm (25°) lens. Camera 1 was used to measure the underside of the steel plate and was operated in the 100 – 650°C calibration range. Camera 1 was 0.58 m below the underside of the steel plate resulting in a field of view of the plate of 0.259 m by 0.195 m, which corresponds to a spatial resolution of 0.4 mm. The emissivity for Camera 1 was set to 0.97 to correspond to the black paint emissivity. Camera 2 measured the firebrand surface temperature and was operated using the 300-2000°C calibration range. The distance between Camera 2 and the firebrand ranged from 0.40 – 0.50 m resulting in a spatial resolution of 0.28 – 0.35 mm of temperature on the firebrand. Camera 2 emissivity was set to a value of $\varepsilon = 0.7$ which is the average of the range of emissivity levels (0.6 – 0.8) reported in the literature for firebrands [6], [9], [21]. ResearchIR software was used to control the cameras, collect data, and produce thermal images.

Wind was provided by a Dayton Model No. 1TDR3 Blower (273 cfm @ free air and 60 Hz), connected to a Staco Energy Products Model 3PN151OB Variable Autotransformer to control the wind speed between 0.5 and 2.0 m/s at the firebrand location. Above wind speeds of 2.0 m/s it was found that the firebrands tended to move on the plate. The blower was set up such that bottom of the blower outlet was flush with the top of the plate and the flow traveled parallel to the surface. The bottom of the plate was shielded from the airflow so that there was only natural convection below the plate. The blower was found to be a good laboratory approximation for wind, providing a uniform flow with less than 0.1 m/s variation across the length of the firebrand. Wind speed was verified prior to each test using an Extech Hot Wire Thermo-Anemometer with a 0.2 – 20 m/s range and 0.1 m/s resolution.

2.2.2 Heat Transfer Measurement

The thermal exposure from firebrands to adjacent surfaces was measured using the inverse heat transfer technique developed by Rippe and Lattimer [19]. The advantage of the inverse heat transfer method is that it measures a heat transfer boundary condition from the firebrand that can then be used to simulate firebrand exposure on a wide variety of surfaces. The technique involves painting a stainless steel plate with a known emissivity paint and exposing one side of the plate to the thermal environment. A series of high-resolution IR thermography images of the unexposed side of the stainless steel plate are recorded during testing. An energy balance on each pixel in the IR thermograph is used to calculate the exposure heat flux at every point on the surface using

$$q''_{exp} + q''_{cond} - q''_{rad,b} - q''_{conv,b} = \frac{\rho V c_p}{A}\frac{dT_s}{dt} \tag{1}$$

where q''_{exp} is the exposure heat flux, q''_{cond} is the net lateral heat flux entering a pixel from its neighbors, $q''_{rad,b}$ is the net radiation flux into the unexposed surface, $q''_{conv,b}$ is the net convection flux into the unexposed surface, ρ is the density of the stainless-steel plate, V is the volume of the pixel, A is the surface area of the pixel, c_p is the specific heat of the stainless steel plate, and dT_s/dt is the time rate of change of the surface temperature of the pixel. The exposure flux can be expressed as a heat flux at standard conditions (surface temperature at 293K as would be measured with a Schmidt-Boelter gauge) using the equation

$$q''_{exp} = q''_o - \varepsilon_f \sigma (T_s^4 - T_0^4) - h_f (T_s - T_0) \tag{2}$$

where q''_0 is the heat flux at standard conditions (surface temperature of 293 K), ε_f is the emissivity of the exposed surface, h_f is the convective heat transfer coefficient on the exposed surface, T_s is the measured surface temperature of the stainless steel plate, and T_0 is the standard temperature taken to be 293 K. All heat fluxes presented in this paper are heat fluxes at the standard condition (surface temperature at 293 K). The key distinction between q''_{exp} and q''_o is that q''_{exp} is the true net heat transfer between the firebrand and the plate accounting for a decreasing temperature difference between firebrand and plate as the plate heats up. q''_o on the other hand, is the heat transfer that would be seen by a plate maintained at a cooler temperature of 293K for the duration of the test. Effects of plate temperature on the burning behavior of the firebrand are ignored.

Rippe and Lattimer showed the uncertainty in the thermal exposure measurements decreased with a larger Δt used in the calculation of the energy storage term in Eq. 1. In this work, Δt of three seconds was used in Eq. 1.

The Nusselt number for natural convection of the heated plate was calculated using the relationships presented by [22] and [23]. For the upper surface of the heated plate,

$$\overline{Nu}_L = 0.54 Ra_L^{1/4} \text{ for } (10^4 \le Ra_L \le 10^7) \tag{3}$$
$$\overline{Nu}_L = 0.15 Ra_L^{1/4} \text{ for } (10^7 \le Ra_L \le 10^{11}) \tag{4}$$

where $\overline{Nu}_L$ is the average Nusslet number, and Ra is the Rayleigh number,

$$Ra_L = \frac{g\beta(T_s - T_\infty)L^3}{\nu\alpha} \tag{5}$$

where g is the acceleration due to gravity, β is the thermal expansion coefficient, T_∞ is the ambient air temperature, ν is the kinematic viscosity, α is the thermal diffusivity, and L is the hydraulic radius of the heated section

$$L = \frac{A_{exp}}{P_{exp}} \tag{6}$$

where A_{exp} is the total area exposed by the firebrand, and P_{exp} is the total perimeter exposed by the firebrand. Similarly, $\overline{Nu}_L$ for the lower surface of the heated plate,

$$\overline{Nu}_L = 0.27 Ra_L^{1/4} \text{ for } (10^5 \leq Ra_L \leq 10^{10}) \tag{7}$$

The Nusselt number for forced convection of the heated plate was calculated using the relationships presented by [24] for fully turbulent and laminar boundary layer conditions over a heated flat plate,

$$\overline{Nu}_L = 0.037\, Re_W^{4/5} Pr^{1/3} \text{ for } (Re_W \geq 5 \times 10^5,\ 0.6 \leq Pr \leq 60) \tag{8}$$

$$\overline{Nu}_L = 0.664\, Re_W^{1/2} Pr^{1/3} \text{ for } (Re_W \leq 5 \times 10^5,\ 0.6 \leq Pr \leq 60) \tag{9}$$

where Re_w is the Reynolds number defined by the plate width, W, and Pr is the Prandtl number.

Rippe and Lattimer [19] conducted an uncertainty analysis of this measurement technique using similar parameters. It was found that the uncertainties in the convection coefficient and local temperature measurements were the two largest contributors to the overall measurement uncertainty. Using the propagation of errors technique it was found that the total measurement uncertainty was 2.63 kW/m^2.

During preliminary testing, it was observed that the Wiener filter recommended by Rippe and Lattimer to reduce the noise in the thermographs prior to the inverse heat transfer calculation resulted in an increase in noise in this application. In this work, the filter was replaced with a 2-D Gaussian filter with a 7 x 7 pixel window. The updated filtering approach reduced the peak measured temperature by approximately 1 °C, and reduced the peak observed heat flux by 10%.

This series of tests were the first to use the inverse heat transfer (IHT) method in a situation where the thermal response of the stainless steel plate was highly dependent on the spatially resolved conductive flux. Verification of the inverse heat transfer (IHT) method is provided in Figure 2 for a local exposure on a steel plate similar to what would occur in the firebrand testing.

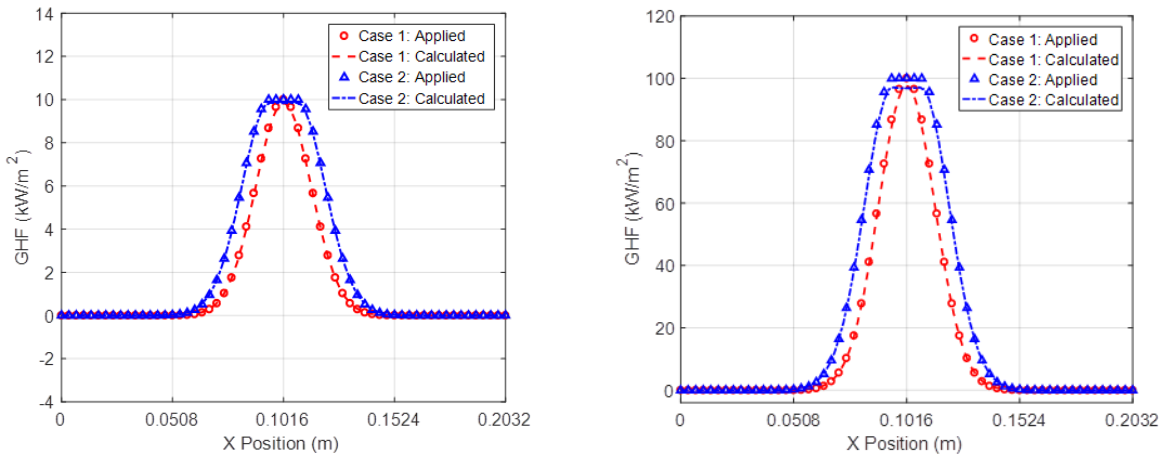

(a) 10 kW/m^2 (b) 100 kW/m^2

Figure 2. Verification for quantifying localized heat transfer using the IHT measurement.

The IHT method was tested by generating artificial thermographs using known exposure profiles in a Finite Element (FE) model in Abaqus. The model included a 0.20 m by 0.18 m plate with continuum heat transfer elements (DC3D8) at a mesh of density of 0.4 mm/element, which was similar to the spatial resolution of the experimental measurements. As seen in Figure 2, two verification scenarios were considered with a local heat flux applied to the center of the plate. Verification Case 1 applied a Gaussian distributed heat flux with a peak value of 10 and 100 kW/m^2 applied at the center with $\sigma = 0.0127$ m in shorter dimension and $\sigma = 0.0254$ m in the longer dimension. Verification Case 2 used the uniform 10 and 100 kW/m^2 heat flux over a 0.025 m x 0.051 m wide rectangle with a Gaussian drop at each edge of the uniform region using the same parameters as Verification Case 1. The error was less than 3%.

2.3 Firebrands

Firebrands were fabricated using oak wood. Six distinct firebrand geometries were manufactured as shown in Figure 3. All firebrands had the same aspect ratio and projected area with the exception of Type 6.

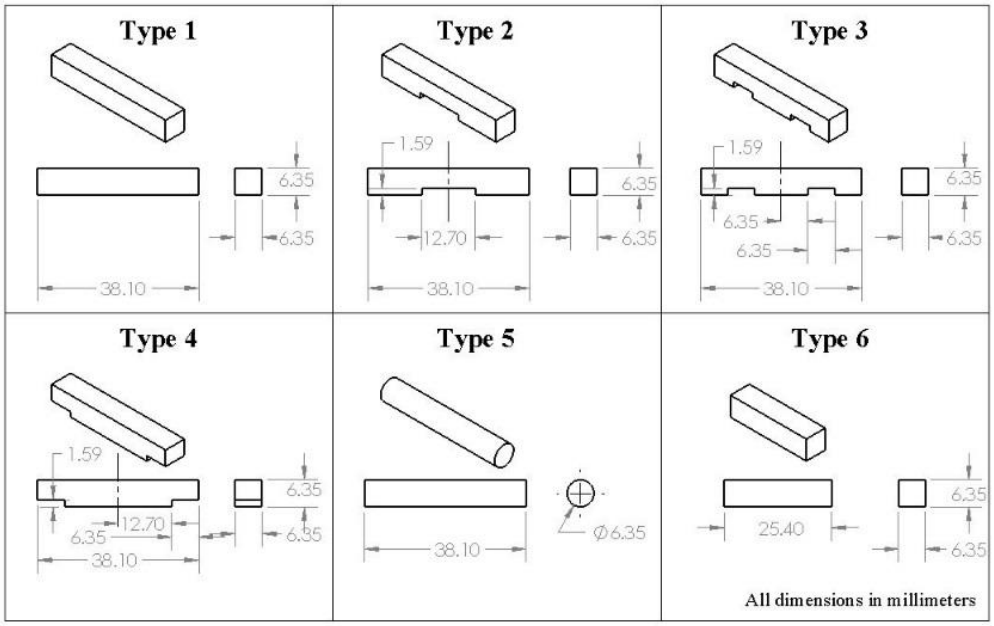

Figure 3. Oak firebrand geometries.

Types 1-4 were all cuboids of the same major dimensions (6.35 mm x 6.35 mm, 38.1 mm long) but with different notches on the face that would be in contact with steel plate surface. The cuboid shape was chosen because it resembles the surface contact of firebrands from bark fragments [15]. The notch depth was 1.59 mm in all cases and spanned the entire width of the firebrand. Type 5 was a cylindrical firebrand (6.35 mm diameter, 38.1 mm long) while Type 6 was a cuboid with no notch and a shorter length (6.35 mm x 6.35 mm, 25.4 mm long). Cylindrical firebrands were selected because they have different surface contact compared with cuboids and they resemble sections of twigs or branches [15], [16]. The cuboid firebrands were manufactured by using a band saw to cut a 38.1 mm x 6.35 mm board into 6.35 mm strips. Notches were installed by hand, using a Dremel rotary cutter. Type 5 firebrands were manufactured by cutting a 6.35 mm round oak dowel into 38.1 mm sections. The moisture content of the firebrands was on average 4.9% by weight with a standard deviation of 0.16%.

Prior to ignition, each firebrand was weighed using an AND HR-202i precision balance with 0.1 mg resolution. The firebrands used for evaluating wind effects were measured using a Sartorius FB6CCE-S scale with a 6200 g range and 0.1 g resolution. To ignite the firebrands, a small propane burner was used. The firebrands were placed in a wire mesh basket over the flames and rotated frequently to ensure even heating on all sides. Heating over the propane flame lasted for 30s for all firebrands. After the 30s heating period, the flame was turned off and the firebrand was allowed to progress in a state of flaming ignition for an additional 10 s before the flame was blown out. The glowing firebrand was then placed in the center of the stainless steel plate using tongs for testing.

2.2.4 Test Procedure and Matrix

A matrix of experiments was designed to characterize the effect of wind and wind orientation on the heat transfer from the different types of firebrands. Each firebrand geometry (Types 1-6) was tested under three conditions as outlined in Table 1. This included a no wind condition, wind direction that was parallel to the long-axis of the firebrand, and wind direction perpendicular to

the long-axis of the firebrand. Experiments with Type 1 firebrands were run twice to quantify the repeatability.

The majority of testing was performed with a wind speed was 1.0 m/s, with the exception of the Type 2 firebrands (cuboid with one centered notch) oriented perpendicular to the wind where the wind speed was varied from 0 – 2.0 m/s. For all tests, the firebrands were left on the plate for 300 seconds. The initial mass of the wood before creating the firebrand is provided in Table 1 along with the firebrand mass after heating and the mass after the 300 s test. The initial firebrand mass before it was put on the plate was approximately 40-50% of the wood initial mass. Results presented in this paper are based on a single firebrand test for each test condition in the matrix provided in Table 1.

2.3. RESULTS

Heat transfer measurements from the different types of firebrands are presented in this section for different wind conditions and firebrand orientations relative to the wind direction. In addition, temperature measurements on the long side of the firebrand and repeatability results are provided.

2.3.1 No Wind

The peak heat flux to the plate with time is provided in Figure 4 for the different types of firebrands tested with no wind. The highest peak heat flux for all firebrands occurred in the initial 25 seconds and then the heat flux decayed with time. Peaks were measured to range from 17-38 kW/m^2 with shorter cuboid (L=25 mm) producing the highest heat flux and the cylindrical cuboid producing the lowest. The cuboidal firebrands were all seen to have similar heat fluxes around 50 s, with variation developing as the test continued. The cylindrical firebrand was measured to have a significantly lower heat flux and decay more rapidly than the cuboids. It was noted during the test that the cuboids progressed in a state of glowing combustion for some time, while the cylinder burned out immediately. The spatial distribution in the heat flux at the time of the highest peak heat flux for the test duration is provided in Figure 5. Except for the cylinder, the heat flux is highest at the distal ends of the firebrands.

Table 1. Firebrand test matrix and mass data.

Type	Description	Wind (m/s)	Wind Orientation	Wood Initial Mass (g)	Mass After Heating (g)	Mass After 300s (g)
1	Cuboid – 6.4 mm x 6.4 mm, 38 mm long	None	N/A	1.221	0.572	0.484
		1.0	Parallel	1.231	0.624	0.386
		1.0	Perpendicular	1.131	0.473	0.238
2	Cuboid – 6.4 mm x 6.4 mm, 38 mm long One centered notch	None	N/A	1.125	0.467	0.357
		None*	N/A	1.1	-	0.3
		0.5*	Perpendicular	1.1	-	0.3
		1.0	Parallel	1.112	0.484	0.331
		1.0	Perpendicular	1.122	0.41	0.208

		1.0*	Perpendicular	1.1	-	0.0
		1.5*	Perpendicular	1.2	-	0.0
		2.1*	Perpendicular	1.1	-	0.0
3	Cuboid – 6.4 mm x 6.4 mm, 38 mm long Two centered notches	None	N/A	1.162	0.55	0.437
		1.0	Parallel	1.128	0.527	0.29
		1.0	Perpendicular	1.092	0.382	0.067
4	Cuboid – 6.4 mm x 6.4 mm, 38 mm long End notches	None	N/A	1.084	0.485	0.405
		1.0	Parallel	1.081	0.512	0.37
		1.0	Perpendicular	1.119	0.495	0.273
5	Cylinder - 6.4 mm diameter, 38 mm long	None	N/A	1.088	0.548	0.524
		1.0	Parallel	1.115	0.554	0.525
		1.0	Perpendicular	1.121	0.551	0.534
6	Cuboid – 6.4 mm x 6.4 mm, 25 mm long	None	N/A	0.81	0.424	0.375
		1.0	Parallel	0.796	0.404	0.326
		1.0	Perpendicular	0.74	0.293	0.158

* Denotes firebrands used to evaluate wind effects.

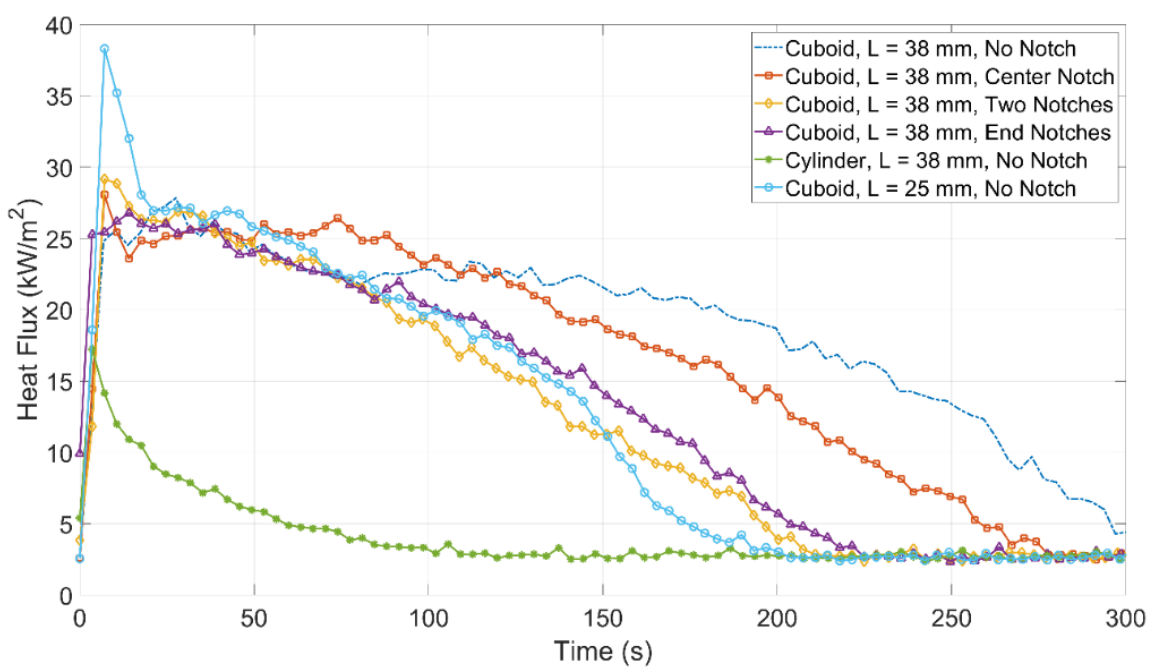

Figure 4. Peak heat flux with time for different types of firebrands with no wind.

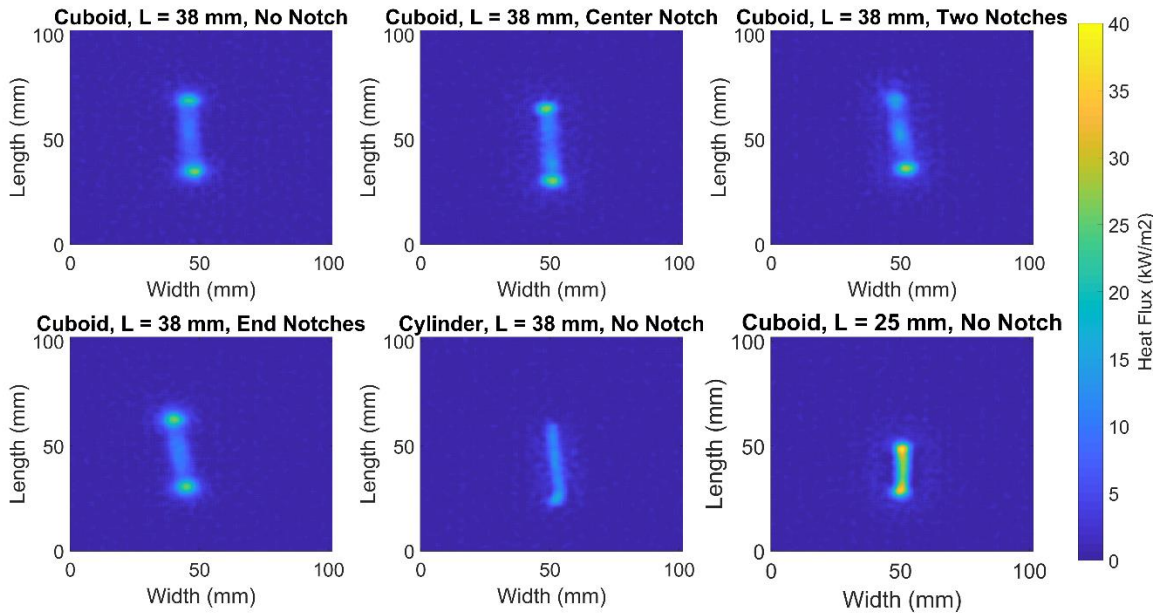

Figure 5. Heat flux distributions at time of highest peak heat flux for different types of firebrands with no wind.

2.3.2 Parallel Wind

The peak heat flux to the plate with time is provided in Figure 6 for the different types of firebrands tested with the long side parallel to 1.0 m/s of wind. Compared with the no wind case in Figure 4, these heat fluxes are generally higher and remain at an elevated level for a longer period of time. The highest peak heat fluxes ranged from 50-65 kW/m^2 except for the cylindrical firebrand which was significantly lower. For this case, the cuboid firebrand exposure remains above 20 kW/m^2 for 115-300 seconds, depending on the type of firebrand. The cylindrical firebrand produced the lowest heat fluxes and had the shortest duration. The highest heat fluxes were measured to be the cuboid with a single notch. The cuboids, L=38 mm produced similar heat fluxes slightly higher heat fluxes for the case with two center notches. The shorter cuboid, L=25 mm, had a similar heat flux level to the longer cuboids but burned out faster than the longer cuboids.

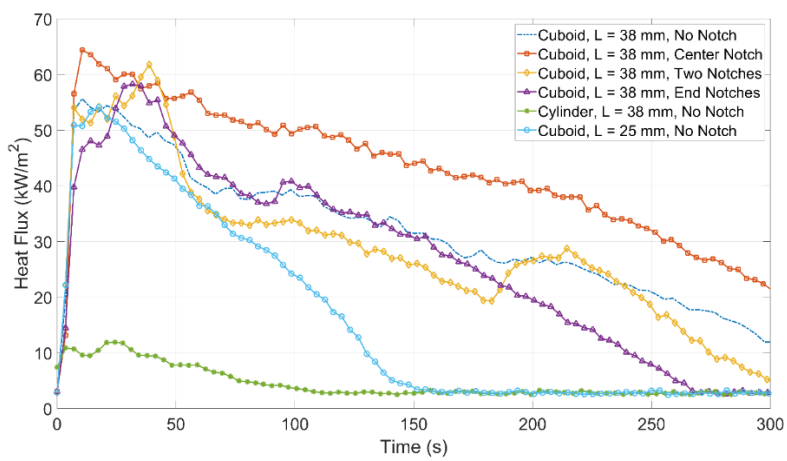

Figure 6. Peak heat flux with time for different firebrands, long side parallel to 1.0 m/s of wind.

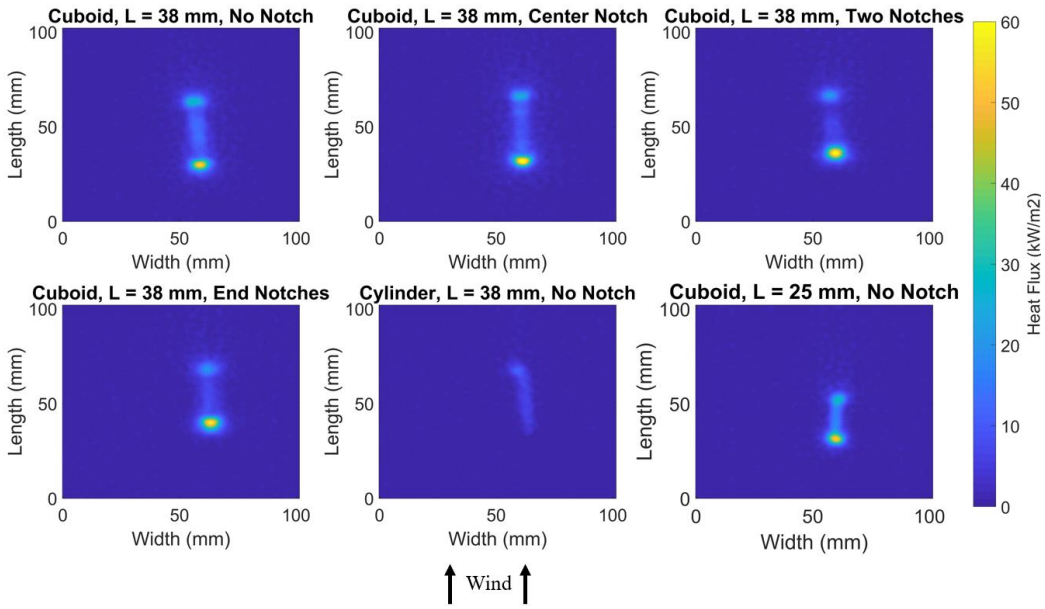

Figure 7. Heat flux distributions at time of highest peak flux for different types of firebrands with long side parallel to 1.0 m/s of wind.

The spatial distribution in heat flux from the firebrands are provided in Figure 7 at the time of the highest peak heat flux. For this case, the highest heat fluxes are generally at the leading edge of the firebrand where the wind initially encounters the firebrand, indicating enhanced char oxidation at the leading edge of the firebrand. The notches in the firebrands are not where the highest heat fluxes were measured, except in the case with the end notches where the leading edge is at the notch location.

2.3.3 Perpendicular Wind

The peak heat flux to the plate with time is provided in Figure 8 for the different types of firebrands tested with the long side perpendicular to 1.0 m/s of wind. In this case, the highest peak fluxes ranged from 50-75 kW/m^2, excluding the cylindrical firebrand which was again much lower. Exposure of greater than 20 kW/m^2 ranged from 200-300 seconds for all cuboids. The cylindrical firebrand produced the lowest heat flux while the large cuboid without notches generated the highest heat fluxes for most of the test. The peak for the cuboid with two notches corresponds to a sudden, rapid progression of glowing combustion across a substantial portion of the firebrand. In general, these firebrand exposures were similar in duration but slightly higher in magnitude compared with the parallel wind case (Figure 6).

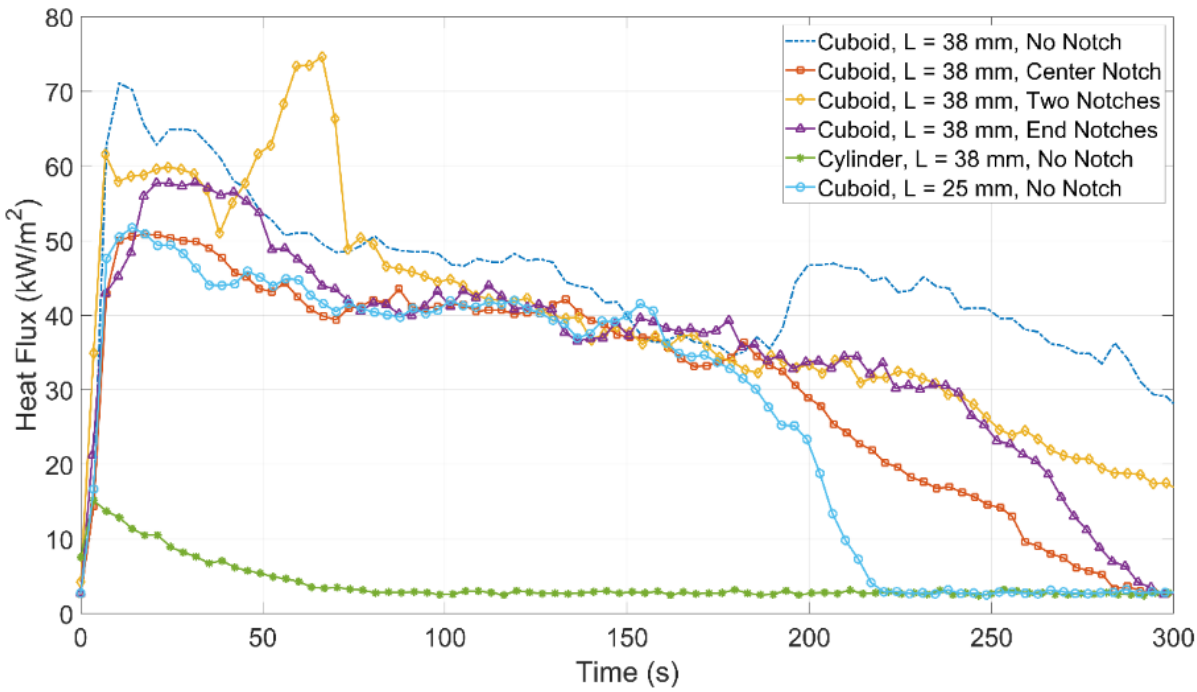

Figure 8. Peak heat flux with time for different types of firebrands with long side perpendicular to 1.0 m/s of wind.

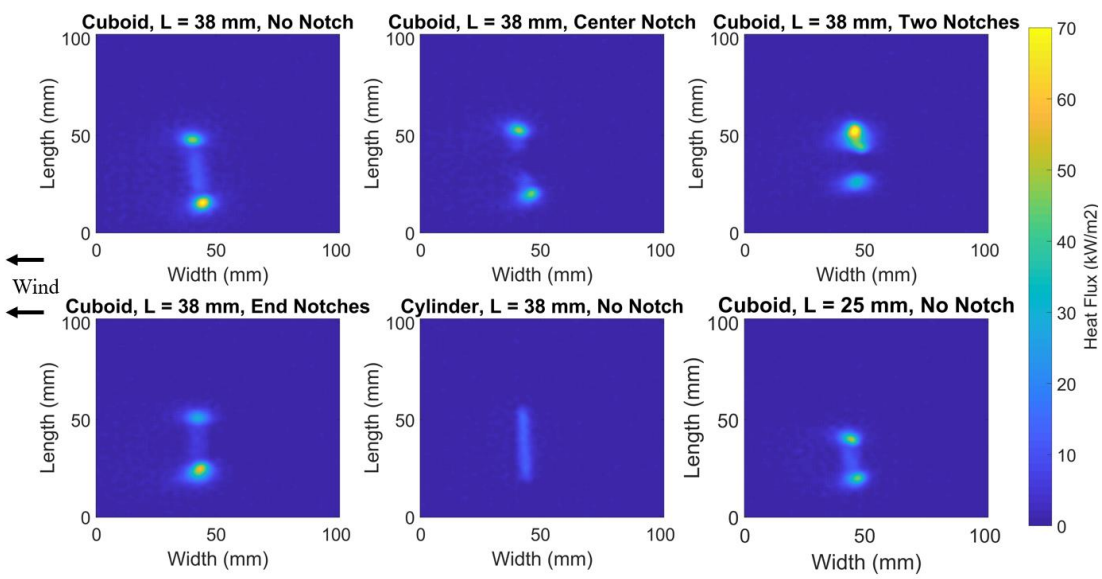

Figure 9. Heat flux distributions at time of highest peak flux for different types of firebrands with long side perpendicular to 1.0 m/s of wind.

Spatial distributions in the firebrand heat flux levels are provided in Figure 9 for the different types of firebrands at the time of the highest peak heat flux level. For this case, the higher heat fluxes are located at the ends of the firebrand, which is attributed to more char oxidation on the ends where there is more surface area.

2.3.4 Firebrand Temperature

The firebrand temperature distribution at the time of the peak temperature is provided in Figure 10. The peak temperatures range from 200-775ºC for cylindrical firebrands to 800-950ºC for the cuboid firebrands. Highest temperatures were measured at the ends where there is more surface area for char oxidation. The reason why the cylindrical firebrands are consistently lower in temperature compared with the cuboids is unknown. One possible explanation is that all the cuboidal firebrands were cut from a single board, while the cylindrical firebrands were made from a dowel rod. It is possible some variation exists between the two sources which affects the combustion properties of the firebrand.

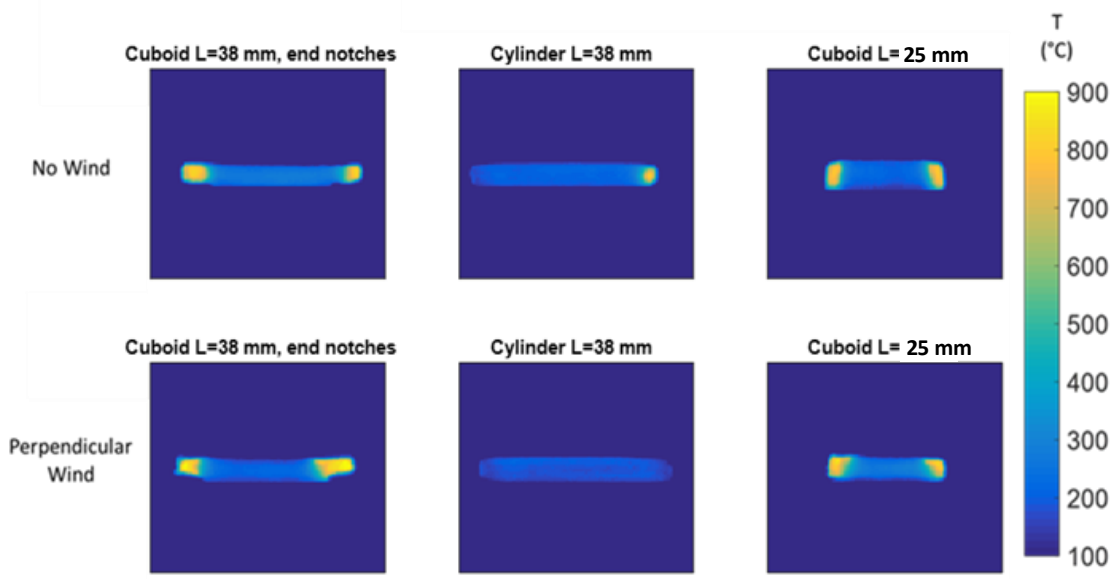

Figure 10. Firebrand temperature distribution at the time of peak temperature for no wind (top row) and firebrand perpendicular to wind at 1.0 m/s (bottom row).

2.3.5 Wind Speed Effects

The effects of wind speed on firebrand heat flux levels are provided in Figure 11 for a cuboid L=38 mm with a one notch in the center and wind perpendicular to the long side of the firebrand. As expected from previous work, increasing the wind speed causes an increase in heat flux level from 20-30 kW/m^2 with low wind speeds (up to 0.5 m/s) to 50-80 kW/m^2 for wind speeds of 1.0 – 2.0 m/s. In addition, the higher wind speeds caused the firebrands to be consumed faster resulting in intense but shorter duration exposures.

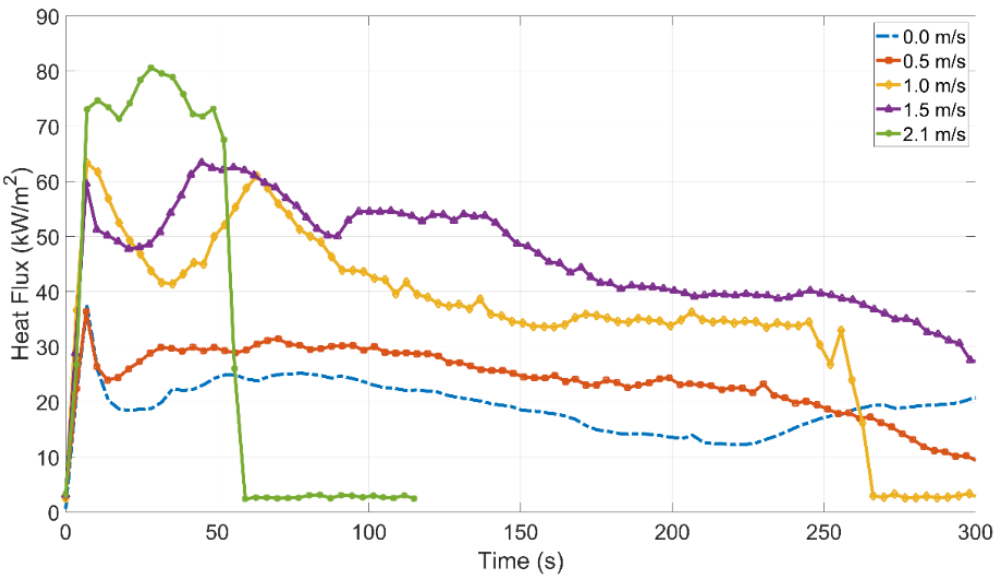

Figure 11. Effect of wind speed on the peak heat flux with time for the cuboid L=38mm, one notch firebrand with the long side perpendicular to the wind.

2.3.6 Repeatability

Experiments with Type 1 firebrands (6.35 mm x 6.35 mm, 38.1 mm long, with no notch) were run twice to gain an estimate of how consistent the heat transfer was from similar firebrands under the same conditions, shown in Figure 12. Sample A firebrands were used in the rest of the paper, Sample B firebrands were exclusively used for the repeatability analysis. Figure 12 shows peak heat fluxes are similar between tests. The average percent difference between Sample A and B across all three wind conditions was determined to be 5-30% during the primary smoldering period (before 190 s) with a more variation observed as the firebrand smoldering began to decay to burn out (after 190 s).

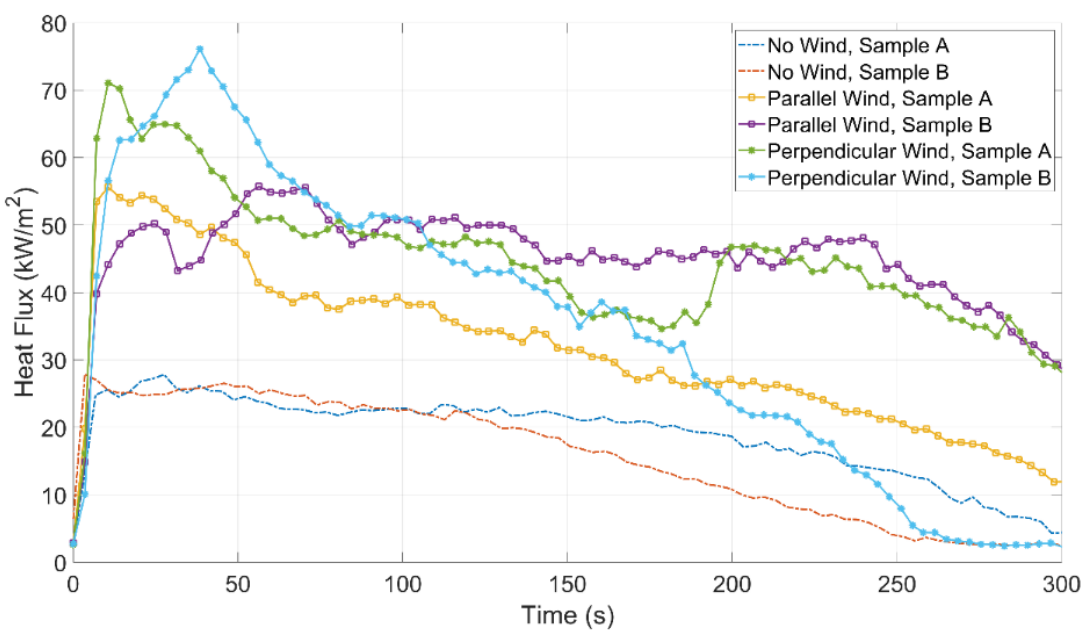

Figure 12. Repeatability of peak heat flux with time (cuboid, L = 38 mm, no notch).

2.4. DISCUSSION

A summary of the peak heat fluxes measured for the different firebrands in this study is provided in Table 2. Summary of heat fluxes measured in this work at different resolutions.. In this table, the heat fluxes are provided at three different resolutions: the inverse heat transfer (IHT) method (0.4x0.4 mm resolution), average over firebrand projected area on the surface, and average over a 12.5 mm x 12.5 mm region.

Table 2. Summary of heat fluxes measured in this work at different resolutions.

Description	Wind (m/s)	Wind Orientation	Peak Heat Flux (kW/m^2)		
			IHT Method (0.4x0.4 mm)	Avg. Over Firebrand	12.5x12.5 mm Region Avg.
Cuboid – 38 mm long No Notch	None	N/A	27.8	13.8	9.8
	1.0	Parallel	55.6	17.9	16.1
	1.0	Perpendicular	71.1	21.6	21.2
Cuboid – 38 mm long One centered notch	None	N/A	28.1	13.9	9.9
	None	N/A	37.3	21.7	19.9
	0.5	Perpendicular	36.4	18.8	23.3
	1.0	Parallel	64.4	17.1	17.8
	1.0	Perpendicular	50.9	15.4	14.4
	1.0	Perpendicular	63.3	35.9	31.6
	1.5	Perpendicular	63.4	32.8	32.9
	2.1	Perpendicular	80.6	36.4	40.2
Cuboid – 38 mm long Two centered notches	None	N/A	29.2	12.3	9.5
	1.0	Parallel	61.7	15.8	18.7
	1.0	Perpendicular	74.6	27.3	31.9
Cuboid – 38 mm long End notches	None	N/A	26.8	15.1	9.9
	1.0	Parallel	58.3	17.2	18.8
	1.0	Perpendicular	57.8	19.4	21.2
Cylinder - 38 mm long	None	N/A	17.2	11.7	5.8
	1.0	Parallel	11.9	9.9	4.7
	1.0	Perpendicular	15.2	12.3	5.6
Cuboid – 25 mm long	None	N/A	38.3	27.0	12.6
	1.0	Parallel	54.2	25.8	16.0
	1.0	Perpendicular	51.7	21.2	14.5

The firebrand average heat flux was calculated to allow for comparison with heat fluxes predicted using an energy balance on the firebrand [6]. The energy balance prediction of heat flux from a cylindrical firebrand (10 mm in diameter, 75 mm long) was 23 kW/m^2 with a 1.3 m/s wind [6]. This is a 46% difference compared with firebrand average heat flux measured in this

study for a cylinder but within 6% of the cuboids. The deviations between the two studies are attributed to the differences in firebrand temperatures.

The 12.5 mm x 12.5 mm average was calculated to compare with measurements using a 12.5 mm diameter heat flux gauge by Hakes et al. [7]. They measured heat fluxes ranging from 7 – 25 kW/m^2 for single cylindrical brands 6.4 – 12.7 mm in diameter and 25 mm long with no wind. This is consistent with the range of 12.5 mm x 12.5 mm average heat flux levels measured in this study shown in Table 2.

The higher resolution heat fluxes are a factor of 2 – 3.5 times higher than the spatially averaged heat fluxes. Some of these heat fluxes are quite localized and the spatial resolution that drives ignition will need to be determined with future experiments of firebrands on combustible materials. Despite this, the technique presented in this paper is able to capture these spatial variations allowing for appropriate averaging to assess the ignition potential of single firebrands and firebrand piles. In addition, the spatial heat flux distributions produced using these measurements also captures the location of the peak heat fluxes which can be uncertain based on the firebrand geometry, contact, and orientation with wind direction.

2.5. CONCLUSION

An experimental study was performed to measure the localized heat fluxes produced by different types of single firebrands onto a horizontal surface under different wind conditions. An inverse heat transfer method using a series of IR thermographs of a stainless steel plate provided spatial heat flux distributions with a 0.4 mm resolution. With the higher resolution, peak heat fluxes were measured to be 25 – 80 kW/m^2, which is 2-3.5 times higher than expected based on lower spatial resolutions and values reported in the literature. Firebrand geometry, wind speed and wind orientation relative to the firebrand all affected the peak heat flux produced by the firebrand and the exposure duration. Firebrand experiments on combustible surfaces are needed to determine the appropriate heat flux resolution to correlate with the ignition of the combustible. In addition, work considering multiple firebrands and firebrand piles is necessary to understand how results from single-firebrand experiments scale for more complex systems.

2.6. ACKNOWLEDGEMENTS

The project was funded through NIST Grant No. 70NANB19H052.

REFERENCES

[1] S. E. Caton, R. S. P. Hakes, D. J. Gorham, A. Zhou, and M. J. Gollner, “Review of Pathways for Building Fire Spread in the Wildland Urban Interface Part I: Exposure Conditions,” *Fire Technol.*, vol. 53, no. 2, pp. 429–473, 2017, doi: 10.1007/s10694-016-0589-z.

[2] R. S. P. Hakes, S. E. Caton, D. J. Gorham, and M. J. Gollner, “A Review of Pathways for Building Fire Spread in the Wildland Urban Interface Part II: Response of Components and Systems and Mitigation Strategies in the United States,” *Fire Technol.*, vol. 53, no. 2, pp. 475–515, 2017, doi: 10.1007/s10694-016-0601-7.

[3] E. Koo, P. J. Pagni, D. R. Weise, and J. P. Woycheese, “Firebrands and spotting ignition in large-scale fires,” *Int. J. Wildl. Fire*, vol. 19, no. 7, pp. 818–843, 2010, doi: 10.1071/WF07119.

[4] S. L. Manzello, “Enabling the investigation of structure vulnerabilities to wind-Driven firebrand showers in wildland-Urban Interface (WUI) fires,” *Fire Saf. Sci. 11*, vol. 11, pp.

83–96, 2014, doi: 10.3801/IAFSS.FSS.11-83.
[5] V. P. Dowling, "Ignition of timber bridges in bushfires," *Fire Saf. J.*, vol. 22, no. 2, pp. 145–168, 1994, doi: 10.1016/0379-7112(94)90070-1.
[6] S. L. Manzello, S. H. Park, and T. G. Cleary, "Investigation on the ability of glowing firebrands deposited within crevices to ignite common building materials," *Fire Saf. J.*, vol. 44, no. 6, pp. 894–900, 2009, doi: 10.1016/j.firesaf.2009.05.001.
[7] R. S. P. Hakes, H. Salehizadeh, M. J. Weston-dawkes, and M. J. Gollner, "Thermal characterization of firebrand piles," *Fire Saf. J.*, vol. 104, no. June 2018, pp. 34–42, 2019, doi: 10.1016/j.firesaf.2018.10.002.
[8] S. L. Manzello and S. Suzuki, "Exposing decking assemblies to continuous wind-driven firebrand showers," *Fire Saf. Sci.*, vol. 11, pp. 1339–1352, 2014, doi: 10.3801/IAFSS.FSS.11-1339.
[9] S. S. Wessies, M. K. Chang, K. C. Marr, and O. A. Ezekoye, "Experimental and Analytical Characterization of Firebrand Ignition of Home Insulation Materials," *Fire Technol.*, vol. 55, no. 3, pp. 1027–1056, 2019, doi: 10.1007/s10694-019-00818-8.
[10] T. J. Ohlemiller, "Smoldering combustion propagation on solid wood," *Fire Saf. Sci. 3*, pp. 565–574, 2006, doi: 10.4324/9780203973493.
[11] P. Ellis, "The Aerodynamic and Combustion Characteristics of Eucalypt Bark - A Firebrand Study," *Disseration, Aust. Natl. Univ. Dep. For.*, p. 205, 2000.
[12] S. L. Manzello, T. G. Cleary, J. R. Shields, A. Maranghides, W. Mell, and J. C. Yang, "Experimental investigation of firebrands: Generation and ignition of fuel beds," *Fire Saf. J.*, vol. 43, no. 3, pp. 226–233, 2008, doi: 10.1016/j.firesaf.2006.06.010.
[13] S. L. Manzello, T. G. Cleary, J. R. Shields, and J. C. Yang, "On the ignition of fuel beds by firebrands," *Fire Mater.*, vol. 30, no. 1, pp. 77–87, 2006, doi: 10.1002/fam.901.
[14] A. Warey, "Influence of thermal contact on heat transfer from glowing firebrands," *Case Stud. Therm. Eng.*, 2018, doi: 10.1016/j.csite.2018.04.018.
[15] A. Filkov *et al.*, "Investigation of firebrand production during prescribed fires conducted in a pine forest," *Proc. Combust. Inst.*, 2017, doi: 10.1016/j.proci.2016.06.125.
[16] S. L. Manzello, A. Maranghides, J. R. Shields, W. E. Mell, Y. Hayashi, and D. Nii, "Mass and size distribution of firebrands generated from burning Korean pine (Pinus koraiensis) trees," *Fire Mater.*, 2009, doi: 10.1002/fam.977.
[17] Y. M. Abul-huda, "Development of a Spatially Resolved Optical Technique for Measuring Heat Flux and Thermal Footprint of Firebrand Piles," *NIST Tech. Note 2052*, p. 28, 2019.
[18] J. Hodges, C. Rippe, S. W. Case, and B. Y. Lattimer, "Predicting the structural response of a compartment fi re using full-field heat transfer measurements," *Fire Saf. J.*, vol. 91, no. March, pp. 471–479, 2017, doi: 10.1016/j.firesaf.2017.03.011.
[19] C. M. Rippe and B. Y. Lattimer, "Full-field surface heat flux measurement using non-intrusive infrared thermography," *Fire Saf. J.*, vol. 78, pp. 238–250, 2015, doi: 10.1016/j.firesaf.2015.10.004.
[20] N. Cholewa, P. T. Summers, S. Feih, A. P. Mouritz, B. Y. Lattimer, and S. W. Case, "A Technique for Coupled Thermomechanical Response Measurement Using Infrared Thermography and Digital Image Correlation (TDIC)," *Exp. Mech.*, vol. 56, pp. 145–164, 2016, doi: 10.1007/s11340-015-0086-1.
[21] J. L. Urban, A. C. Fernandez-pello, M. Vicariotto, and D. Dunn-Rankin, "Temperature Measurement of Glowing Embers with Color Pyrometry," *Fire Technol.*, vol. 55, no. 3, pp. 1013–1026, 2019, doi: 10.1007/s10694-018-0810-3.
[22] R. J. Goldstein, E. M. Sparrow, and D. C. Jones, "Natural convection mass transfer

adjacent to horizontal plates," *Int. J. Heat Mass Transf.*, vol. 16, no. 5, pp. 1025–1035, 1973, doi: 10.1016/0017-9310(73)90041-0.

[23] J. R. Lloyd and W. R. Moran, "Natural convection adjacent to horizontal surface of various planforms," *J. Heat Transfer*, vol. 96, no. 4, pp. 443–447, 1974, doi: 10.1115/1.3450224.

[24] F. P. Incropera, D. P. DeWitt, T. L. Bergman, and A. S. Lavine, *Fundamentals of Heat and Mass Transfer*, 6th ed. John Wiley & Sons, 2007.

[25] P. Deb *et al.*, "Causes of the Widespread 2019–2020 Australian Bushfire Season," *Earth's Futur.*, vol. 8, no. 11, 2020, doi: 10.1029/2020EF001671.

[26] M. Ward *et al.*, "Impact of 2019–2020 mega-fires on Australian fauna habitat," *Nat. Ecol. Evol.*, vol. 4, no. 10, pp. 1321–1326, 2020, doi: 10.1038/s41559-020-1251-1.

[27] A. I. Filkov, T. Ngo, S. Matthews, S. Telfer, and T. D. Penman, "Impact of Australia's catastrophic 2019/20 bushfire season on communities and environment. Retrospective analysis and current trends," *J. Saf. Sci. Resil.*, vol. 1, no. 1, pp. 44–56, 2020, doi: 10.1016/j.jnlssr.2020.06.009.

[28] M. Turco *et al.*, "Climate drivers of the 2017 devastating fires in Portugal," *Sci. Rep.*, vol. 9, no. 1, pp. 1–8, 2019, doi: 10.1038/s41598-019-50281-2.

[29] K. Lagouvardos, V. Kotroni, T. M. Giannaros, and S. Dafis, "Meteorological conditions conducive to the rapid spread of the deadly wildfire in eastern attica, Greece," *Bull. Am. Meteorol. Soc.*, vol. 100, no. 11, pp. 2137–2145, 2019, doi: 10.1175/BAMS-D-18-0231.1.

[30] T. Brown, S. Leach, B. Wachter, and B. Gardunio, "THE NORTHERN CALIFORNIA 2018 EXTREME FIRE SEASON," *Bull. Am. Meteorol. Soc.*, vol. 95, no. 9, pp. S1–S96, 2014, doi: 10.1175/1520-0477-95.9.s1.1.

[31] D. M. Theobald and W. H. Romme, "Expansion of the US wildland-urban interface," *Landsc. Urban Plan.*, vol. 83, no. 4, pp. 340–354, 2007, doi: 10.1016/j.landurbplan.2007.06.002.

[32] W. Mell and Alexander Maranghides, "NIST Technical Note 1635: A Case Study of a Community Affected by the Witch and Guejito Fires," 2009.

[33] N. A. McArthur and P. Lutton, "Ignition of exterior building details in bushfires: An experimental study," *Fire Mater.*, vol. 15, no. 2, pp. 59–64, 1991, doi: 10.1002/fam.810150204.

[34] A. Filkov, D. Kasymov, V. Zima, and O. Matvienko, "Experimental investigation of surface litter ignition by bark firebrands," *AIP Conf. Proc.*, vol. 1698, no. January, 2016, doi: 10.1063/1.4937859.

[35] S. Santamaria *et al.*, "Investigation of Structural Wood Ignition By Firebrand Accumulation," *First Int. Conf. Struct. Saf. under Fire Blast*, no. July 2016, pp. 1–13, 2015.

[36] E. D. Bearinger, J. L. Hodges, F. Yang, C. M. Rippe, and B. Y. Lattimer, "Localized heat transfer from firebrands to surfaces," *Fire Saf. J.*, vol. 120, no. April 2020, p. 103037, 2021, doi: 10.1016/j.firesaf.2020.103037.

[37] Z. Tao, B. Bathras, B. Kwon, B. Biallas, M. J. Gollner, and R. Yang, "Effect of firebrand size and geometry on heating from a smoldering pile under wind," *Fire Saf. J.*, no. May, p. 103031, 2020, doi: 10.1016/j.firesaf.2020.103031.

[38] J. R. Lloyd and W. R. Moran, "Natural Convection Adjacent To Horizontal Surface of Various Planforms.," *Am. Soc. Mech. Eng.*, vol. 96, no. 74-WA/HT-66, pp. 443–447, 1974, doi: 10.1115/1.3450224.

[39] T. Conners, "Distinguishing Softwoods from Hardwoods," *Agric. Nat. Resour. Publ.*, p. 105, 2015.

[40] S. X. Li, J. Zhao, P. Lu, and Y. Xie, "Maximum packing densities of basic 3D objects," *Chinese Sci. Bull.*, vol. 55, no. 2, pp. 114–119, 2010, doi: 10.1007/s11434-009-0650-0.
[41] R. P. Zou, X. Y. Lin, A. B. Yu, and P. Wong, "Packing of cylindrical particles with a length distribution," *J. Am. Ceram. Soc.*, vol. 80, no. 3, pp. 646–652, 1997, doi: 10.1111/j.1151-2916.1997.tb02880.x.
[42] D. Thomas, D. Butry, S. Gilbert, D. Webb, and J. Fung, "The Costs and Losses of Wildfires: A Literature Survey (NIST Special Publication 1215)," 2017, [Online]. Available: https://doi.org/10.6028/NIST.SP.1215.
[43] S. Wang, X. Huang, H. Chen, N. Liu, and G. Rein, "Ignition of low-density expandable polystyrene foam by a hot particle," *Combust. Flame*, vol. 162, no. 11, pp. 4112–4118, 2015, doi: 10.1016/j.combustflame.2015.08.017.
[44] R. M. Hadden, S. Scott, C. Lautenberger, and C. C. Fernandez-Pello, "Ignition of Combustible Fuel Beds by Hot Particles: An Experimental and Theoretical Study," *Fire Technol.*, vol. 47, no. 2, pp. 341–355, 2011, doi: 10.1007/s10694-010-0181-x.
[45] A. Ganteaume *et al.*, "Spot fires: Fuel bed flammability and capability of firebrands to ignite fuel beds," *Int. J. Wildl. Fire*, vol. 18, no. 8, pp. 951–969, 2009, doi: 10.1071/WF07111.
[46] C. Lautenberger and A. C. Fernandez-Pello, "Spotting ignition of fuel beds by firebrands," *WIT Trans. Modelling Simul.*, vol. 48, pp. 603–612, 2009, doi: 10.2495/CMEM090541.
[47] H. S. Carslaw and J. C. Jaeger, *Conduction of Heat in Solids*, 2nd ed. London: Oxford University Press, 1959.
[48] J. G. Quintiere, "A simulation model for fire growth on materials subject to a room-corner test," *Fire Saf. J.*, vol. 20, no. 4, pp. 313–339, 1993, doi: 10.1016/0379-7112(93)90053-S.
[49] SFPE, *Engineering Guide - Piloted Ignition of Solid Materials Under Radiant Exposure*. Society of Fire Protection Engineers, 2002.
[50] A. Tewarson, "Generation of Heat and Chemical Compounds in Fires," in *The SFPE Handbook of Fire Protection Engineering*, 1995, p. Section 3-Chapter 4.
[51] E. D. Bearinger, B. Y. Lattimer, J. Hodges, C. Rippe, and A. Kapahi, "Statistical Assessment of Parameters Affeting Firebrand Pile Heat Transfer to Surfaces," *Curr. under Rev. by Front. Mech. Eng.*

3. STATISTICAL ASSESSMENT OF PARAMETERS AFFECTING FIREBRAND PILE HEAT TRANSFER TO SURFACES

Elias Bearinger, Brian Lattimer, Jonathan Hodges, Christian Rippe, Anil Kapahi

ABSTRACT

Firebrands are known to cause ignition of structures far from the primary fire front, resulting in significant damage to structures before firefighting can be attempted. To make structures more resilient to firebrand ignition, a better understanding of the heat transfer from firebrands to surfaces is needed. This paper provides a statistical assessment of different parameters expected to have an impact on the heat transfer from firebrand piles. This includes a range of variables that may affect the burning of firebrand piles including wood moisture content, wood type (hardwood or softwood), wood density, wood state (live, dead, or artificial), wind, pile mass, firebrand diameter, and firebrand length which may impact the heat transfer from firebrand piles. Using design of experiments, a test matrix was developed that permitted a statistical analysis to be performed to quantify which factors most significantly impact the heat transfer to the surface. Statistically significant impacts on heat transfer were observed with variations in wind, firebrand length, and the interaction between firebrand length and diameter interaction. These results support existing knowledge that wind, pile porosity, and pile height all affect the heat transfer from firebrand piles. In addition, significant impact on heat transfer were observed between artificial and natural firebrands, suggesting that laboratory experiments using surrogate firebrands such as wood dowels may overestimate the heat transfer observed from natural firebrands.

3.1. INTRODUCTION

For much of the world, uncontrolled wildfires present a serious and reoccurring threat to life, property, and the environment. The recent 2019-2020 fire season in Australia for example was so severe that it was named the Black Summer [25], with a cumulative 97,000 km^2 of vegetation burned [26]. Tragically, Australia's Black Summer resulted in the destruction of 3,000 homes and 33 direct fatalities [27]. This type of destruction from wildland fires has been increasingly seen around the world. The 2017 fires in Portugal killed 112 people [28]. In 2018, fires in Greece burned 3,000 houses [29]. In the United States, the 2018 Camp Fire alone killed 85 people and destroyed 19,000 structures [30]. Much of the human toll from these fires occurred in the wildland urban interface (WUI), the confluence of rural and developed environments. As the wildland urban interface continues to expand [31], there is a pressing need to design structures to withstand the potential destruction caused by wildfires.

Wildfires produce airborne pieces of burning vegetation and debris known as firebrands, which have been shown to be a prominent mode of home ignition [32]. Firebrands are particularly dangerous due to their lofting potential. The high winds associated with wildland fires can transport these firebrands 1-2 km from the fire front [3], where they have been witnessed to cause home ignition without direct flame contact. Experimental work has shown that during wind-driven firebrand showers, firebrands can accumulate in piles and easily ignite common building materials [8]. Understanding heat transfer from piles of firebrands is an important step in engineering fire-resistant structures.

One of the difficulties in identifying the risk of a structure igniting due to firebrand piles is the uncertainty and variability in the heat transfer from fires to surfaces. Early work in the field conducted by McArthur and Lutton investigated the ignition of mock building assemblies by radiata pine wood cribs at 3-5% moisture content. Crib masses from 0.8 – 12.0 g were tested in absence of wind and it was found that burning damage to the structure increased with crib mass [33]. Dowling collected embers from burned wood cribs which were then used to test ignition of timber bridges. It was found that 7.0 g of firebrands deposited in a 10 mm gap was sufficient to cause ignition with no wind applied [5].

Experiments were conducted by Manzello et al. [12] using machined Douglas fir firebrands to assess ignition in various fuel beds. The firebrands were cylindrical and came in two sizes. The first size had a diameter of 5 mm and a length of 51 mm, while second size had diameter of 10 mm and length of 76 mm. Experiments included tests with single and groups of four firebrands. It was found that increasing the number of deposited glowing firebrands led to an increased likelihood of ignition when all other factors were held constant. Increasing firebrand size and wind speed also led to increased ignition [12]. In another similar study, also by Manzello et. al., ponderosa pine disks were used for firebrands [13]. The authors point out that compared with disks, approximately half the mass of cylindrical Douglas fir firebrands are required to cause ignition under identical conditions [12].

Filkov et al. [34] investigated the effects of firebrand size, firebrand quantity, and wind speed on the ignition of pine needle beds at 9.3% moisture content. The firebrands were made from pine bark 5mm thick with lengths and width dimensions of 10 x 10, 15 x 15, 20 x 20, 25 x 25, and 30 x 30 mm depending on the experiment. Firebrand quantity ranged from 1 to 10, and wind speed was varied between 0 and 3 m/s. It was found that the ignition of the fuel beds depended on the size and quantity of firebrands, with ignition being more likely with a greater quantity of large firebrands. For a given firebrand size and quantity, the likelihood of ignition increased with wind speed [34].

Two separate studies investigated the ignition of recipient fuels by firebrand piles based on the geometric configuration of the piles and the substrate. Santamaria et al. used slices of bark to assess ignition on flat and angled (120°) configurations and concluded that ignition depends on pile mass [35]. Manzello, Park, and Cleary [6] also looked at the effect of configuration using plywood and oriented strand board with ponderosa pine firebrands. The size of a crevice between two boards was varied by changing the crevice angle. Results show that there was an interplay between configuration, wind, and mass/number of firebrands. Generally, the likelihood of ignition increased with increasing wind speed and decreasing crevice angle [6].

The studies mentioned so far have mainly relied on binary observation data to assess heat transfer from firebrand piles (i.e. the pile did or did not cause ignition under certain conditions). Hakes et al. [7] were some of the first to characterize the heat transfer from firebrand piles. Heat flux data was taken with both a 1.27 cm water-cooled heat flux gauge (WC-HFG) and an array of thin-skin calorimeters (TSC). The TSC's were used to resolve the distribution of heat flux across the surface area but suffered from poor spatial resolution (1.5 cm). All firebrands used in this study were 25 mm long, with diameters of 6.35, 9.5, and 12.7 mm. Deposited piles masses ranged from 0.1 to 9.6 g, and cases with and without wind were tested. It was found that for a given firebrand diameter, increasing the pile mass resulted in increased heat flux and duration. Additionally, it was found that if two piles had the same mass, the diameter of the firebrands within the piles made little difference on the recorded heat flux, a finding at odds with previous studies which point to firebrand geometry as an important parameter [12]. It was also found that

wind substantially increased the heat flux from the firebrand pile but shortened the burning duration [7]. Bearinger et al. conducted a similar study where heat fluxes were measured at a high resolution (0.4 mm x 0.4 mm) using inverse heat transfer with infrared thermography [36]. The authors' observed local heat fluxes significantly higher than the critical heat fluxes for many building materials in single firebrand configurations which were not expected to cause ignition from previous studies.

Tao et al. [37] further investigated the effects of firebrand size and geometry on heat transfer from piles of firebrands. In this study, a combination of firebrands collected from natural vegetation and those made from commercially available materials such as dowel rods were used. Piles were subjected to 0.5 – 1.4 m/s winds in a wind tunnel and heat flux measurements were again taken using a water-cooled heat flux gauge and TSC array. It was noted that based on the type of firebrand, piles exhibited differing bulk densities (i.e. some piles were more porous). The pile porosity was found to have a significant impact on the measured heat transfer, but there are likely competing effects between oxygen availability and reradiation within the pile. There also appeared to be a difference in the heat transfer from piles made with natural firebrands compared with those made from dowel rods. As found in all previous studies, increasing wind led to increased heat flux [37].

It is apparent that there are many factors that could potentially affect the heat transfer from firebrand piles. Some of these factors such as pile mass, wind speed, firebrand size, and whether the firebrand is made from natural or processed wood have been at least partially explored in previous work. Other factors such as wood moisture content and density have received little attention. The goal of this work is to test the effect of as many independent factors as possible and statistically evaluate their importance. It must be noted that some factors, such as pile mass and number of firebrands for a given firebrand shape, are not independent and therefore cannot be separately investigated. Additionally, this work employs a rigorous statistical framework used to evaluate whether there is a significant difference between the different factors. This work explores the effect of eight factors including wood moisture content, wood type (hardwood or softwood), wood density, wood state (live, dead, or artificial), wind speed, pile mass, firebrand diameter, and firebrand length on the heat transfer from firebrand piles.

3.2. EXPERIMENTAL METHODS

A series of experiments were conducted using a custom testing apparatus to investigate the effects of the wood moisture content, wood type (hardwood or softwood), wood density, wood state (live, dead, or artificial), wind speed, pile mass, firebrand diameter, and firebrand length on the heat transfer from firebrand piles. High resolution heat transfer measurements from the firebrand piles were collected through time by a method of inverse heat transfer (IHT) using thermographs from an infrared (IR) camera. These results were then statistically analyzed to determine the significance of the various factors. Details of the experiments and analysis are described in the following sections.

3.2.1. Experimental Setup

3.2.1.1. Testing Apparatus

A custom experimental apparatus was developed for this testing (shown in Figure 13) consisting of a wind tunnel, support structure, two infrared cameras, an RGB camera, a wire mesh cage, and a black 304 stainless steel plate. The wind tunnel is 2.4 m long by 0.31 m wide with a flow-conditioning section in the middle. The wind tunnel exit is 0.31 m wide and 0.10 m high with a

uniform flow across 90% of the opening. The flow through the tunnel is driven by an American Fan Company AF-8 blower, controlled by a 1 hp, 3-phase AC motor and a Reliance Electric SP500 variable speed drive. The maximum flow rate for the tunnel is 3.5 m/s corresponding to volumetric flow rate of 0.106 m^3/s (225 cfm).

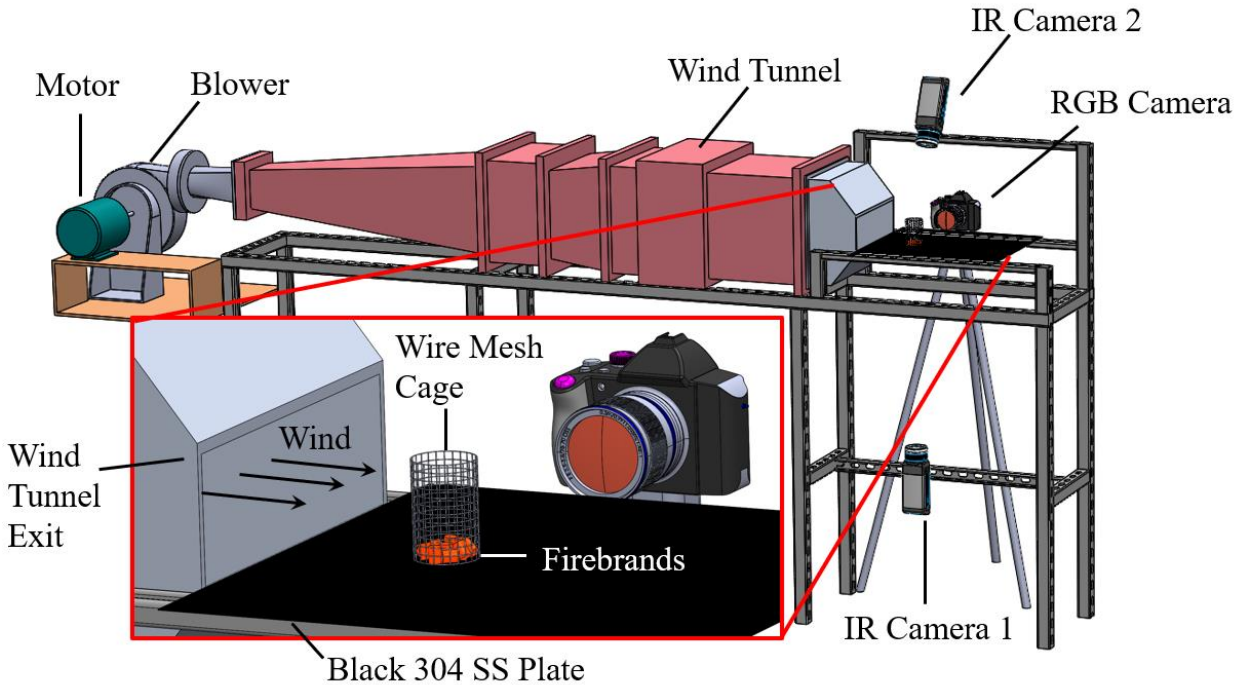

Figure 13. Test apparatus used to evaluate heat transfer from firebrand piles under various conditions. Note image insert contains close view of measurement area.

The firebrand piles were supported on a 304 stainless steel plate having dimensions 457 mm x 457 mm x 0.762 mm. The plate was painted black on both sides using Rust-oleum™ High Heat black enamel paint. The paint thickness was approximately 20 μm and has been shown by Cholewa et al. to have an emissivity of $\varepsilon = 0.97$ [20]. The plate was clamped to the support structure and carefully leveled such that the top face of the plate aligned with lower edge of the wind tunnel exit. A thin piece of aluminum tape (not pictured in Figure 13) connected the inside of the wind tunnel exit to the top side of the plate, ensuring no wind reached the underside of the plate.

Two FLIR A655sc infrared (IR) cameras were used in the testing and controlled by ResearchIR™ acquisition software. The A655sc cameras record in the longwave infrared spectrum (7.5-14.0 μm), have 640 x 480 pixel resolution, and both used 25° lenses. Both cameras recorded at 3.13 Hz, with the data being down-sampled to 0.28 Hz post-process. IR Camera 1 was used to measure the temperature on the underside of the stainless steel plate. IR Camera 1 was operated in the 100-650 °C mode with an emissivity equal to that of the plate ($\varepsilon = 0.97$) and was positioned 0.648 m below the bottom surface of the plate meaning each pixel corresponded to a 0.44 mm x 0.45 mm rectangular area on the plate's surface. IR Camera 2 was placed at a distance of 0.37 m from the pile center and was used to measure firebrand temperature. IR Camera 2 was operated in the 300-2000 °C mode with an emissivity of $\varepsilon = 0.9$ assumed for the firebrands. Additionally, a Nikon D3200 SLR camera (RGB Camera in Figure 13) recorded video of the burning pile in the visible spectrum. IR Camera 2 and the RGB Camera provided

qualitative information about the burning of the pile. Plate temperature data from IR Camera 1 was used for the inverse heat transfer calculations.

Firebrand piles have been observed to accumulate on flat surfaces with external wind and remain in a pile due to the larger surrounding pile preventing them from moving [10]. To quantify the heat flux from small piles of firebrands, the firebrands in this study were placed inside a lightweight cage made of steel mesh with dimensions shown in Figure 14. In addition to keeping the firebrands from prematurely blowing off the plate, the cage helped the pile maintain a circular shape with diameter of 50 mm. The 6.3 mm by 6.3 mm gridding was sufficiently porous to allow wind to access the pile while still securing small firebrands.

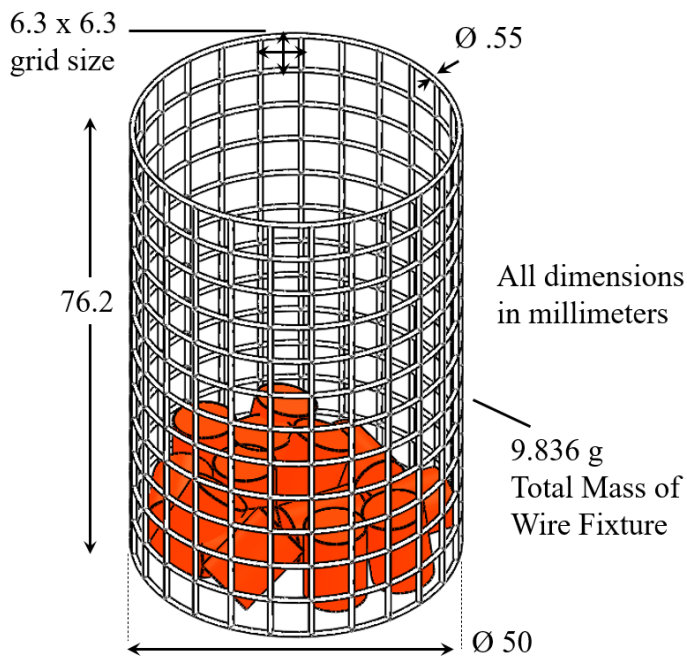

Figure 14. Galvanized steel wire cage used to constrain firebrand piles (shown in red)

3.2.1.2. Inverse Heat Transfer

Inverse heat transfer (IHT) analysis is the method through which the stainless steel plate temperature measurements recorded with IR Camera 1 are used to calculate heat flux from the firebrands onto a horizontal surface. The advantage of this method is that heat flux measurements can be resolved with the same spatial and temporal resolution as recorded by the infrared camera.

The IHT method using infrared images was originally developed by Rippe and Lattimer [19] and relies on a thermally-thin interstitial medium (in this case the black 304 SS plate) of known optical and thermal properties between the infrared camera and the heat source. The infrared camera is used to obtain a series of 2D temperature measurements of the unexposed side of the plate through time. Each pixel recorded by the camera corresponds to a small, discrete area on the plate and a known temperature. By knowing each temperature value through time and ambient conditions, an energy balance can be conducted on every pixel to obtain a temporally-resolved 2D heat flux map.

The net heat flux to each pixel, q''_{exp}, is the combined flux from all modes of heat transfer on the exposed side of the plate and is determined by an energy balance on the pixel

$$q''_{exp} = q''_{stor} - q''_{cond} + q''_{rad,b} + q''_{conv,b} \tag{1}$$

where q''_{stor} is rate of energy storage, q''_{cond} is the conduction flux into the pixel of interest from its neighbors, and $q''_{rad,b}$ and $q''_{conv,b}$ are the radiation and convection fluxes from the plate's unexposed surface.

The storage term depends on the thermal properties of the plate material and the pixels time rate of temperature change

$$q''_{stor} = \frac{\rho V C_p}{A}\frac{dT_s}{dt} \tag{2}$$

In Eqn. (2), $\rho = 7{,}900\ kg/m^3$ is the density of the plate, V and A are the volume and surface area of a discrete pixel element, respectively, and $C_p = 515\ J/kg\ \cdot K$ is the specific heat capacity of the plate material. The calculation of the storage term also depends on the time rate of surface temperature change for the given pixel, dT_s/dt. Since the plate is assumed to be thermally thin, the entire pixel element is assumed to be at T_S.

As the plate temperature increases, the true net heat flux from the firebrand pile to the plate will decrease as the temperature difference is minimized. For this reason, it is convenient to express the measured heat transfer as the heat flux that would be experienced by a surface maintained at a standard temperature of 20 °C (293K). This is also equivalent to the heat flux that would be measured with a water-cooled heat flux gauge. This heat flux at the standard temperature, q''_0, is calculated using

$$q''_0 = q''_{exp} + \varepsilon\sigma(T_s^4 - 293^4) + h_f(T_s - 293) \tag{3}$$

where h_f is the convective heat transfer coefficient of the exposed side of the plate. All heat flux values presented in this work are the heat flux at standard temperature, q''_0, as described in Eqn. (3).

The convective heat transfer coefficients, h_f, used in the analysis was determined using the Nusselt number, $\overline{Nu}_L$, the thermal conductivity of air, k_f, and the hydraulic length of the heated section, L.

$$h_f = \frac{\overline{Nu}_L k_f}{L} \tag{4}$$

For calculations on the top of the plate, the hydraulic length, L, is simply the distance of the pile center from the leading edge of the plate (shown in Eqn. (5)). For calculations of the natural convection on the underside of the plate, L is found using Eqn. (6)

$$L = 0.0256\ m \text{ for top of plate} \tag{5}$$

$$L = A_s/P \text{ for bottom of plate} \tag{6}$$

where A_s is the surface area of the plate (m^2) and P is the perimeter (m).

The calculation of the Nusselt number itself depends on whether wind is applied during the test, and differs for the top and bottom sides of the plate. For tests with wind applied to the firebrands, the Nusselt number on the top of the plate was calculated using forced convection relationships from Incropera et al. [24] which depend on the Reynolds number, Re_L, at the pile location

$$\overline{Nu}_L = 0.037 Re_L^{4/5} Pr^{1/3} \text{ for } (Re_L \geq 5 \times 10^5) \tag{7}$$

$$\overline{Nu}_L = 0.664 Re_L^{1/2} Pr^{1/3} \text{ for } (Re_L \leq 5 \times 10^5) \tag{8}$$

where $\mathrm{Pr} = 0.72$ was used for all tests.

The Reynolds number, Re_L, was calculated using

$$Re_L = \frac{UL}{v} \tag{9}$$

where U is the flow velocity, and $v = 15.06 \times 10^{-6}\ m^2/s$ is the kinematic viscosity of air at 293K.

For natural convection on the top surface of the plate in cases with no external wind applied, the Nusselt number was found using Eqn. (10) or (11) from Lloyd and Moran [38]

$$\overline{Nu}_L = 0.54 Ra_L^{1/4} \text{ for } (10^4 \leq Ra_L \leq 10^7) \tag{10}$$

$$\overline{Nu}_L = 0.15 Ra_L^{1/3} \text{ for } (10^7 \leq Ra_L \leq 10^{11}) \tag{11}$$

where Ra_L is the Rayleigh number calculated by

$$Ra_L = \frac{g\beta(T_s - T_\infty)L^3}{v\alpha} \tag{12}$$

where g is the acceleration due to gravity, β is the thermal expansion coefficient, T_∞ is the ambient air temperature, v is the kinematic viscosity, α is the thermal diffusivity, and L is the hydraulic length of the heated section. All properties were taken to be values at ambient temperature.

The underside of the plate was never exposed to forced convection due to external wind, so the Nusselt number for the underside of the plate used in all tests was determined using the following natural convection correlation from [24]

$$\overline{Nu}_L = 0.27 Ra_L^{1/4} \text{ for } (10^5 \leq Ra_L \leq 10^{10}) \tag{13}$$

The above approach was previously verified for measuring heat transfer at this scale over the range of heat fluxes expected for firebrand piles [36]. All properties were taken to be values at ambient temperature.

3.2.1.3. Experimental Procedure

The details pertaining to each separate experiment will be discussed in the following sections. Unless otherwise stated, the wood used to make the firebrands was harvested from living trees in the Eastern United States. A single tree of each species provided wood for all tests to reduce

variability. To make the unburned firebrands, tree branches were cut to length using a bandsaw and bark was left intact. The length tolerance for firebrands was +/- 0.5 mm relative to the reported lengths in Table 3. Due to imperfections in the natural samples, some variability existed in the diameter of the firebrands. A diameter tolerance of +/- 1 mm was specified and samples not within this window were discarded. Prior to testing, the firebrands were dried to 0% moisture content (MC) by storing them in a thermal chamber at 75°C, for several days. It was confirmed that this time and temperature was sufficient to bring the samples to <0.3% MC.

Prior to each test, the metal cage shown in Figure 14 was centered 127 mm from leading edge of the 304 SS plate. For tests with wind, the wind tunnel was started and the wind speed inside the metal cage was verified using an Extech Hot Wire Thermo-Anemometer with 0.1 m/s resolution. A custom funnel was placed on top of the cage to facilitate firebrand placement. Initially it was found that during tests with wind, the firebrands were blown to the trailing edge of the cage during the placement process. For this reason, a wind shield was added in front of the cage during the setup and removed at the start of testing. Data acquisition using the IR and RGB cameras was started prior to the heating of the firebrand pile.

To make the firebrand pile, a carefully measured mass of unburned firebrands was heated in a wire mesh basket over a propane flame. Heating times and initial masses of unburned firebrands are recorded in the following sections. Once the firebrands reached a state of self-sustaining flaming combustion, the propane was turned off. The firebrands were allowed to flame and transition to smoldering combustion while the mass was monitored using a Sartorius FB6CCE-S scale with 0.1 g resolution. Once the total mass of the firebrands reached the desired deposited mass, the glowing firebrands were poured into the funnel and allowed to fall randomly within the cage. The funnel and wind shield were removed, and the firebrand pile burned unhindered until the peak temperature within the pile dropped below 100°C, at which point the test was ended. The firebrand piles left some residue on the plate during burning, so no more than two tests were conducted on the same plate.

3.2.2. Design of Experiments

A series of five separate experiments were designed to evaluate the effects of the eight chosen factors on the heat transfer from firebrand piles, see Table 3. For each factor, a high and a low level were chosen. These high and low values were chosen to represent the extremes that would likely be seen in a realistic wildfire scenario, but in some cases were subject to constraints of the experimental setup. Four completely randomized experimental designs (CRDs) were used to independently assess the main effects of wood moisture content, wood type, wood density, and wood state on the heat transfer from firebrand piles. A full factorial design was then used to evaluate the main effects and all interactions of pile mass, wind speed, firebrand diameter, and firebrand length.

Table 3. Experiments used to evaluate the effect of eight factors on heat transfer from firebrand piles

Test Name	Experiment Design	Factor Levels	Wind Speed (m/s)	Firebrand Wood Material	Firebrand Sizes (L x D) (mm)
Moisture Content Study	Completely Randomized Design	0%, 25%	2.0	N. Red Oak	(12.5 x 9.50)
Wood Type Study	Completely Randomized Design	Hardwood, Softwood	2.0	Yellow Poplar, E. White Pine	(12.5 x 9.50)
Density Study	Completely Randomized Design	548, 870 kg/m3	2.0	Yellow Poplar, N. Red Oak	(12.5 x 9.50)
Wood Mode Study	Completely Randomized Design	Natural - Live, Natural - Dead, Artificial	2.0	N. Red Oak	(12.5 x 9.50)
Full Factorial Study	Full Factorial Design	Pile Mass: 1.5, 3.0 g Wind Speed: 0.0, 2.0 m/s Firebrand Diameter: 4.75, 9.50 mm Firebrand Length: 12.5, 50.0 mm	0.0 or 2.0	N. Red Oak	(12.5 x 4.75) (12.5 x 9.50) (50.0 x 4.75) (50.0 x 9.50)

3.2.2.1.Moisture Content Study

To assess the impact of starting moisture content on the heat transfer from firebrand piles, a CRD experiment was designed with two moisture content levels (0% and 25%) as shown in Table 4. One replication was conducted per treatment for a total of four experiments. Prior to heating, all the firebrands used in this study had length of 12.5 mm, diameter of 9.5 mm, and were made from live N. Red Oak ($\rho = 870\ kg/m^3$) branches. A wind speed of 2.0 m/s was used for all tests. To reduce experimental bias, tests were run in a random order. The moisture content was calculated using

$$MC = \frac{(m - m_{dry})}{m_{dry}} \times 100 \qquad (14)$$

where m is the mass and m_{dry} is the dry mass. The moisture content was assessed on the pile level. Initially, all firebrands were dried to 0% MC. Firebrands used for the 25% MC tests were rehydrated by storing them in an airtight container filled with damp cloth. The firebrands were turned frequently to ensure even saturation and the total mass was checked periodically until the pile reached the desired moisture content. The rehydration process typically took 24-27 hours.

The test details are provided in Table 4. The piles at 25% MC had to be heated substantially longer to reach self-sustaining combustion, which was attributed to the fact that more energy was

required to also drive off the moisture in the wood before ignition would occur. The number of wood samples used in the testing was determined by preserving the initial mass of wood. The deposited mass is the mass of smoldering firebrands deposited onto the plate and was constant in all tests.

Table 4. Test matrix used to assess the effect of starting moisture content on the heat transfer from firebrand piles.

Test	Pile Moisture Content (%)	Heating Time (s)	Initial Firebrand Count	Initial Wood Mass (g)	Deposited Pile Mass (g)
Test 1	0	30	33	22.0	3.1
Test 2	0	30	36	21.8	3.1
Test 3	25	75	27	22.2	3.0
Test 4	25	75	28	22.4	2.9

3.2.2.2. Wood Type Study

Differences exist in the basic cellular structure of hardwoods and softwoods. These differences include the presence of wood fibers and vessels in hardwoods, making them porous, and an abundance of tracheid cells in softwoods [39]. To explore the effect of firebrand wood type on the heat transfer from firebrand piles, a CRD study was designed. To have similar densities between treatments, Yellow Poplar ($\rho = 548\ kg/m^3$) was selected for the hardwood and E. White Pine ($\rho = 586\ kg/m^3$) was selected for the softwood. Prior to heating, all the firebrands used in this study had a length of 12.5 mm, diameter of 9.5 mm, and were made from live branches dried to 0% MC. A wind speed of 2.0 m/s was used for all tests. As shown in Table 5, each factor was repeated in duplicate yielding four total tests with tests run in a randomized order. The number of wood samples used in the testing was determined by preserving the initial mass of wood. The deposited mass is the mass of smoldering firebrands deposited onto the plate and was constant in all tests.

Table 5. Test matrix used to assess the effect of firebrand wood type on the heat transfer from firebrand piles.

Test	Wood Type	Heating Time (s)	Initial Firebrand Count	Initial Wood Mass (g)	Deposited Pile Mass (g)
Test 1	Hardwood	30	49	21.9	3.0
Test 2	Hardwood	30	50	22.1	3.0
Test 3	Softwood	30	44	22.1	3.1
Test 4	Softwood	30	45	22.1	3.1

3.2.2.3. Density Study

The effect of firebrand wood density on pile heat transfer has received little attention in the literature. To evaluate the impact of this parameter, a CRD using Yellow Poplar ($\rho = 548\ kg/m^3$) and N. Red Oak ($\rho = 870\ kg/m^3$) was conducted. Both Yellow Poplar and N. Red Oak are hardwoods. As before, firebrands used in this study had length of 12.5 mm, diameter of 9.5 mm before heating, and were made from live branches dried to 0% MC. A wind speed of 2.0 m/s was used for all tests. Each factor was repeated in duplicate, yielding four total tests as shown in Table 6 performed in randomized order. The initial wood mass and deposited pile mass were kept constant during the testing.

Table 6. Test matrix used to assess the effect of firebrand wood density on the heat transfer from firebrand piles.

Test	Wood Density (kg/m³)	Heating Time (s)	Initial Firebrand Count	Initial Wood Mass (g)	Deposited Pile Mass (g)
Test 1	548	30	49	21.9	3.0
Test 2	548	30	50	22.1	3.0
Test 3	870	30	32	22.3	3.1
Test 4	870	30	32	22.1	3.0

3.2.2.4. Wood State Study

Much of the previous work in the field of firebrand research has used dowels or other commercially-available processed woods to simulate firebrands naturally occurring in wildfires. These “artificial” firebrands typically lack bark, have very consistent sizes, and are made from wood harvested from the trunk of trees instead of the branches. It is unclear how well these artificial firebrands simulate natural results. Tao et. al. [37] has reported some differences in heat transfer between piles made with natural and artificial firebrands. For cases using natural firebrands, a difference may also exist between firebrands made from living or dead wood.

To explore the effect of firebrand wood state (live, dead, artificial), a CRD experiments was conducted with three levels of a single factor. Each factor was replicated for a total of six tests, shown in Table 7. The unburned live ($\rho = 870\ kg/m^3$) and dead ($\rho = 664\ kg/m^3$) firebrands were collected from different branches of the same N. Red Oak tree in early autumn when it was easy to distinguish between live and dead tree limbs. The unburned artificial firebrands ($\rho = 627\ kg/m^3$) were cut from commercially available N. Red Oak dowel rods. All firebrands used in this study had length of 12.5 mm, diameter of 9.5 mm prior to heating, and were dried to 0% MC. A wind speed of 2.0 m/s was used for all tests with a randomized run order. The wood mass and applied firebrand mass were kept constant in the study.

Table 7. Test matrix used to assess the effect of firebrand wood mode on the heat transfer from firebrand piles.

Test	Wood Mode	Heating Time (s)	Initial Firebrand Count	Initial Wood Mass (g)	Deposited Pile Mass (g)
Test 1	Artificial	30	33	22.0	3.1
Test 2	Artificial	30	33	22.0	3.1
Test 3	Natural - Live	30	32	22.1	3.2
Test 4	Natural - Live	30	33	21.9	3.1
Test 5	Natural - Dead	30	40	22.2	3.2
Test 6	Natural - Dead	30	40	21.9	3.1

3.2.2.5. Full Factorial Study

The previously described experiments have examined the effect of a single factor with different levels. While the main effects associated with each factor are important, the interaction between factors may be significant as well and cannot be evaluated using single-factor CRDs. Recent studies have pointed to a complex influence of pile mass, pile bulk density, and wind speed on the heat transfer from firebrand piles [7], [37]. Pile bulk density is related to pile porosity or the percentage of the pile volume occupied by gases instead of smoldering firebrands. Porosity is of particular interest due to its effect on oxygen availability and reradiation within the pile.

The porosity can be attributed to the packing density of the cylindrical firebrands which has been shown to depend on the aspect ratio ($AR = L/D$) and thus the firebrand length and diameter [40], [41]. To capture the complexity of this interactions, the effects of pile mass, wind speed, firebrand diameter, and firebrand length were evaluated in a 2^k full factorial experiment. A high and low level were chosen for each factor and all possible combinations of factor levels were evaluated. The addition of a center point (combination of average levels for each factor) brought the number of tests to 17. The complete test matrix can be found in Table 8. All firebrands used in this study were cut from live N. Red Oak branches and dried to 0% MC. The run order of the experiments was randomized. Due to the time required to run the full factorial test matrix, replication was not feasible.

Table 8. Full-factorial test matrix used to assess the effect of unburned firebrand length and diameter, pile mass, and wind speed on the heat transfer from firebrand piles.

Test	Unburned Firebrand Length (mm)	Unburned Firebrand Diameter (mm)	Pile Mass (g)	Wind Speed (m/s)	Heating Time (s)	Initial Firebrand Count	Initial Wood Mass (g)	Actual Deposited Pile Mass (g)
Test 1	12.50	4.75	1.50	0.0	12	65	11.0	1.6
Test 2	50.00	4.75	1.50	0.0	15	14	11.3	1.6
Test 3	12.50	9.50	1.50	0.0	15	17	11.0	1.6
Test 4	50.00	9.50	1.50	0.0	30	4	11.0	1.6
Test 5	12.50	4.75	3.00	0.0	30	126	22.1	3.0
Test 6	50.00	4.75	3.00	0.0	30	29	22.0	2.9
Test 7	12.50	9.50	3.00	0.0	30	35	22.2	3.1
Test 8	50.00	9.50	3.00	0.0	30	8	22.2	3.1
Test 9	12.50	4.75	1.50	2.0	15	60	11.1	1.4
Test 10	50.00	4.75	1.50	2.0	15	15	11.1	1.6
Test 11	12.50	9.50	1.50	2.0	15	17	11.0	1.6
Test 12	50.00	9.50	1.50	2.0	30	4	11.0	1.6
Test 13	12.50	4.75	3.00	2.0	30	127	22.0	3.0
Test 14	50.00	4.75	3.00	2.0	30	28	21.9	2.9
Test 15	12.50	9.50	3.00	2.0	30	33	22.3	3.1
Test 16	50.00	9.50	3.00	2.0	30	8	22.6	3.2
Test 17	31.25	7.13	2.25	1.0	22.5	16	16.4	2.3

3.2.3. Analysis

Additional analysis was conducted on the data to quantify the local heat flux values for each test and provide sufficient data to perform the DOE statistical analysis.

3.2.3.1. Data Processing

The infrared images from IR Camera 1 were used to generate high resolution maps of the heat flux through time. Each pixel corresponded to a 0.44 mm × 0.45 mm area on the underside of the 304 SS plate. Since the pile diameter was 50 mm there were ~9,900 pixels per image

representing a discrete location under the pile. While this high spatial resolution is valuable for visualizing the distributed heat fluxes under the pile, it is unlikely that the ~0.5 mm length scale is relevant to ignition. High heat flux into a single 0.44 mm × 0.45 mm surface element would quickly dissipate through lateral conduction if the surrounding material were at a lower temperature. Conversely, taking the average flux under the entire pile with time would dilute higher measured values and may under-predict ignition.

To remedy this length-scale issue, the pixels under each pile were divided into twenty-nine 6.6 mm × 6.75 mm (15 × 15 pixel) grids that were totally within the pile boundaries, as shown in Figure 15. The grid array was centered on the pile and grids lying even slightly outside the pile were not considered. This produced 29 different time-temperature heat flux plots. However, the statistical evaluation required a single value for each test and so the heat fluxes from these twenty-nine grid values had to be distilled into a single metric. For each grid location, the average heat flux over the initial 120 s of the firebrand exposure was used to represent grid heat flux. This 120 s averaging time was based on a review of the temporal heat flux data, where the highest heat fluxes most often occurred in the initial 120 s. In order to reduce the 29 average heat fluxes to a single value for the statistical analysis, the 75th percentile of all of the heat fluxes in the pile was used (i.e., which is the heat flux where 75% of the 29 measured heat fluxes in the pile were less than this value). The end goal of this research is to relate these heat fluxes to the ignition of building materials. As a result, this higher heat flux value was selected to assess where the most severe exposures would for a given firebrand pile.

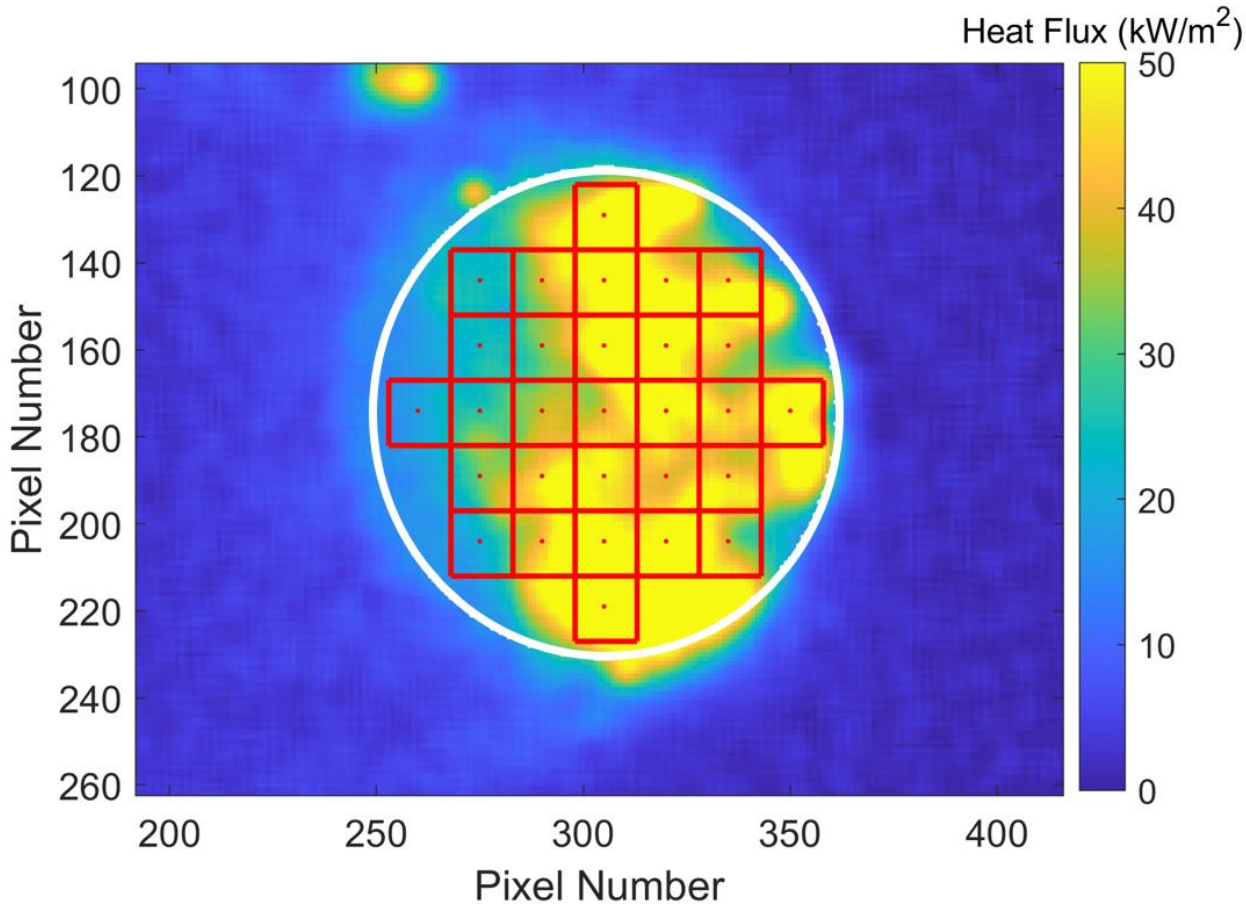

Figure 15. 6.6 mm × 6.75 mm grids (shown in red) lying totally within the bounds of the 50 mm circular pile (shown in white)

3.2.3.2. Statistical Analysis

Three different experimental designs were used in these studies: one-factor CRDs with two treatment levels, one-factor CRD's with three treatment levels, and full factorial designs. For all cases, the objective of the statistical analysis was to determine whether the factor in question significantly affected the heat transfer from firebrand piles.

3.2.3.2.1. CRD Experiments with Two Treatment Levels

The analysis of the CRD experiments with two treatment levels (Moisture Content Study, Wood Type Study, and Density Study) was conducted using one-way analysis of variance (ANOVA) to assess whether there was a statistically significant difference in the mean, μ, of the two treatment levels. Analysis was conducted using Minitab v.19 software at the 95% confidence level ($\alpha = 0.05$) and equal variance was assumed between groups. The null hypothesis, H_0, was that there was no significance between μ_1 and μ_2 and was rejected for p-values < 0.05. Factors where the null hypothesis were rejected were assumed to have an effect on the heat transfer from firebrand piles. The null and alternate (H_a) hypotheses are

$$H_0: \mu_1 = \mu_2 \,; H_a: \mu_1 \neq \mu_2 \tag{15}$$

3.2.3.2.2. CRD Experiments with Three Treatment Levels

For the CRD experiment with three treatment levels (Wood State Study), Fisher's Least Significant Difference (LSD) method was chosen to conduct the pairwise comparison on the categorical treatment level means (μ_1, μ_2, μ_3) in Minitab v.19. Fisher's method is essentially a set of individual t tests but uses the pooled standard deviation and is more powerful than conservative techniques such as Tukey's method. The Type I error rate is set for each individual contrast and does not take into account that the same data is used for multiple comparisons. A 95% confidence level was specified for each of the individual contrasts, meaning that the simultaneous confidence level for the comparison as a whole was 90.17%. The null and alternate hypotheses for the CRD with three treatment levels are

$$H_0: \mu_1 = \mu_2 = \mu_3 \,; H_a: At\ least\ one\ mean\ significantly\ different \tag{16}$$

3.2.3.2.3. Full Factorial Design

The full factorial design was a 2^k experimental structure that evaluated the main effects and all interactions of wind, pile mass, firebrand diameter, and firebrand length. A main effect was defined as the effect on the heat transfer from the firebrand pile caused by one of the four independent variables (e.g. heat transfer increased with increasing wind). An interaction was defined as a relationship where the effects of one independent variable on the heat transfer from the firebrand pile depended on the level of another independent variable (i.e. wind affects heat transfer from firebrand piles differently for different firebrand sizes). Four-way analysis of variance (ANOVA) was used to assess whether each main effect or interaction had a significant effect on the pile heat transfer. For each term, the null hypothesis was that there was no effect; p-values < 0.05 indicated that the null hypothesis should be rejected, and the term significantly impacted the pile heat transfer. The center point was not included in the model.

3.3. RESULTS

The results from the statistical analysis of the experimental data are presented in the following subsections.

3.3.1. Data Overview

The data for the tests consisted of the average flux within each grid at every point in time. Figure 16 shows the grid average flux with time for each of the twenty-nine grids in Full Factorial Test 15. This plot illustrates a trend that is seen in much of the data where the test was characterized by high initial fluxes that decreased with time. The average flux value for each grid was calculated for the first 120s of the test, resulting in twenty-nine individual values with distributions like those shown in Figure 17. From these distributions, the 75th percentile 120s-average grid flux was selected and used as the metric for the test statistics. This value is shown in red in Figure 17.

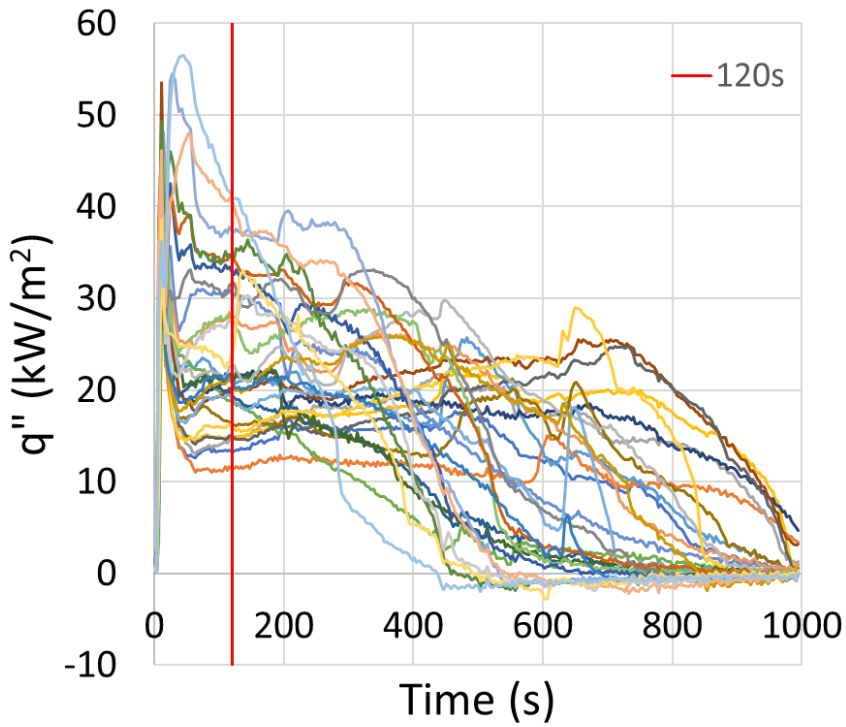

Figure 16. Grid heat flux values through time for example test. Vertical red line indicates the 120 s mark.

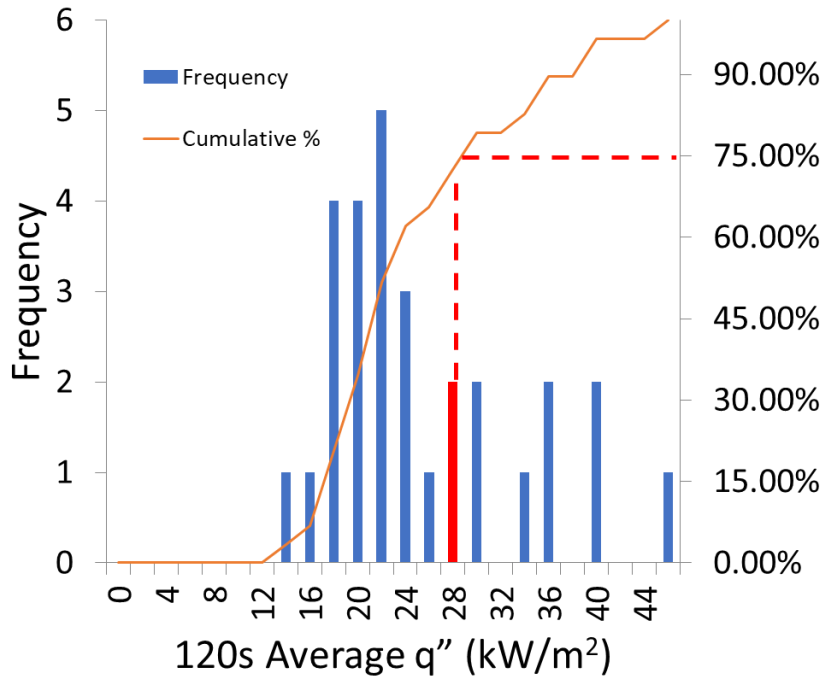

Figure 17. Histogram of 120s averages for each of twenty-nine grids within a test. 75th percentile heat flux value is shown in red.

3.3.2. Moisture Content Study

The effects of starting moisture content of the unburned firebrands were statistically analyzed using the one-way ANOVA. The results are summarized in Table 9. Piles made from firebrands with a starting moisture content of 0% were found to have a mean heat flux of 33.42 kW/m^2, while piles made from firebrands with 25% starting MC were found to have a mean heat flux of 38.81 kW/m^2, a difference of 5.39 kW/m^2. The p-value of 0.075, indicates that this difference does not meet the threshold for statistical significance and there is a >5% chance of observing a difference at least this large assuming the null hypothesis is true. For this reason, the null hypothesis could not be rejected, and it was concluded that firebrand starting moisture content does not have a significant effect on firebrand pile heat transfer. This result was somewhat expected since the moisture was believed to be driven off during burning to form the firebrand.

Table 9. Summary of the statistical analysis of the effect of starting moisture content of unburned firebrands on the heat transfer from firebrand piles.

%MC	Mean (kW/m^2)	σ (kW/m^2)	N	Hypotheses	p-value	Conclusions
0%	33.42	1.93	2	$H_0: \mu_1 = \mu_2$	0.075	Fail to reject H_0. Starting moisture content does not affect heat transfer from firebrand piles
25%	38.81	1.07	2	$H_a: \mu_1 \neq \mu_2$		

The interval plot for the moisture content study is shown in Figure 18. The heat flux value shown on the y-axis is the 75th percentile of 120 s average for grids within each group. The central black marker shows the mean while the interval bars show the extent of the 95% confidence interval for each group. The 95% confidence interval denotes the range of values which have a 95% chance of including the true population mean for that group. Due to the limited number of samples for each group, the interval plot was generated using the pooled standard deviation ($\sigma_{pooled} = 1.565$) for all four tests in the moisture content study. The significant overlap in the 95% confidence intervals for the 0% and 25% MC show why it was not possible to reject the null hypothesis for this study.

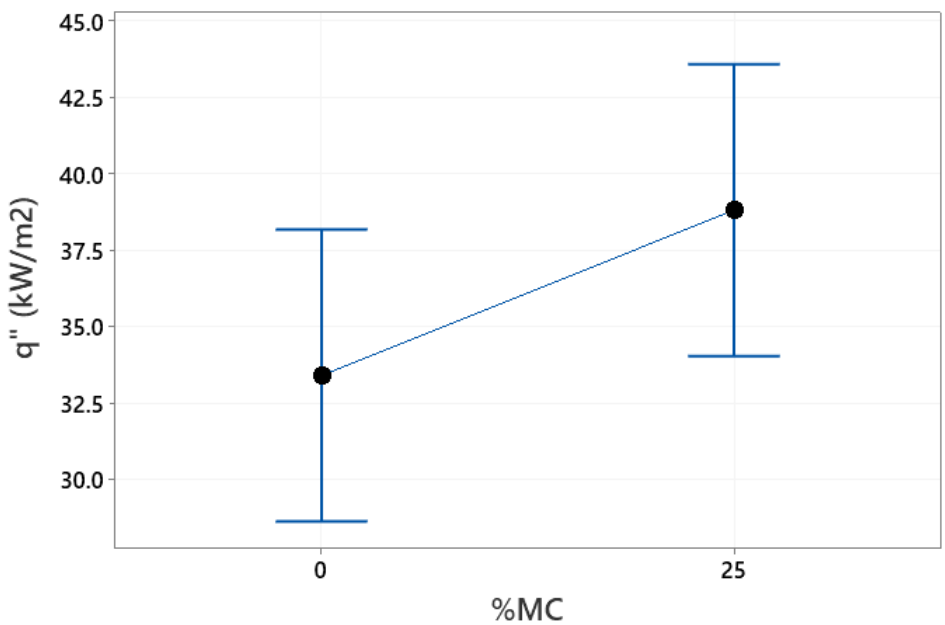

Figure 18. Interval plot showing the 95% CI for each group in the moisture content study.

3.3.3. Wood Type Study

One-way ANOVA was used to evaluated whether there was a significant difference in heat transfer from firebrand piles made with firebrands from hardwood and softwood branches. Summary of the results can be found in Table 10 while the interval plot is shown in Figure 19. The mean heat flux from firebrand piles made with hardwood firebrands was found to be 39.27 kW/m^2, while the mean for the piles with softwood firebrands was 45.35 kW/m^2. The difference of 6.08 kW/m^2 and resulting p-value of 0.346 means the null hypothesis could not be rejected. It was therefore concluded that firebrand wood type does not significantly affect heat transfer from firebrand piles. As before, the interval plot was generated using the pooled standard deviation ($\sigma_{pooled} = 4.970$).

Table 10. Summary of the statistical analysis of the effect of firebrand wood type on the heat transfer from firebrand piles.

Wood Type	Mean (kW/m^2)	σ (kW/m^2)	N	Hypotheses	p-value	Conclusions
Hardwood	39.27	2.93	2	$H_0: \mu_1 = \mu_2$	0.346	Fail to reject H_0. Wood type does not affect heat transfer from firebrand piles
Softwood	45.35	6.39	2	$H_a: \mu_1 \neq \mu_2$		

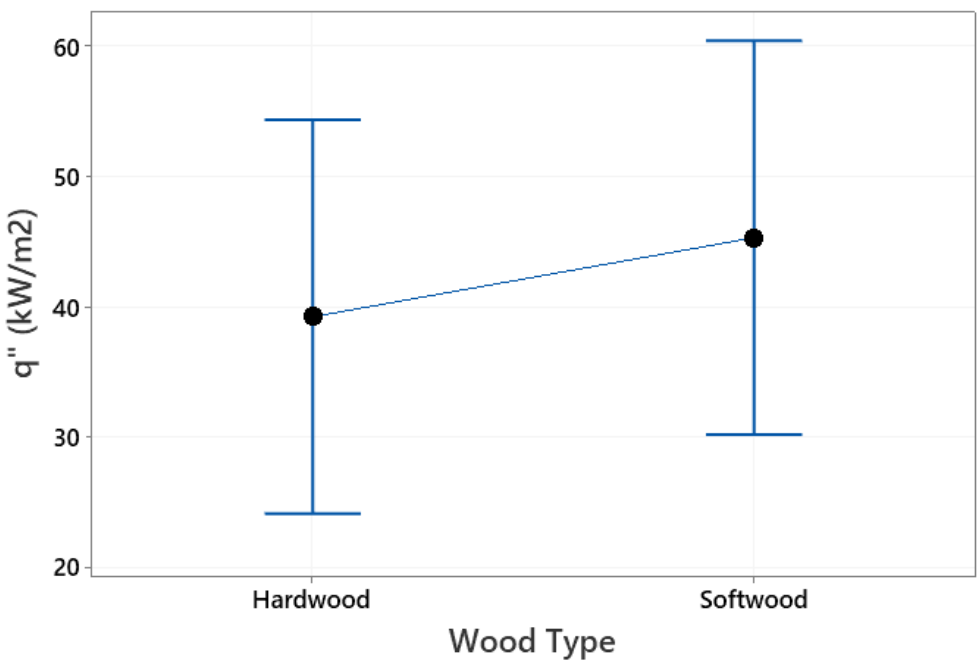

Figure 19. Interval plot showing the 95% CI for each group in the wood type study.

3.3.4. Density Study

The density study used two types of hardwood firebrands with different unburned dry densities to evaluate whether this parameter influenced heat transfer from firebrand piles. The statistical results are summarized in Table 11. One-way ANOVA was once again used to evaluate the results. It should be noted that the low density data set used in the density study is the same as the hardwood data set from the wood type study. It was found that for low density wood (Yellow Poplar, $\rho = 548\ kg/m^3$) the mean heat flux value was 39.27 kW/m^2. The high-density wood (N. Red Oak, $\rho = 870\ kg/m^3$) had a mean heat flux of 34.33 kW/m^2, a difference of 4.94 kW/m^2. The p-value was 0.286, an order of magnitude higher than the 0.05 threshold for significance. For this reason, the null hypothesis could not be rejected, and it was concluded that firebrand wood density does not significantly affect the heat transfer from firebrand piles. The interval plot of the results, seen in Figure 20, shows significant overlap in the 95% confidence interval range of heat flux from piles with firebrands made from different densities.

Table 11. Summary of the statistical analysis of the effect of unburned firebrand dry density on the heat transfer from firebrand piles.

Wood Dry Density (kg/m^3)	Mean (kW/m^2)	σ (kW/m^2)	N	Hypotheses	p-value	Conclusions
548	39.27	2.93	2	$H_0: \mu_1 = \mu_2$	0.286	Fail to reject H_0. Wood density does not affect heat transfer from firebrand piles
870	34.33	3.87	2	$H_a: \mu_1 \neq \mu_2$		

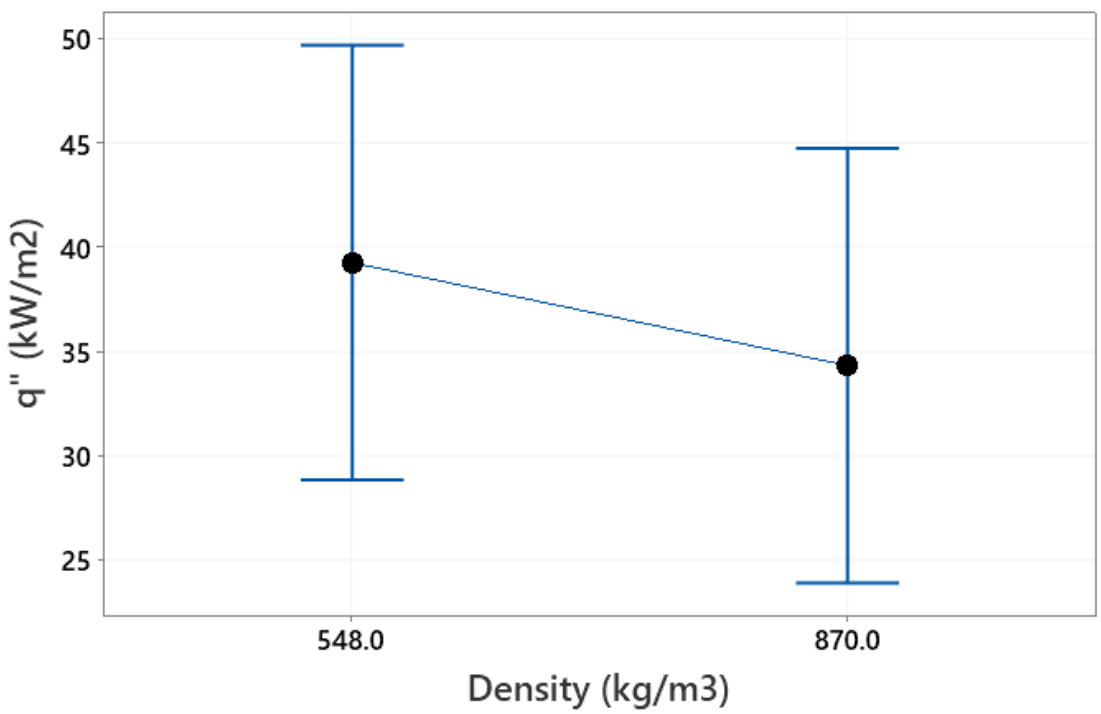

Figure 20. Interval plot showing the 95% CI for each group in the density study.

3.3.5. Wood State Study

The wood state study was a CRD experiment with three treatment levels used to assess whether a difference existed in heat transfer from piles made of live, dead, or artificial firebrands. Both live and dead samples were collected from natural tree branches while artificial firebrand were cut from commercially available dowel rods. Fisher's method was used at the individual 95% confidence level to determine if any of the treatment means were significantly different, with results shown in Table 12. The output of Fisher's Pairwise Comparison is the ordered letter report. Treatment levels that do not share a letter have significantly different means.

Table 12. Summary of the statistical analysis of the effect of wood mode on the heat transfer from firebrand piles.

Wood State	Mean (kW/m^2)	σ (kW/m^2)	N	Ordered Letter Report	Hypotheses	Conclusions
Artificial	48.88	2.96	2	A	$H_0: \mu_1 = \mu_2 = \mu_3$ $H_a: At\ least\ one\ mean\ significantly\ different$	Reject H_0. Heat transfer from piles made with artificial firebrands is significantly different from piles made from live or dead firebrands. No significant difference exists in heat transfer between piles made with live and dead firebrands
Live	36.25	3.98	2	B		
Dead	35.68	3.63	2	B		

As seen in Table 12, piles made with artificial firebrands have a mean heat flux value of 48.88 kW/m^2 which is significantly different the mean value of 36.25 kW/m^2 for piles consisting of live firebrands and 35.68 kW/m^2 for piles consisting of dead firebrands. The ordered letter report confirms that no significant difference exists between piles made of live and dead firebrands. Fisher's method also gives the p-values for the simultaneous test of the difference in treatment level means, shown in Table 13. The null hypothesis for each test is that there is no significant difference between treatment means.

Table 13. Fisher's individual tests for difference of means

Difference of Treatment Levels	Difference of Means (kW/m^2)	Adjusted p-value	Conclusion
Dead - Artificial	-12.63	0.038	Artificial and dead firebrands result in significantly different heat transfer
Live - Artificial	-13.20	0.034	Artificial and live firebrands result in significantly different heat transfer
Live - Dead	-0.58	0.881	No significant difference in heat transfer between live and dead firebrands

Finally, the results for the wood state study can be visualized using the interval plot in Figure 21. The heat transfer from piles consisting of artificial firebrands is higher than that from piles consisting of live or dead firebrands.

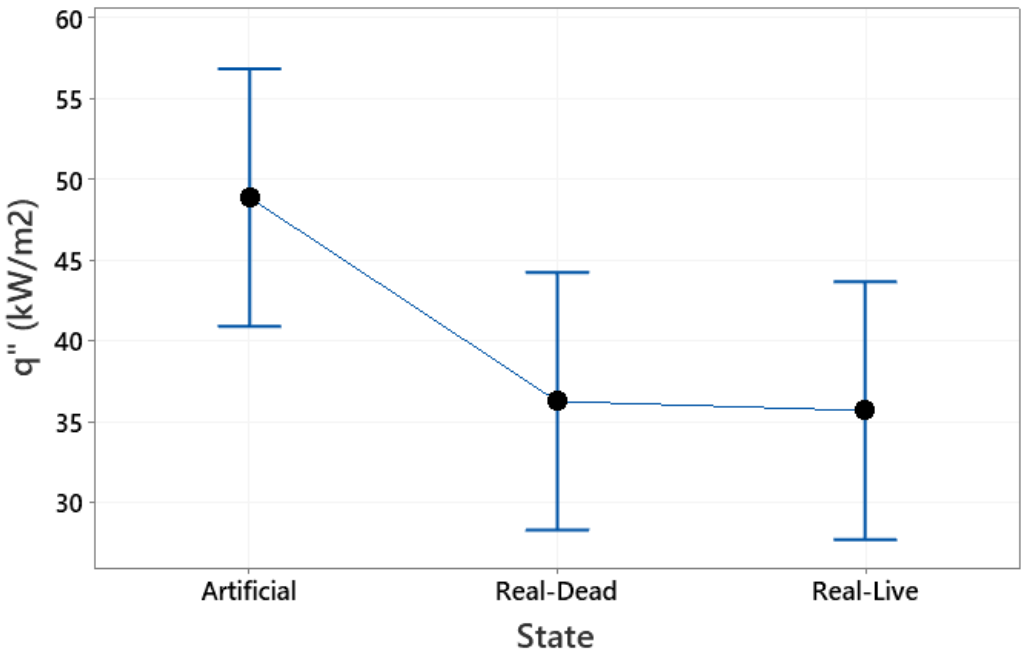

Figure 21. Interval plot showing the 95% CI for each group in the wood state study

3.3.6. Full Factorial Study

The full factorial matrix evaluated the main effects and interactions of pile mass, wind speed, firebrand diameter, and firebrand length on the heat transfer from firebrand piles. Four-way ANOVA determined whether each main effect or interaction had a significant effect on the heat transfer. The Pareto chart of the standardized effects, shown in Figure 22a, shows the effects of each term ranked from largest to smallest with the threshold for statistical significance denoted by the red dashed line. The standardized effects are t-statistics used to test the null hypothesis that the term has no effect, with larger t-statistics corresponding to smaller p-values. The main effects are denoted by A, B, C, or D for firebrand length, firebrand diameter, pile mass, and wind, respectively. Interactions are denoted using the appropriate combination of letters.

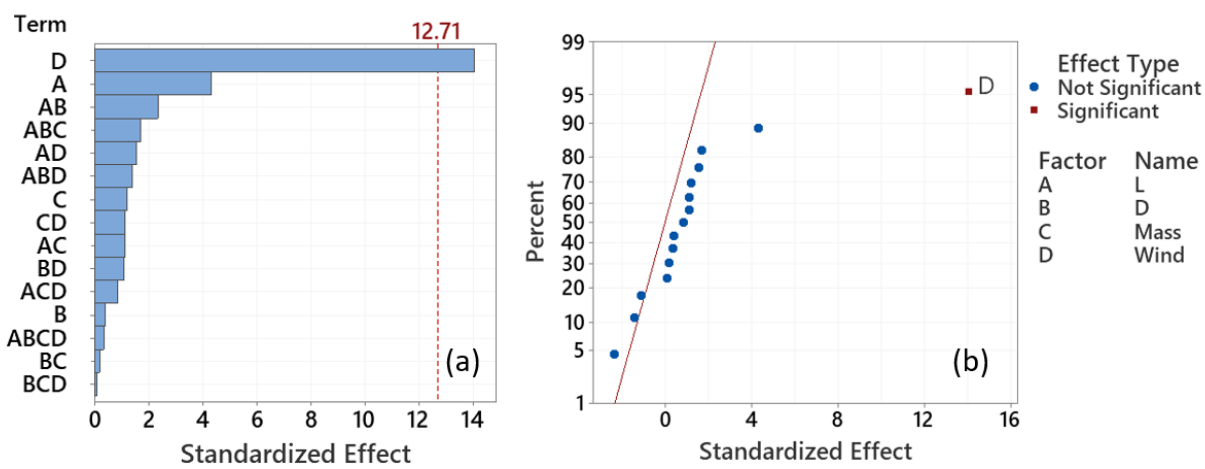

Figure 22. Pareto chart (a) and normal plot (b) for the full factorial tests with all terms included

Figure 22a shows the effects when all terms are included in the model and reveals that the wind main effect has by far the largest impact on heat flux from firebrand piles and is the only term that meets the criteria for statistical significance. The center point run (Test 17) was not included in the model and instead provided a single degree of freedom for error (df_E) in the ANOVA analysis.

To improve the model, insignificant high-order interactions can be removed and the model redeveloped with more df_E. In physical systems, high-order interactions consisting of three or more terms are rarely physically significant. The Pareto chart in Figure 22a, shows that the 4th order interaction between length, diameter, mass, and wind (ABCD) does not appear to be important. The same is true for the length-mass-wind (ACD) and diameter-mass-wind (BCD) 3rd order interactions. These terms were removed, and the model was redeveloped now with four degrees of freedom for error. Results are shown in Figure 23. With the improvements made to the model, three terms are statistically significant: wind, firebrand length, and the length-diameter interaction. The main effects of pile mass (C) and firebrand diameter (B) were found to have a statistically insignificant impact on the heat flux.

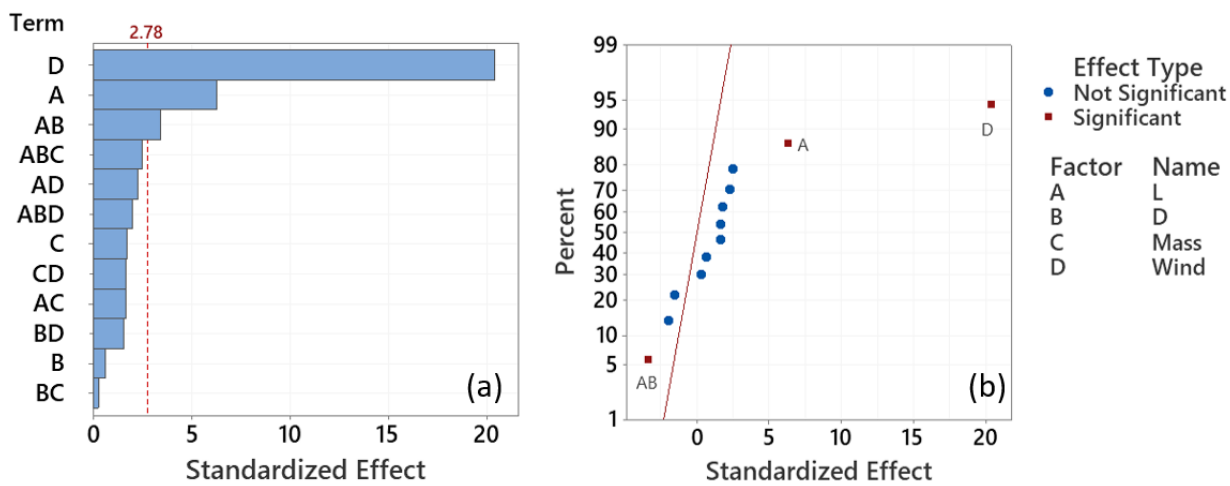

Figure 23. Pareto chart (a) and normal plot (b) for the full factorial tests with ABCD, ACD, and BCD terms removed

While the Pareto chart Figure 23a is useful for comparing the magnitudes of the standardized effects, the normal plot shown in Figure 23b shows the directionality of the effects. Effects greater than zero increase the heat firebrand pile when the effect is increased. For example, as wind increases, so does the heat transfer from pile. Effects less than zero reduce the response when their value is increased. The length-diameter interaction seems to have this type of negative feedback response with the heat flux. The red line in Figure 23b represents the response if the effect from all main effects and interactions were zero.

3.4. DISCUSSION

Many of the results found in these experiments agree well with the developing knowledge of heat transfer from individual firebrands and firebrand piles. The moisture content study showed that the moisture content of the unburned firebrands had no effect on the heat transfer from firebrand piles. The important caveat is that the firebrands in this study were heated until they reached a state of flaming combustion, likely driving off any internal moisture in the process. In

a real fire scenario, branches with more moisture may be less likely to form a firebrand in the first place. Firebrands with 25% MC had to be heated 2.5 times longer than those at 0% MC to reach the same state of self-sustaining flaming. This suggests that moisture content may play an important role in the actual formation of firebrands during a wildfire scenario, but not on the burning and heat transfer from an existing firebrand.

The wood type study found that there was no significant difference in heat transfer between Yellow Poplar and E. White Pine, a hardwood and a softwood with similar densities. These results were generalized to say that the wood type does not affect the heat transfer from firebrand piles despite there being fundamental biological differences between hardwoods and softwoods. The closely related density study showed that there were also no differences in pile heat transfer based on the starting dry density of the wood used to make the firebrands.

The wood state study showed that the heat transfer was not statistically different between piles made with firebrands collected from live or dead tree branches. There was however a statistically significant difference between natural firebrands (from live or dead wood) and artificial firebrands made from dowel rods. This result was also reported by Tao et. al. [37]. For the limited data collected in this study, the artificial firebrands generated higher mean heat fluxes compared with the natural firebrands. This finding has important ramifications as many previous firebrand studies have used artificial firebrands to simulate wildfire scenarios. Based on these results, using artificial firebrands may overestimate heat transfer of more realistic firebrands. For cases involving safety testing of building materials, a modest overestimation of the heat transfer may not be undesirable and artificial firebrands have the distinct advantage of consistent sizing and ample availability.

The full factorial study explored the influence of the main effects and interactions of firebrand length, firebrand diameter, pile mass, and wind on the heat transfer from firebrand piles. It was found that wind, firebrand length, and the length-diameter interaction were statistically significant and the most important parameters governing the heat transfer from firebrand piles. It is very well understood that wind increases heat flux from embers, so this result was anticipated. It has previously been established that pile height and porosity are important factors in determining the heat flux from firebrand piles [37]. The packing density, a measurement of porosity, depends on the ratio of the length and diameter for randomly oriented cylinders [40], [41]. It is suspected that this is the reason for the significant length-diameter interaction. The length of the firebrands also appeared to be important. The length of the firebrands is an important parameter in determining the height of the pile, particularly in these tests using the cage where wall effects may have prevented longer firebrands from lying flat.

Pile mass, which has been the metric used to quantify a firebrand pile most likely to cause ignition [7], was found to be statistically insignificant in the full-factorial study. The significant dependence of the heat flux on the wind and firebrand geometric details points to the importance of airflow into the pile and less on the overall mass of the pile. For example, the firebrand aspect ratio can be changed which will significantly affect the heat transfer while maintaining the same pile mass. This result suggests that future firebrand pile experiments should be quantified / varied based on firebrand geometric details and not on pile mass.

3.5. CONCLUSION

A series of experiments were conducted to test the effect of wood moisture content, wood type (hardwood or softwood), wood density, wood state (live, dead, or artificial), wind speed, pile mass, firebrand diameter, and firebrand length on the heat transfer from firebrand piles. A statistically rigorous framework was employed to design the experiments so that the results could be used to determine whether each factor had a significant effect on the heat flux. A method of inverse heat transfer analysis yielded high spatial resolution data under the firebrand piles that was then subdivided into twenty-nine grids for each test. Using the 75th percentile of the 120s grid average fluxes, it was found that wood moisture content, wood type, and density did not affect the heat transfer. Differences did exist in heat transfer from piles consisting of natural firebrands and firebrands made dowels. The result suggests firebrands made from artificial materials such as dowel rods may result in higher heat fluxes than expected from natural firebrands in actual wildfire scenarios. Finally, a full factorial matrix was used to explore the main effects and interactions of firebrand length, firebrand diameter, pile mass, and wind. Wind, firebrand length, and the length-diameter interaction were all found to be significant after insignificant terms were dropped from the model. These results fit well with existing knowledge that wind, pile porosity, and pile height all affect the heat transfer from firebrand piles. Firebrand pile mass was found to be statistically insignificant. Based on these results, the firebrand geometric details are more important to quantify rather than overall mass when assessing the magnitude of heat flux from the pile and its potential to ignite combustible surfaces.

REFERENCES

[1] S. E. Caton, R. S. P. Hakes, D. J. Gorham, A. Zhou, and M. J. Gollner, "Review of Pathways for Building Fire Spread in the Wildland Urban Interface Part I: Exposure Conditions," *Fire Technol.*, vol. 53, no. 2, pp. 429–473, 2017, doi: 10.1007/s10694-016-0589-z.

[2] R. S. P. Hakes, S. E. Caton, D. J. Gorham, and M. J. Gollner, "A Review of Pathways for Building Fire Spread in the Wildland Urban Interface Part II: Response of Components and Systems and Mitigation Strategies in the United States," *Fire Technol.*, vol. 53, no. 2, pp. 475–515, 2017, doi: 10.1007/s10694-016-0601-7.

[3] E. Koo, P. J. Pagni, D. R. Weise, and J. P. Woycheese, "Firebrands and spotting ignition in large-scale fires," *Int. J. Wildl. Fire*, vol. 19, no. 7, pp. 818–843, 2010, doi: 10.1071/WF07119.

[4] S. L. Manzello, "Enabling the investigation of structure vulnerabilities to wind-Driven firebrand showers in wildland-Urban Interface (WUI) fires," *Fire Saf. Sci. 11*, vol. 11, pp. 83–96, 2014, doi: 10.3801/IAFSS.FSS.11-83.

[5] V. P. Dowling, "Ignition of timber bridges in bushfires," *Fire Saf. J.*, vol. 22, no. 2, pp. 145–168, 1994, doi: 10.1016/0379-7112(94)90070-1.

[6] S. L. Manzello, S. H. Park, and T. G. Cleary, "Investigation on the ability of glowing firebrands deposited within crevices to ignite common building materials," *Fire Saf. J.*, vol. 44, no. 6, pp. 894–900, 2009, doi: 10.1016/j.firesaf.2009.05.001.

[7] R. S. P. Hakes, H. Salehizadeh, M. J. Weston-dawkes, and M. J. Gollner, "Thermal characterization of firebrand piles," *Fire Saf. J.*, vol. 104, no. June 2018, pp. 34–42, 2019, doi: 10.1016/j.firesaf.2018.10.002.

[8] S. L. Manzello and S. Suzuki, "Exposing decking assemblies to continuous wind-driven firebrand showers," *Fire Saf. Sci.*, vol. 11, pp. 1339–1352, 2014, doi: 10.3801/IAFSS.FSS.11-1339.

[9] S. S. Wessies, M. K. Chang, K. C. Marr, and O. A. Ezekoye, "Experimental and Analytical Characterization of Firebrand Ignition of Home Insulation Materials," *Fire Technol.*, vol. 55, no. 3, pp. 1027–1056, 2019, doi: 10.1007/s10694-019-00818-8.

[10] T. J. Ohlemiller, "Smoldering combustion propagation on solid wood," *Fire Saf. Sci. 3*, pp. 565–574, 2006, doi: 10.4324/9780203973493.

[11] P. Ellis, "The Aerodynamic and Combustion Characteristics of Eucalypt Bark - A Firebrand Study," *Disseration, Aust. Natl. Univ. Dep. For.*, p. 205, 2000.

[12] S. L. Manzello, T. G. Cleary, J. R. Shields, A. Maranghides, W. Mell, and J. C. Yang, "Experimental investigation of firebrands: Generation and ignition of fuel beds," *Fire Saf. J.*, vol. 43, no. 3, pp. 226–233, 2008, doi: 10.1016/j.firesaf.2006.06.010.

[13] S. L. Manzello, T. G. Cleary, J. R. Shields, and J. C. Yang, "On the ignition of fuel beds by firebrands," *Fire Mater.*, vol. 30, no. 1, pp. 77–87, 2006, doi: 10.1002/fam.901.

[14] A. Warey, "Influence of thermal contact on heat transfer from glowing firebrands," *Case Stud. Therm. Eng.*, 2018, doi: 10.1016/j.csite.2018.04.018.

[15] A. Filkov *et al.*, “Investigation of firebrand production during prescribed fires conducted in a pine forest,” *Proc. Combust. Inst.*, 2017, doi: 10.1016/j.proci.2016.06.125.

[16] S. L. Manzello, A. Maranghides, J. R. Shields, W. E. Mell, Y. Hayashi, and D. Nii, “Mass and size distribution of firebrands generated from burning Korean pine (Pinus koraiensis) trees,” *Fire Mater.*, 2009, doi: 10.1002/fam.977.

[17] Y. M. Abul-huda, “Development of a Spatially Resolved Optical Technique for Measuring Heat Flux and Thermal Footprint of Firebrand Piles,” *NIST Tech. Note 2052*, p. 28, 2019.

[18] J. Hodges, C. Rippe, S. W. Case, and B. Y. Lattimer, “Predicting the structural response of a compartment fi re using full-field heat transfer measurements,” *Fire Saf. J.*, vol. 91, no. March, pp. 471–479, 2017, doi: 10.1016/j.firesaf.2017.03.011.

[19] C. M. Rippe and B. Y. Lattimer, “Full-field surface heat flux measurement using non-intrusive infrared thermography,” *Fire Saf. J.*, vol. 78, pp. 238–250, 2015, doi: 10.1016/j.firesaf.2015.10.004.

[20] N. Cholewa, P. T. Summers, S. Feih, A. P. Mouritz, B. Y. Lattimer, and S. W. Case, “A Technique for Coupled Thermomechanical Response Measurement Using Infrared Thermography and Digital Image Correlation (TDIC),” *Exp. Mech.*, vol. 56, pp. 145–164, 2016, doi: 10.1007/s11340-015-0086-1.

[21] J. L. Urban, A. C. Fernandez-pello, M. Vicariotto, and D. Dunn-Rankin, “Temperature Measurement of Glowing Embers with Color Pyrometry,” *Fire Technol.*, vol. 55, no. 3, pp. 1013–1026, 2019, doi: 10.1007/s10694-018-0810-3.

[22] R. J. Goldstein, E. M. Sparrow, and D. C. Jones, “Natural convection mass transfer adjacent to horizontal plates,” *Int. J. Heat Mass Transf.*, vol. 16, no. 5, pp. 1025–1035, 1973, doi: 10.1016/0017-9310(73)90041-0.

[23] J. R. Lloyd and W. R. Moran, “Natural convection adjacent to horizontal surface of various planforms,” *J. Heat Transfer*, vol. 96, no. 4, pp. 443–447, 1974, doi: 10.1115/1.3450224.

[24] F. P. Incropera, D. P. DeWitt, T. L. Bergman, and A. S. Lavine, *Fundamentals of Heat and Mass Transfer*, 6th ed. John Wiley & Sons, 2007.

[25] P. Deb *et al.*, “Causes of the Widespread 2019–2020 Australian Bushfire Season,” *Earth’s Futur.*, vol. 8, no. 11, 2020, doi: 10.1029/2020EF001671.

[26] M. Ward *et al.*, “Impact of 2019–2020 mega-fires on Australian fauna habitat,” *Nat. Ecol. Evol.*, vol. 4, no. 10, pp. 1321–1326, 2020, doi: 10.1038/s41559-020-1251-1.

[27] A. I. Filkov, T. Ngo, S. Matthews, S. Telfer, and T. D. Penman, “Impact of Australia’s catastrophic 2019/20 bushfire season on communities and environment. Retrospective analysis and current trends,” *J. Saf. Sci. Resil.*, vol. 1, no. 1, pp. 44–56, 2020, doi: 10.1016/j.jnlssr.2020.06.009.

[28] M. Turco *et al.*, “Climate drivers of the 2017 devastating fires in Portugal,” *Sci. Rep.*, vol. 9, no. 1, pp. 1–8, 2019, doi: 10.1038/s41598-019-50281-2.

[29] K. Lagouvardos, V. Kotroni, T. M. Giannaros, and S. Dafis, “Meteorological conditions

conducive to the rapid spread of the deadly wildfire in eastern attica, Greece," *Bull. Am. Meteorol. Soc.*, vol. 100, no. 11, pp. 2137–2145, 2019, doi: 10.1175/BAMS-D-18-0231.1.

[30] T. Brown, S. Leach, B. Wachter, and B. Gardunio, "THE NORTHERN CALIFORNIA 2018 EXTREME FIRE SEASON," *Bull. Am. Meteorol. Soc.*, vol. 95, no. 9, pp. S1–S96, 2014, doi: 10.1175/1520-0477-95.9.s1.1.

[31] D. M. Theobald and W. H. Romme, "Expansion of the US wildland-urban interface," *Landsc. Urban Plan.*, vol. 83, no. 4, pp. 340–354, 2007, doi: 10.1016/j.landurbplan.2007.06.002.

[32] W. Mell and Alexander Maranghides, "NIST Technical Note 1635: A Case Study of a Community Affected by the Witch and Guejito Fires," 2009.

[33] N. A. McArthur and P. Lutton, "Ignition of exterior building details in bushfires: An experimental study," *Fire Mater.*, vol. 15, no. 2, pp. 59–64, 1991, doi: 10.1002/fam.810150204.

[34] A. Filkov, D. Kasymov, V. Zima, and O. Matvienko, "Experimental investigation of surface litter ignition by bark firebrands," *AIP Conf. Proc.*, vol. 1698, no. January, 2016, doi: 10.1063/1.4937859.

[35] S. Santamaria *et al.*, "Investigation of Structural Wood Ignition By Firebrand Accumulation," *First Int. Conf. Struct. Saf. under Fire Blast*, no. July 2016, pp. 1–13, 2015.

[36] E. D. Bearinger, J. L. Hodges, F. Yang, C. M. Rippe, and B. Y. Lattimer, "Localized heat transfer from firebrands to surfaces," *Fire Saf. J.*, vol. 120, no. April 2020, p. 103037, 2021, doi: 10.1016/j.firesaf.2020.103037.

[37] Z. Tao, B. Bathras, B. Kwon, B. Biallas, M. J. Gollner, and R. Yang, "Effect of firebrand size and geometry on heating from a smoldering pile under wind," *Fire Saf. J.*, no. May, p. 103031, 2020, doi: 10.1016/j.firesaf.2020.103031.

[38] J. R. Lloyd and W. R. Moran, "Natural Convection Adjacent To Horizontal Surface of Various Planforms.," *Am. Soc. Mech. Eng.*, vol. 96, no. 74-WA/HT-66, pp. 443–447, 1974, doi: 10.1115/1.3450224.

[39] T. Conners, "Distinguishing Softwoods from Hardwoods," *Agric. Nat. Resour. Publ.*, p. 105, 2015.

[40] S. X. Li, J. Zhao, P. Lu, and Y. Xie, "Maximum packing densities of basic 3D objects," *Chinese Sci. Bull.*, vol. 55, no. 2, pp. 114–119, 2010, doi: 10.1007/s11434-009-0650-0.

[41] R. P. Zou, X. Y. Lin, A. B. Yu, and P. Wong, "Packing of cylindrical particles with a length distribution," *J. Am. Ceram. Soc.*, vol. 80, no. 3, pp. 646–652, 1997, doi: 10.1111/j.1151-2916.1997.tb02880.x.

[42] D. Thomas, D. Butry, S. Gilbert, D. Webb, and J. Fung, "The Costs and Losses of Wildfires: A Literature Survey (NIST Special Publication 1215)," 2017, [Online]. Available: https://doi.org/10.6028/NIST.SP.1215.

[43] S. Wang, X. Huang, H. Chen, N. Liu, and G. Rein, "Ignition of low-density expandable polystyrene foam by a hot particle," *Combust. Flame*, vol. 162, no. 11, pp. 4112–4118,

2015, doi: 10.1016/j.combustflame.2015.08.017.

[44] R. M. Hadden, S. Scott, C. Lautenberger, and C. C. Fernandez-Pello, "Ignition of Combustible Fuel Beds by Hot Particles: An Experimental and Theoretical Study," *Fire Technol.*, vol. 47, no. 2, pp. 341–355, 2011, doi: 10.1007/s10694-010-0181-x.

[45] A. Ganteaume *et al.*, "Spot fires: Fuel bed flammability and capability of firebrands to ignite fuel beds," *Int. J. Wildl. Fire*, vol. 18, no. 8, pp. 951–969, 2009, doi: 10.1071/WF07111.

[46] C. Lautenberger and A. C. Fernandez-Pello, "Spotting ignition of fuel beds by firebrands," *WIT Trans. Modelling Simul.*, vol. 48, pp. 603–612, 2009, doi: 10.2495/CMEM090541.

[47] H. S. Carslaw and J. C. Jaeger, *Conduction of Heat in Solids*, 2nd ed. London: Oxford University Press, 1959.

[48] J. G. Quintiere, "A simulation model for fire growth on materials subject to a room-corner test," *Fire Saf. J.*, vol. 20, no. 4, pp. 313–339, 1993, doi: 10.1016/0379-7112(93)90053-S.

[49] SFPE, *Engineering Guide - Piloted Ignition of Solid Materials Under Radiant Exposure*. Society of Fire Protection Engineers, 2002.

[50] A. Tewarson, "Generation of Heat and Chemical Compounds in Fires," in *The SFPE Handbook of Fire Protection Engineering*, 1995, p. Section 3-Chapter 4.

[51] E. D. Bearinger, B. Y. Lattimer, J. Hodges, C. Rippe, and A. Kapahi, "Statistical Assessment of Parameters Affeting Firebrand Pile Heat Transfer to Surfaces," *Curr. under Rev. by Front. Mech. Eng.*

4. PREDICTING IGNTION FROM EXPOSURE TO FIREBRAND PILES

Elias Bearinger, Brian Lattimer, Jonathan Hodges

ABSTRACT
A simple engineering model was developed for using time-varying heat fluxes from firebrand piles to predict the ignition of common materials. The model requires known material thermal properties and heat flux values to make its predictions. To assess the model, piloted and spontaneous ignition properties of nylon, pressure-treated southern yellow pine decking, and composite decking were developed through cone calorimeter testing. A series of twelve firebrand pile tests were run to obtained representative heat fluxes. The measured heat fluxes were used in conjunction with the material properties to predict probability of ignition and time to ignition. These predictions were validated through experiments.

4.1. INTRODUCTION

The destruction caused by wildfires continues to be an issue of tremendous concern and poses a severe risk to many communities around the world. Each year in the United States alone, wildfires are estimated to cause $71.1 to $347.8 billion in total economic damages [42], destroy thousands of structures, and result in dozens of fatalities [30]. Firebrands, small pieces of burning material generated by fires, are responsible for many of the home ignitions that occur in these fire disaster scenarios [32]. Firebrand can be lofted up to 2 km by high winds [3], further complicating efforts to protect structures. Work by Manzello and Suzuki [8] has shown that firebrands can accumulate in piles in wind-driven conditions greatly increasing the potential to ignite building assemblies.

Several studies [5], [6], [8], [12], [13], [33]–[35], have experimentally investigated the ability of firebrand piles to ignite various fuels. Other research [43], [44] has looked at ignition of fuels by heated metal particles, but few studies have modeled ignition by firebrands or firebrand piles.

Warey [14] developed a theoretical model of heat transfer between cylindrical and disk shaped firebrands with a fuel substrate, but did not relate this to ignition. Ganteaume et al. [45] developed logistic models for probability of ignition for various firebrand/fuel combinations, providing an empirical method for determining whether ignition would occur for select cases. To understand the fundamental physical processes involved in the ignition of fuel beds by firebrands, Lautenberger and Fernandez-Pello [46] created an advanced coupled model combining computational fluid dynamics, heat transfer, and pyrolysis models.

One notable study conducted by Wessies et al. [9], developed an ignition model for firebrands or firebrand piles using a using heat and mass transfer analysis. The model predicts the temperature evolution of the firebrands and accounts for a porous layer of ash that grows along the firebrand with time, reducing the ease of oxygen availability. The firebrand is assumed to be radiatively coupled with a fuel and using the predicted temperature of the firebrand, the fuel temperature and

pyrolizate generation can be modeled. The model includes ignition criteria based on the mass flux of generated fuel vapors.

The goal of this work was to provide a simple engineering model to predict the ignition of common building materials by firebrand piles. The model used time-varying heat flux data measured directly from tests on firebrand piles and experimentally determine thermal properties of several common building materials. The model was applied to nylon, pressure-treated southern yellow pine deck board, and composite deck board made from wood fibers and plastic. Ignition predictions were made for various fuel/pile combinations and validated through experiments.

4.2. METHODS

The objective of this work was to develop and validate an engineering model that can be used to predict the ignition of building material by piles of firebrands. To accomplish this goal, a model was developed and validated against an exact theoretical solution. Thermal properties of common materials were obtained experimentally and used in conjunction with heat flux data collected from firebrand piles to predict which pile/material combinations would ignite. Finally, physical tests were run to assess the accuracy of the model's prediction.

4.2.1. Ignition Model

An ignition model using material properties developed through cone calorimeter testing was employed to predict whether the time-varying heat fluxes from firebrand piles would be able to ignite common building materials. Originally developed by Carslaw and Jaeger [47] to analyze temperatures within a solid exposed to an incident heat flux, the model was adopted by Quintiere [48] to assess ignition. The model predicts the surface temperature rise of the material for an incident flux which varies temporally as a function of τ using the Duhamel integral

$$T_s = \left(\frac{1}{\pi k \rho c}\right)^{1/2} \int_0^t \frac{q''(\tau)}{\sqrt{t-\tau}} d\tau + T_0; \qquad Ignition: T_s > T_{ig} \tag{17}$$

where $q''(\tau) = q''_e(\tau) - q''_{cr}$ and t is the moment of interest in time. $q''_e(\tau)$ is the exposure heat flux from the firebrand pile and q''_{cr} is the critical heat flux (explained in detail in Section 2.2). Ignition is predicted when the surface temperature, T_s, rises above the ignition temperature of the material. The integral in Eqn. 1 is evaluated numerically using the exposure flux measured under the firebrand piles. To avoid instability in the numerical integration as τ approaches t, a small relaxation factor, δ, was added to the denominator of the integrand. It was found that using a δ approximately equal to 10% of the time step in the recorded flux data yielded the best results.

The numeric integration and relaxation factor were validated against an exact solution for a theoretical parabolic exposure flux. The exposure flux had the form

$$q'' = A(Bt - t^2) \tag{18}$$

where $A = 4q''_{max}/t_{dur}^2$, and $B = t_{dur}$, the duration of $q'' > 0$. For the validation case $q''_{max} = 60\ kW/m^2$ and $t_{dur} = 150s$ were chosen, resulting in the parabolic exposure flux shown in Figure 24.

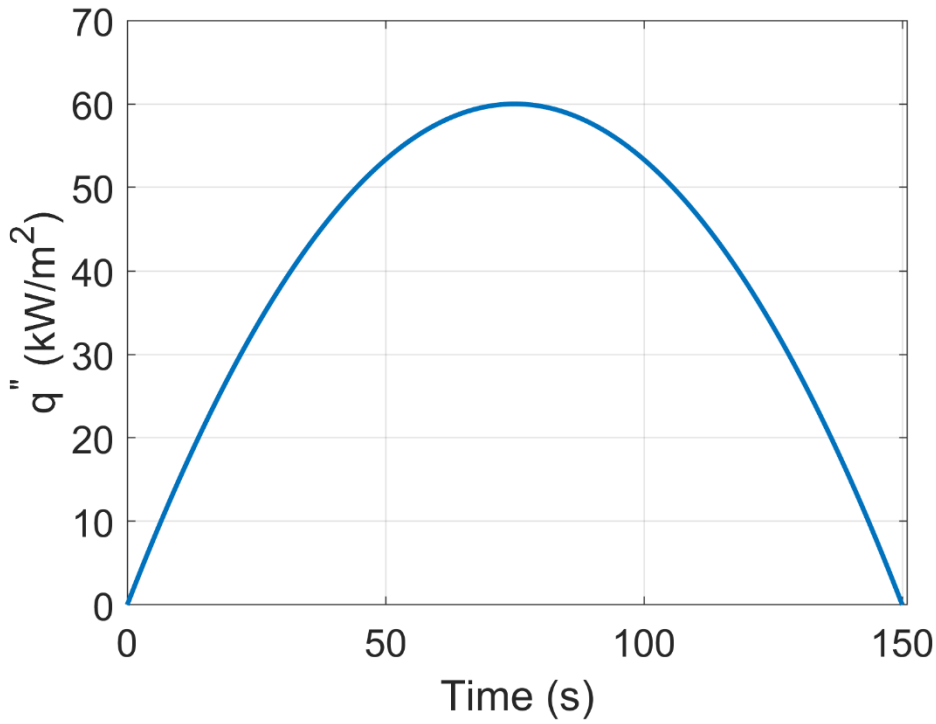

Figure 24. The parabolic heat flux used to validate the numeric integration technique.

The exact solution for the surface temperature rise, ΔT_s, was obtained using the Duhamel integral

$$\Delta T_s = \left(\frac{1}{\pi k \rho c}\right)^{1/2} \int_0^t \frac{A(B\tau - \tau^2)}{\sqrt{\mathrm{t} - \tau}} d\tau \tag{19}$$

And can be shown to be

$$\Delta T_s = \left(\frac{1}{\pi k \rho c}\right)^{1/2} \left[\frac{4}{3} A B t^{3/2} - \frac{16}{15} A t^{5/2}\right] \tag{20}$$

where t is the time of interest. This expression now gives an exact solution for the surface temperature rise due to the incident flux against which the numeric estimation can be compared.

To obtain the numeric integration, the parabolic flux was sampled every 1s, giving discretized data similar to what is recorded in the firebrand experiments. A relaxation factor of $\delta = 0.1$ was used and results were compared with the exact solution for $k\rho c = 0.237$, as shown in Figure 25. As can be seen, excellent agreement exists between the numeric and exacts solutions for the surface temperature rise over the duration of the test.

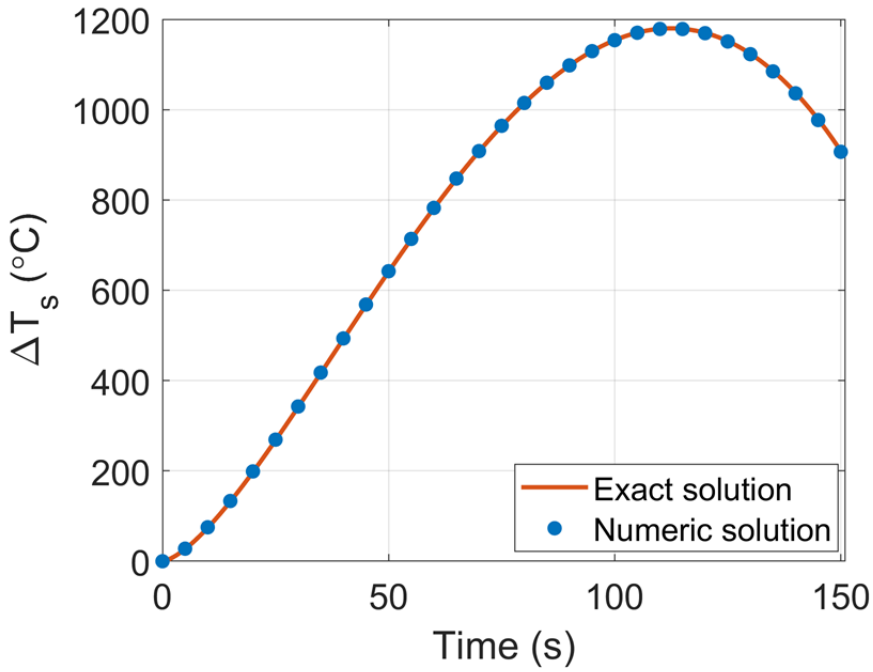

Figure 25. Comparison of the exact solution and numeric estimation of the surface temperature rise for parabolic exposure flux.

4.2.2. Material Properties

The thermal properties of three building materials were experimentally determined. The materials tested were nylon, pressure treated southern yellow pine deck board, and composite deck board made from wood fibers and plastic. The thermal properties for the specific materials were important inputs into the ignition model and were experimentally determined for both piloted and spontaneous ignition using a cone calorimeter.

The three materials were assumed to be thermally thick, meaning that the physical thickness of the material is larger than the depth of thermal diffusion over the time-scales of interest and that significant thermal gradients exist within the material. Under this assumption, it has been shown [49] that the time to ignition, t_{ig}, for a given exposure heat flux, q_e'', can be modeled by

$$t_{ig} = \frac{\pi}{4} kpc \frac{\left(T_{ig} - T_0\right)^2}{(q_e'' - q_{cr}'')^2} \tag{21}$$

Where k is the thermal conductivity, ρ is the density, c is the specific heat capacity, T_{ig} is the ignition temperature of the material, and T_0 is the starting temperature. q_{cr}'' is the critical heat flux: the exposure heat flux value for which the time to ignition goes to infinity.

The time to ignition was experimentally measured for each material using a range of incident heat flux values. Uniform, constant exposure fluxes were provided by a cone calorimeter as shown in Figure 26. 100 mm × 100 mm samples were cut from the materials and dried to 0% MC by storing them in a thermal chamber at 75 °C for several days. The southern yellow pine and the composite deck boards had a thickness of 25.4 mm. while the nylon had a thickness of

12.7 mm. Prior to testing, the samples were allowed to cool to room temperature and the bottom and sides of the sample were wrapped in aluminum foil, leaving only the top of the sample exposed to the incident radiant flux. The heater temperature was set, and heat flux was validated using a water-cooled heat flux gauge. The aluminum-wrapped sample was placed in the holder (shown in the inset in Figure 26) and ceramic wool was used to insulate the bottom of the sample so direct contact with the holder did not occur. To start the testing, the sample and holder were centered 25.4 mm beneath the bottom of the heater. The time between the sample being placed under the heater and the onset of flaming ignition was measured, giving t_{ig}. Tests lasting longer than 20 minutes without flaming ignition were said not to ignite. For piloted ignition tests, a continuous spark was provided a few millimeters above the center of the heated sample.

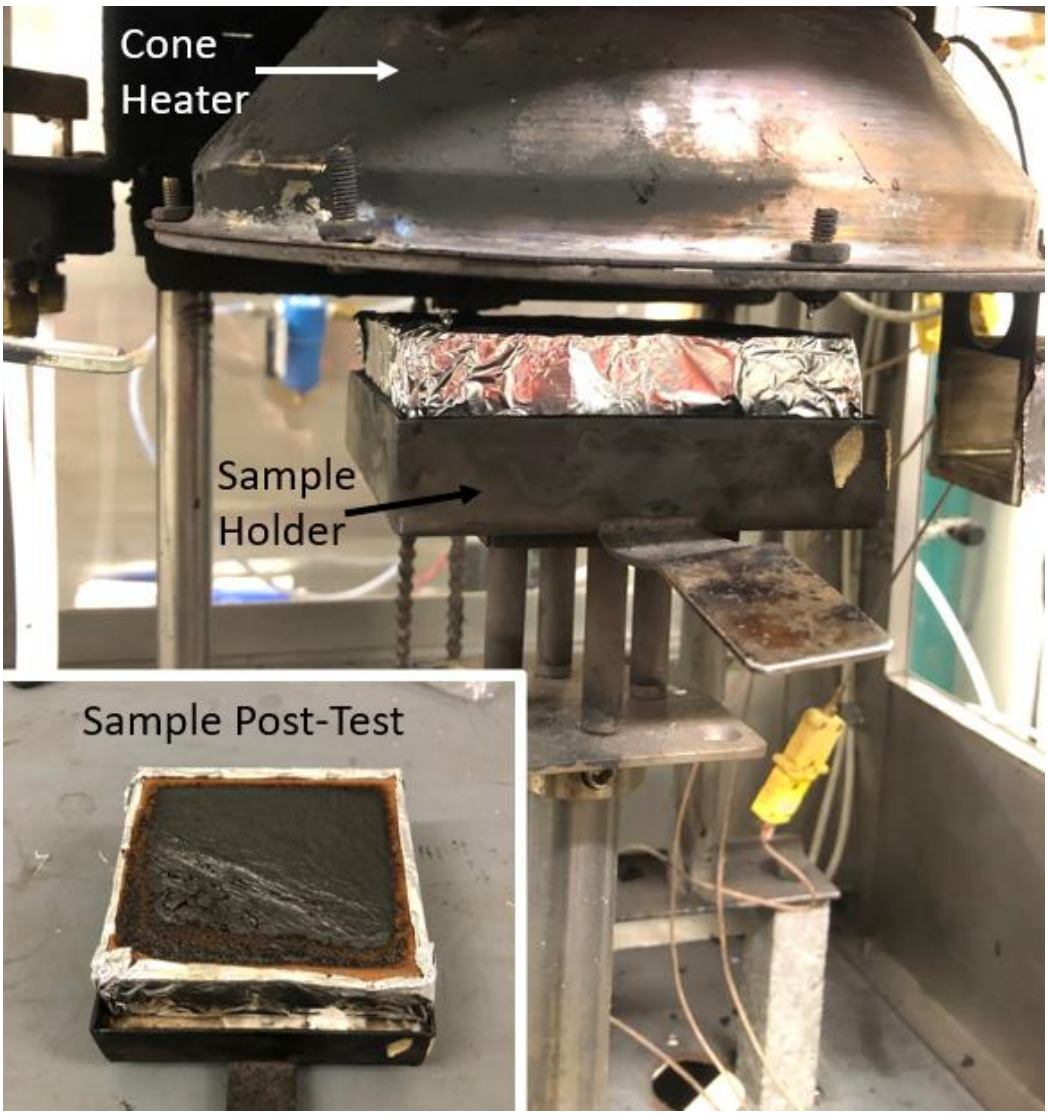

Figure 26. Cone calorimeter testing apparatus

The minimum heat flux, q''_{min}, is defined as the minimum flux required to ignite the sample in 20 minutes or less. q''_{min} was found experimentally by decreasing the exposure flux until ignition was not observed and was bracketed within +/- 1 kW/m^2 by a test where ignition did occur and a test where ignition did not occur. q''_{min} was taken to be the average of these bracketing tests.

For both piloted and spontaneous ignition, $1/\sqrt{t_{ig}}$ scales approximately linearly with the exposure flux, q_e''. By plotting $1/\sqrt{t_{ig}}$ versus q_e'', important material properties, including the thermal response parameter and the critical flux, can be calculated. The thermal response parameter (TRP), originally identified by Tewarson [50], is a combination of the thermal inertia of the material, $k\rho c$, and the temperature rise required for ignition, $T_{ig} - T_0$:

$$TRP = \sqrt{k\rho c}\left(T_{ig} - T_0\right) \tag{22}$$

Combining Eqn. 5 with Eqn. 6 and raising the resultant equation to the $-1/2$ power yields

$$\frac{1}{\sqrt{t_{ig}}} = \frac{1}{\sqrt{\frac{\pi}{4}}TRP} q_e'' + \frac{-1}{\sqrt{\frac{\pi}{4}}TRP} q_{cr}'' \tag{23}$$

an equation of the form $y = mx + y_0$ where q_e'' is the independent variable. The slope, m, of the linear best-fit line from the plot of the $1/\sqrt{t_{ig}}$ versus q_e'' is used to find TRP by

$$TRP = \frac{1}{\sqrt{\frac{\pi}{4}}m} \tag{24}$$

Similarly, the critical flux can be found using the y-intercept of the best-fit line, y_0:

$$q_{cr}'' = \left(-\sqrt{\frac{\pi}{4}}TRP\right) y_0 \tag{25}$$

The ignition temperature, T_{ig}, is found using the measured q_{min}'' and a surface energy balance at steady state. The net heat flux absorbed by the material, q_{net}'', is equal to the exposure flux less the heat transferred away from the material through convection and reradiation to the surroundings.

$$q_{net}'' = q_e'' - \varepsilon\sigma(T_s^4 - T_0^4) - h(T_s - T_0) \tag{26}$$

where ε is the emissivity, σ is the Stefan-Boltzmann constant, T_s is the surface temperature of the material, and h is the convective heat transfer coefficient.

At steady-state, $q_{net}'' \approx 0$, and as such $q_e'' = q_{min}''$ and $T_s = T_{ig}$, resulting in

$$q_{min}'' = \varepsilon\sigma\left(T_{ig}^4 - T_0^4\right) + h(T_{ig} - T_0) \tag{27}$$

The expression shown above in Eqn. 11 was iteratively solved for T_{ig} using $\varepsilon = 0.9$, $h = 0.015 kW/m^2K$, and $T_0 = 293K$.

Finally, Eqn. 5 was used to derive the thermal inertia of the material

$$k\rho c = \left(\frac{TRP}{T_{ig} - T_0}\right)^2 \tag{28}$$

This process was conducted for each of the three tested materials for both piloted and spontaneous ignition, yielding TRP, $k\rho c$, T_{ig}, q''_{min}, and q''_{cr} for all cases.

4.2.3. Experimental Setup

A series of experiments were run to measure exposure heat fluxes from realistic firebrand piles. The measured heat fluxes were then used with the ignition model and fuel thermal properties to predict whether ignition would occur. The experimental setup and data collection technique is identical to that used by Bearinger et al. [51].

The experimental setup (shown in Figure 27) consisted of a wind tunnel, two infrared cameras, an RGB camera, a wire mesh cage, and a 304SS plate painted black with high-emissivity paint. The exit of the wind tunnel was 0.31m wide by 0.10m high and provided a uniform flow across 90% of the outlet with a maximum volumetric flow rate of 0.106 m^3/s (225 cfm). The flow was generated by an American Fan Company AF-8 blower driven by a 1 hp, 3-phase AC motor controlled with a variable speed drive.

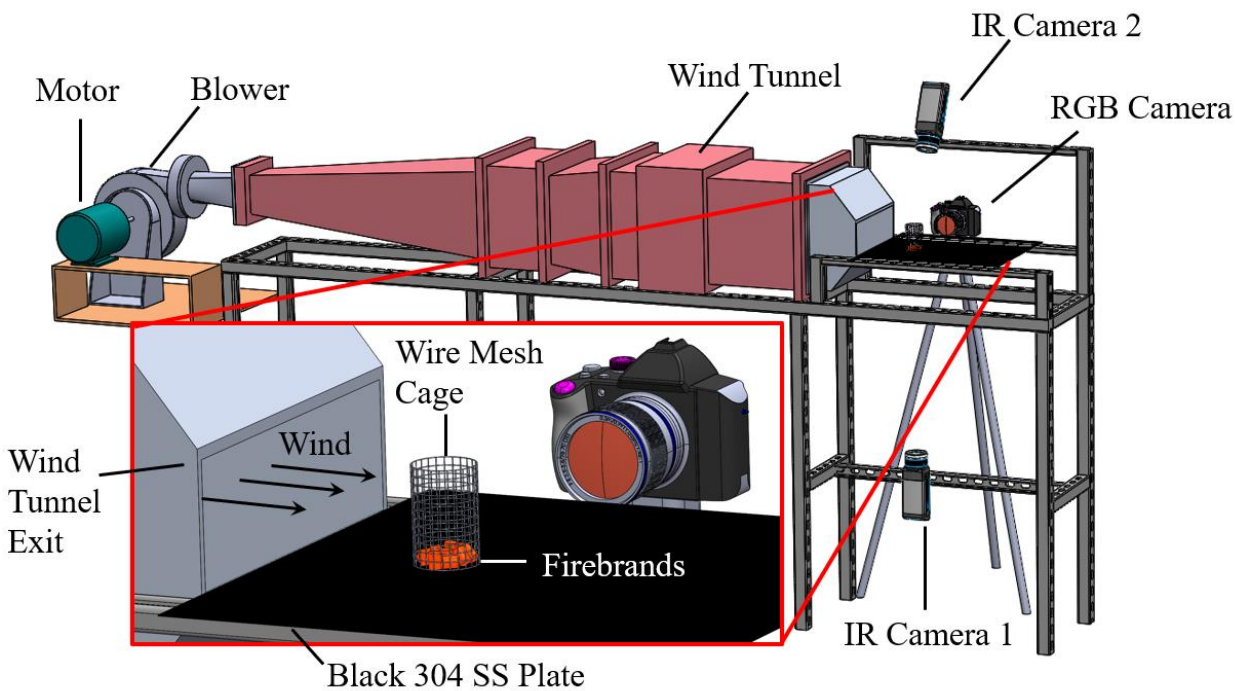

Figure 27. Experimental setup used to measure exposure flux from firebrand piles

The firebrand piles were contained in a lightweight steel mesh cage and supported on a 0.762 mm thick stainless-steel plate. The cage had dimensions shown in Figure 28, and was necessary to keep the firebrand piles from blowing off the plate. The piles rested directly only the black

stainless-steel plate which was painted on each side with approximately 20 μm of Rust-oleum™ High Heat black enamel paint. Experiments by Cholewa et al. [20] showed this paint to have an emissivity of $\varepsilon = 0.97$. The plate temperature was recorded by IR Camera 1, mounted 0.37m beneath the bottom surface. At this distance, each pixel in the camera display corresponded to a 0.44 mm × 0.45 mm area under the underside of the plate.

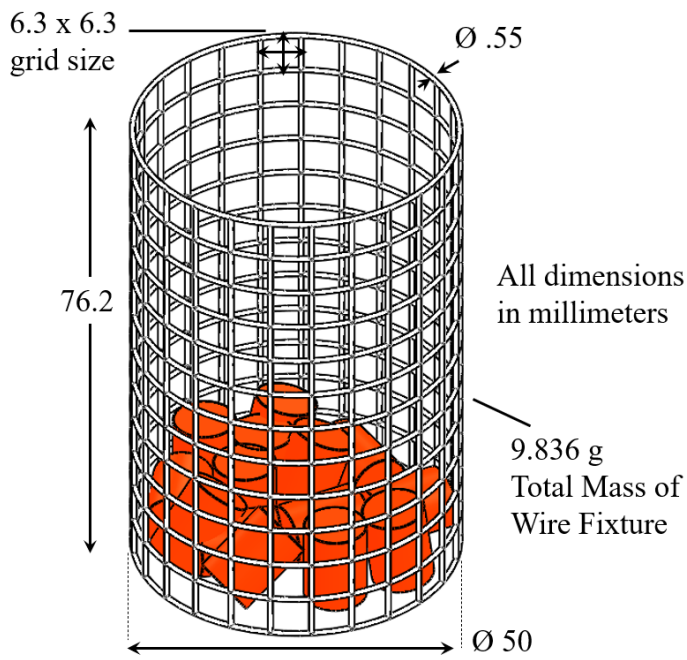

Figure 28. Steel wire cage used to constrain the firebrand piles (shown in red)

Heat flux measurements were taken using a technique known as inverse heat transfer (IHT) analysis. Developed by Rippe and Lattimer [19], this method of IHT relies on thermographs recorded by infrared (IR) cameras to produce distributed heat flux measurements with spatial resolutions <0.5 mm. The IHT technique requires a thermally-thin, interstitial plate (Black 304 SS Plate in Figure 27) of known optical and thermal properties, situated between the heat source (i.e. the firebrand piles) and the infrared camera. Described in great detailed by Rippe and Lattimer [19], and Bearinger et al. [36], the basic premise of the IHT technique is that each pixel on the IR camera corresponds to a small, discrete element on the interstitial plate. The IR camera continuously measures the temperature of each one of these elements, allowing an energy balance to be conducted on each pixel at every instance in time, shown in Figure 29. For any given element of interest, the element temperature, T, the temperatures of the surrounding pixels, and the ambient temperature, T_∞, are known. The only unknown is the exposure heat flux, q''_{exp}.

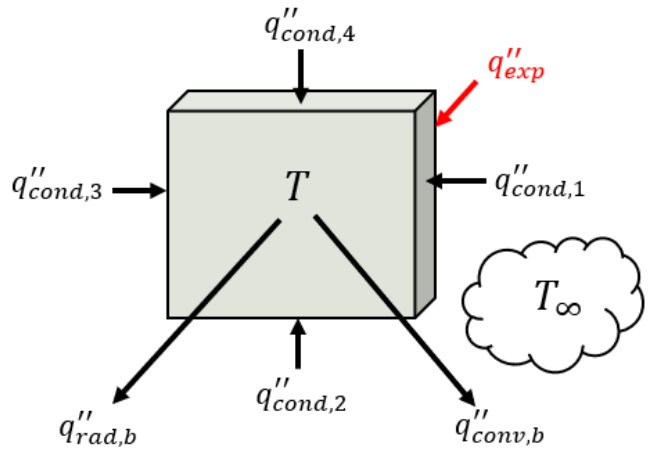

Figure 29. Energy balance conducted on each pixel to resolve distributed heat flux measurements.

The unknown exposure flux is simply the difference between a storage term, q''_{stor}, and the net heat flux into the pixel.

$$q''_{exp} = q''_{stor} - \sum q''_{cond} + q''_{rad,b} + q''_{conv,b} \tag{29}$$

where q''_{cond} is the conduction flux from the contiguous pixels and $q''_{rad,b}$ and $q''_{conv,b}$ are the radiation and convection losses from the underside of the plate, respectively. The storage term depends on the time rate of temperature change, dT/dt, of the pixel of interest

$$q''_{stor} = \frac{\rho V c}{A}\frac{dT}{dt} \tag{30}$$

where $\rho = 7{,}900\ kg/m^3$ is the density of the plate, V and A are the volume and surface area of a discrete pixel element, respectively, and $c = 515\ J/kg\ \cdot K$ is the specific heat capacity of the plate material.

The IHT method was chosen due to the high spatial and temporal resolution it provides. Each 0.44 mm × 0.45 mm pixel was effectively its own heat flux gauge allowing distributed maps of the heat flux under the firebrand pile to resolved with a temporal resolution of 0.28 Hz. The high spatial resolution meant that the 50 mm diameter firebrand pile corresponded to ~9,900 discrete pixels. Following a method developed by Bearinger et al. [51] the pile was subdivided into twenty-nine 15 × 15 pixel grids lying completely within the pile boundaries, shown in Figure 30. Each grid corresponded to 6.6 mm × 6.75 mm area on the plate.

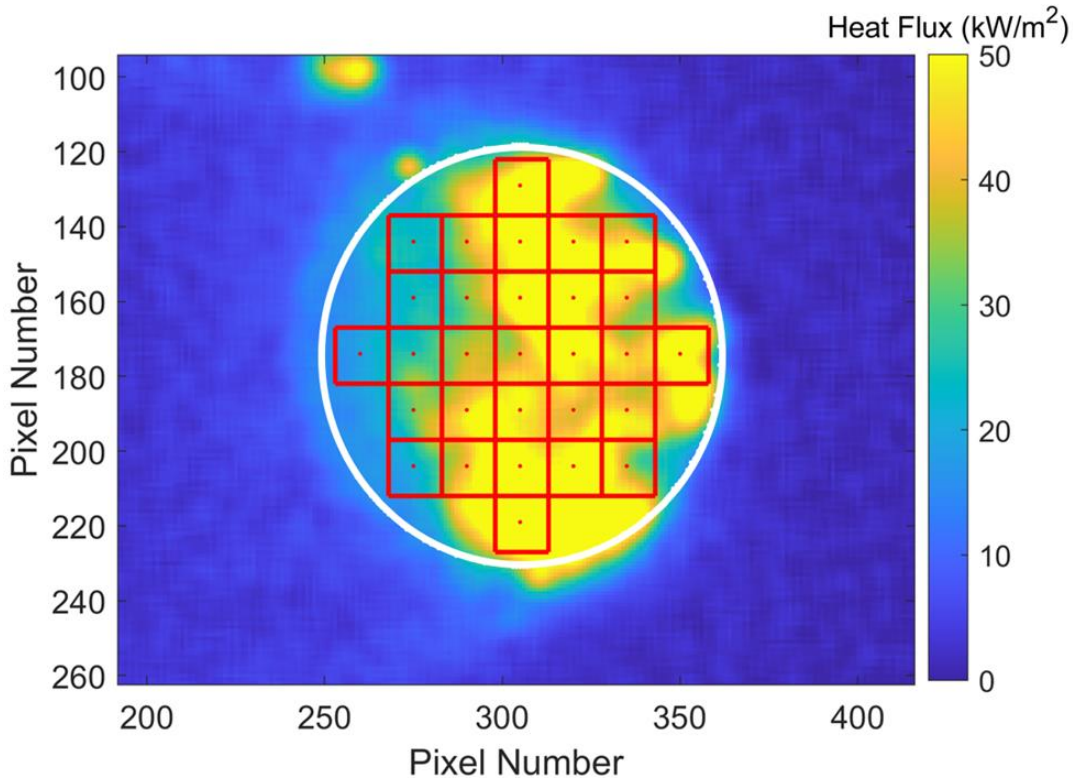

Figure 30. 6.6 mm × 6.75 mm grids (shown in red) lying totally within the bounds of the 50 m circular pile (shown in white).

At each point in time, the average heat flux of all the pixels within each grid was computed, resulting in twenty-nine heat flux versus time curves for each test, as shown in Figure 31. Ignition was assessed at the grid level using each of the grid fluxes as q_e''. Using the ignition model in Eqn. 1 and the experimentally-developed material properties, each grid heat flux was analyzed to see if ignition would be expected within that particular grid. This process was completed twenty-nine times for each test, corresponding to the twenty-nine individual grid values. The number of grids where ignition was predicted was used to compute the probability of ignition for that test, p_{ig}, defined as

$$p_{ig} = \frac{N_{ig}}{N_{Tot}} \tag{31}$$

where N_{ig} is the number of grids where ignition was predicted and N_{Tot} is the total number of grids (i.e. 29).

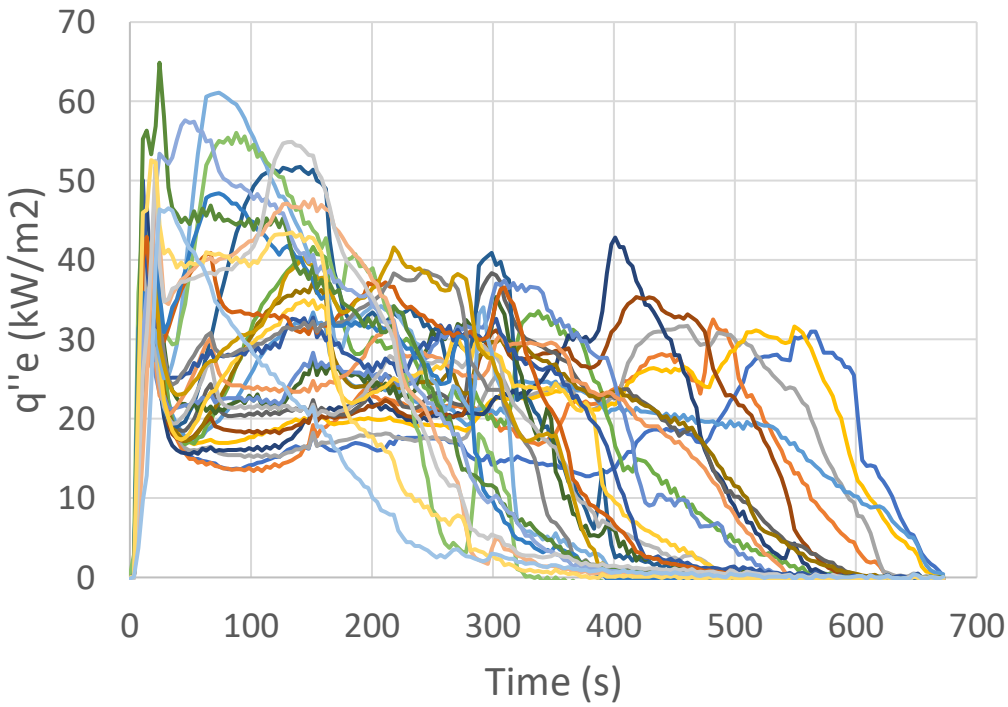

Figure 31. Heat flux data from all 29 grids from a single test plotted through time

4.2.4. Heat Flux Tests

A series of tests were run to obtain heat flux data for the ignition prediction. Using a variety of pile configurations and wind speeds, different heat flux levels could be achieved. The test matrix (shown in Table 14), used firebrands made from 4 different wood materials: N. Red Oak, Yellow Poplar, E. White Pine, and Loblolly Pine. Half the tests used "real" firebrands collected directly from live tree branches. The other half of the tests used "artificial" firebrands made from commercially available dowel rods. Two firebrand diameters (4.76 and 9.53 mm) and two firebrand lengths (12.5 and 50.0 mm) were used, with values reported for unburned firebrand dimensions. The mass of the deposited quantity of smoldering firebrands was either 1.5 or 3.0 g depending on the test. Two different pile moisture contents were used as well, with 0% and 25% being tested, as measured on a dry mass basis. Finally, wind speeds of either 0 or 2.0 m/s were used. The wind speed has been shown to be a highly significant variable in controlling the heat flux from firebrand piles and was measured in the center of the wire mesh cage using an Extech Hot Wire Thermo-Anemometer with 0.1 m/s resolution.

Firebrands were heated using the same method described by Bearinger et al. [51], where a carefully measured mass of unburned firebrands was heated in a mesh basket over a propane flame for a specified period of time. For piles with a deposited mass of 1.5 g, 11.0 g of wood pieces were heated for 15 s, while piles with a deposited mass of 3.0 g used 22.0 g of wood pieces heated for 30 s. Once the heating period was complete, the firebrands were allowed to continue unhindered from a state of flaming combustion to a state of smoldering combustion. The mass of the smoldering firebrands was carefully monitored. Once the group of firebrands reached the specified mass, data acquisition was started and the firebrands were deposited into the wire mesh cage through a custom-made funnel. In tests with wind, it was found that firebrands tended to be blown to the trailing edge of the pile during the placement process. To

remedy this issue, a wind shield (not pictured in Figure 27), was added on the upstream side of the pile during the prior to the start of the test. The wind shield was quickly removed once the smoldering firebrand were deposited within the cage.

Table 14. Firebrand pile test matrix

Test #	Wood State	Firebrand Wood Material	Initial Firebrand Diameter (mm)	Initial Firebrand Length (mm)	Pile Mass (g)	Wind (m/s)	Moisture Content (%)
1	Real	N. Red Oak	4.76	12.5	1.5	2	25
2	Real	E. White Pine	9.53	12.5	1.5	0	25
3	Artificial	Loblolly Pine	4.76	50	1.5	0	0
4	Real	N. Red Oak	9.53	12.5	3	0	0
5	Real	E. White Pine	9.53	50	1.5	2	0
6	Real	Loblolly Pine	4.76	50	3	0	25
7	Artificial	Loblolly Pine	9.53	12.5	3	2	0
8	Artificial	N. Red Oak	9.53	50	1.5	2	25
9	Artificial	Yellow Poplar	9.53	50	3	0	25
10	Real	Yellow Poplar	4.76	50	3	2	0
11	Artificial	E. White Pine	4.76	12.5	3	2	25
12	Artificial	Yellow Poplar	4.76	12.5	1.5	0	0

4.2.5. Ignition Tests

The ignition predictions were validated by running a series of firebrand pile tests on the combustible materials. Tests 7, 8, and 9 from Table 14 were each run on dry samples of nylon, pressure treated southern yellow pine (SYP) deck board, and composite deck board made from wood fibers and plastic, resulting in nine tests total. The testing procedure was identical to that of the heat transfer measurement tests described in Section 2.4, with the important exception that now the fuel samples were supported on the 304 SS plate and the firebrands placed on top of the combustible material, as shown in Figure 32. As before, wind speeds inside the cage were validated using a hotwire anemometer. In all cases the fuel samples were 100 mm wide and 100 mm long and dried to 0% moisture content. The SYP and the composite decking had a thickness of 25.4 mm while the nylon had a thickness of 12.7 mm. Time to ignition for the samples was measured from the time the full pile had been deposited within the cage. Ignition was defined as the presence of sustained flaming and tests that did not transition to flaming ignition with 20 minutes were said not to ignite.

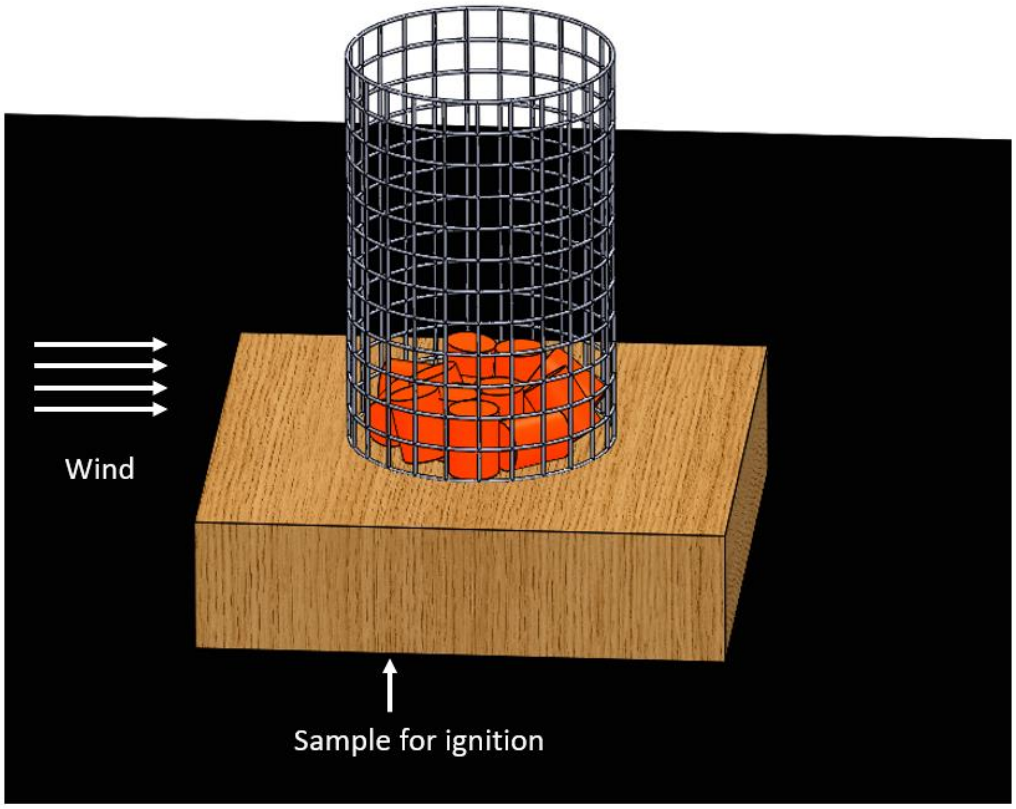

Figure 32. Setup used to test ignition of fuel samples by firebrand piles

4.3. RESULTS

The overarching objective of this work was to develop an engineering model to predict the ignition of building materials from firebrand exposure. The validation of this engineering model required several important steps. First, material properties of three common building materials were obtained through cone calorimeter testing. Next, these material properties were used with representative heat flux values to determine the probability and time to ignition for various pile/fuel combinations. Finally, the accuracy of the prediction methods was assessed by conducting physical ignition tests.

4.3.1. Material Properties

The material properties were found by exposing each of the three fuel materials to different radiant heat flux exposures in a cone calorimeter and measuring the time to ignition, t_{ig}. Piloted and spontaneous ignition tests were run for each material. $1/\sqrt{t_{ig}}$ scales linearly with the exposure flux, and the plot of $1/\sqrt{t_{ig}}$ versus q_e'' is the source from which many of the material properties are derived. The plots for each of the materials tested can be seen for piloted ignition in Figure 33 and spontaneous ignition in Figure 34.

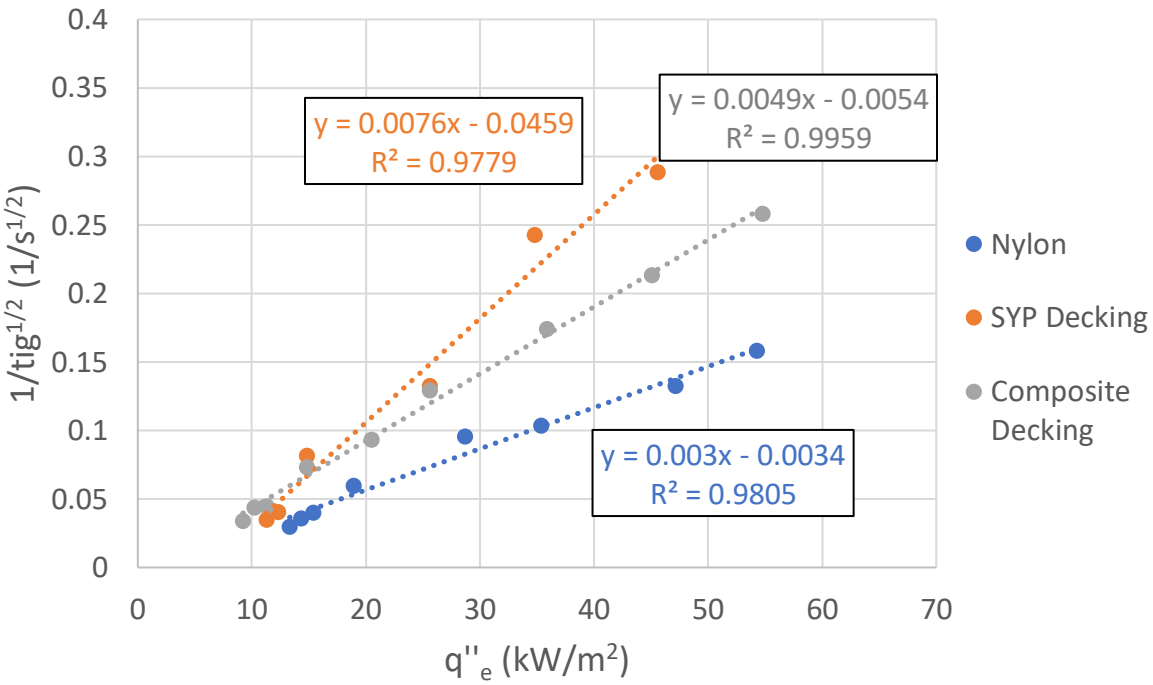

Figure 33. $\mathbf{1/\sqrt{t_{ig}}}$ versus exposure flux for piloted ignition of building materials.

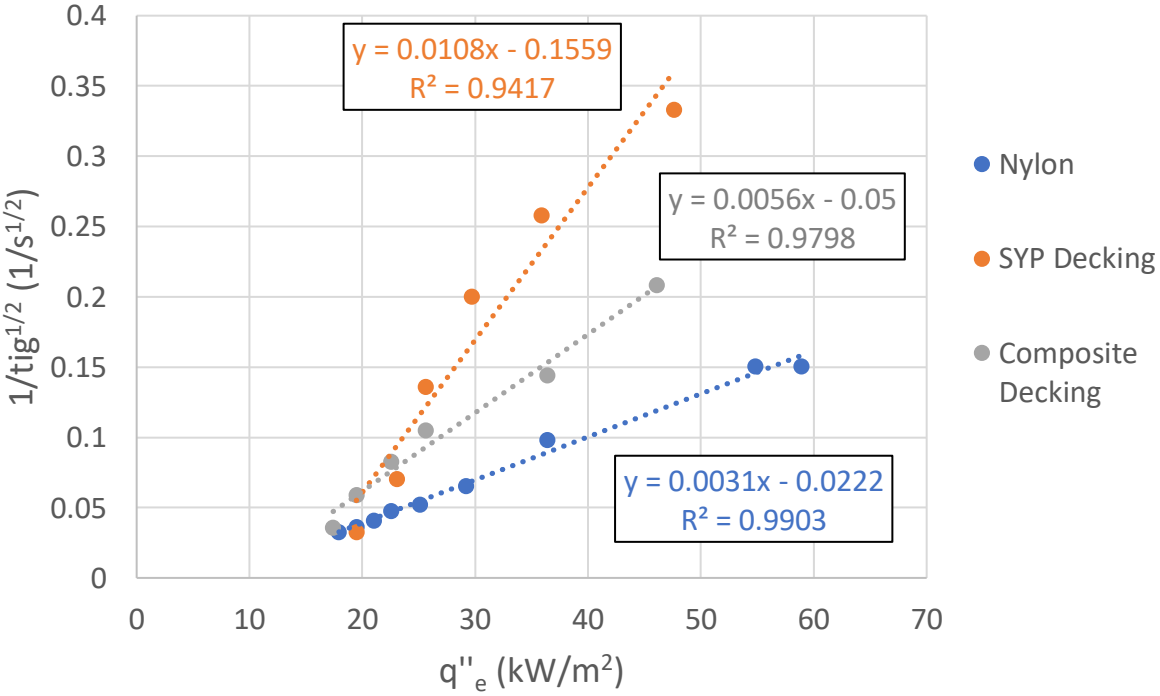

Figure 34. $\mathbf{1/\sqrt{t_{ig}}}$ versus exposure flux for spontaneous ignition of building materials.

Figure 33 and Figure 34 show the same trend for both the piloted and spontaneous ignition, with the SYP decking having the highest slope and smallest (most negative) y_0, followed by the composite decking. The nylon had the lowest slope and largest (least negative) value for y_0. The high R^2 values indicate that the trendlines fit the experimental data well. The slope and intercept values from the trendlines were used to calculate the thermal response parameter (TRP), the thermal inertia ($k\rho c$), the ignition temperature (T_{ig}), and the minimum (q''_{min}) and the critical (q''_{cr}) heat flux values. Results are shown in Table 15.

Table 15. Thermal properties of common materials

Material	Ignition Type	TRP $(kWs^{\frac{1}{2}}/m^2)$	$k\rho c$ (kW^2s/m^4K^2)	T_{ig} (K)	q''_{min} (kW/m^2)	q''_{cr} (kW/m^2)
Nylon	Piloted	375.86	1.234	631.32	12.80	1.14
	Spontaneous	368.28	0.847	693.25	17.41	7.25
SYP Decking	Piloted	148.73	0.237	598.53	10.76	6.05
	Spontaneous	104.08	0.062	711.18	18.95	14.38
Composite Decking	Piloted	230.69	0.740	561.17	8.71	1.11
	Spontaneous	202.11	0.263	687.01	16.90	8.95

The TRP of the materials shows a consistent trend for both piloted and spontaneous ignition. The SYP decking has the lowest TRP and the nylon has the highest, with the TRP of the composite decking material falling in between. For a given material, the TRP is lower for spontaneous ignition than piloted ignition. The TRP values of nylon, however, are quite similar for spontaneous and piloted ignition, with a difference of just 2% between to the two cases. The $k\rho c$ values show similar trends. $k\rho c$ is known as the thermal inertia and represents the tendency of a material to resist fluctuations in temperature. A noticeable difference exists in the $k\rho c$ values for piloted and spontaneous ignition. This may be due in part to a temperature dependence issue. The spontaneous ignition tests required higher exposure heat fluxes to induce ignition, increasing the material temperature and amount of surface char, potentially influencing some of thermal parameters such as $k\rho c$.

Ignition temperatures and minimum heat fluxes varied based on ignition type. Piloted ignition could be achieved at lower surface temperature than spontaneous ignition. The SYP decking was found to have the highest spontaneous ignition temperature ($T_{ig} = 711.18K$) and minimum flux ($q''_{min} = 18.95\ kW/m^2$). The composite decking had the lowest piloted ignition temperature ($T_{ig} = 561.17K$) and minimum heat flux ($q''_{min} = 8.71\ kW/m^2$). The critical flux, the heat flux for which the ignition time goes to infinity, followed similar trends.

4.3.2. Pile Heat Fluxes

A series of twelve experiments were run to measure heat transfer from firebrand piles to a horizontal surface under various conditions. The results for each pile were divided into twenty-nine grids, with the average heat flux within each grid being recorded through time. This time-varying data was then used to predicted ignition on a grid-by-grid basis. To compare with work

by Bearinger et al. [51], the 120 s average was computed for each grid, resulting in twenty-nine values for each test. The 75th percentile 120 s average grid heat flux (q''_{120s}) was then identified and used as a single value to represent the severity of heat flux exposure for each test. The q''_{120s} values for each of the twelve tests are shown in Figure 35. These values range from 6.4 kW/m^2 (Test 12) to 43.6 kW/m^2 (Test 10).

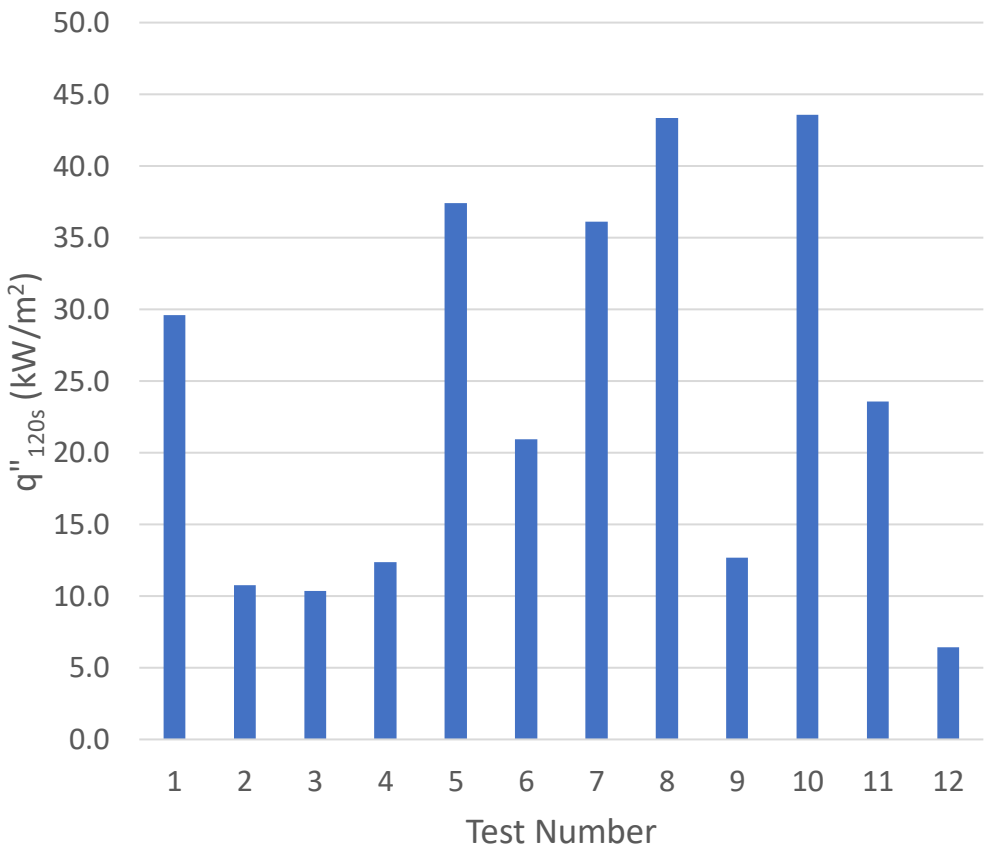

Figure 35. 75th percentile 120s average grid heat flux values

4.3.3. Ignition Prediction

The time-varying heat flux curves for each of the 29 grids in every test were used to predict ignition on the grid level. The percentage of grids predicted to ignite for each test was defined as the probability of ignition, p_{ig}. It was unknown whether the ignition of fuels by smoldering firebrands behaved more as piloted or spontaneous ignition and due to the difference in ignition behavior between these two cases, results were calculated for both, as shown Table 16. Of the three materials, nylon was the least likely to ignite. There were no tests where $p_{ig} = 1$ for nylon for either the piloted or spontaneous results. The SYP decking had three tests (Tests 5, 7, and 10), however, for which 100% of the grids were expected to experience ignition for both piloted and spontaneous results. Similarly, Tests 7 and 10 had $p_{ig} = 1.0$ for the composite decking. Tests 2, 3, and 12 had $p_{ig} = 0$ for all materials.

Table 16. Probability of ignition of each test on common materials

Test	q''_{120s} (kW/m^2)	Probability of Ignition					
		Nylon		SYP Decking		Composite Decking	
		Piloted	Spontaneous	Piloted	Spontaneous	Piloted	Spontaneous
1	29.6	0.59	0.21	0.97	0.93	0.97	0.86
2	10.8	0.00	0.00	0.00	0.00	0.00	0.00
3	10.4	0.00	0.00	0.00	0.00	0.00	0.00
4	12.3	0.07	0.00	0.21	0.00	0.45	0.00
5	37.4	0.59	0.28	1.00	1.00	1.00	0.97
6	20.9	0.00	0.00	0.72	0.21	0.86	0.14
7	36.1	0.97	0.93	1.00	1.00	1.00	1.00
8	43.4	0.62	0.59	0.90	0.86	0.83	0.83
9	12.7	0.00	0.00	0.07	0.00	0.21	0.00
10	43.6	0.72	0.59	1.00	1.00	1.00	1.00
11	23.6	0.55	0.14	0.97	0.97	0.93	0.93
12	6.4	0.00	0.00	0.00	0.00	0.00	0.00

For the modeling, t_{ig} was defined as the time taken for the surface temperature, T_s, within the grid to exceed the ignition temperature of the material when the time-varying heat flux data was used. Every grid where ignition was predicted had its own t_{ig}, resulting in up to twenty-nine values per tests. For reporting purposes, the minimum time to ignition for any grid was selected. The minimum $t_{ig}$was chosen because it represents the minimum time under which ignition could occur, a meaningful metric for fire safety engineering. The t_{ig} calculated using the time-varying heat could be compared with the time to ignition ($t_{ig,120s}$) calculated using the time-invariant q''_{120s}. These results are shown for piloted ignition in Table 17 and spontaneous ignition in Table 18. Cases where $p_{ig} = 0$ or $q''_{120s} < q''_{cr}$ were excluded.

Table 17. Times to ignition based on piloted results

Test	q''_{120s} (kW/m^2)	Nylon		SYP Decking		Composite Decking	
		t_{ig} (s)	$t_{ig,120s}$ (s)	t_{ig} (s)	$t_{ig,120s}$ (s)	t_{ig} (s)	$t_{ig,120s}$ (s)
1	29.6	63.4	136.9	24.6	31.5	31.7	51.5
2	10.8	--	1197.8	--	787.6	--	448.8
3	10.4	--	1303.1	--	939.1	--	488.1
4	12.3	858.9	881.3	91.5	439.3	123.2	330.5
5	37.4	35.2	84.2	21.1	17.7	24.6	31.7
6	20.9	--	282.5	45.8	78.6	63.4	106.2
7	36.1	52.8	90.5	17.6	19.3	21.1	34.1
8	43.4	38.7	62.1	21.1	12.5	24.6	23.4
9	12.7	--	829.4	323.8	394.9	285.1	311.1
10	43.6	35.2	61.5	14.1	12.4	21.1	23.1
11	23.6	70.4	219.9	28.2	56.7	42.2	82.7
12	6.4	--	3936.7	--	112641.8	--	1467.5

Table 18. Times to ignition based on spontaneous results

Test	q''_{120s} (kW/m^2)	Nylon		SYP Decking		Composite Decking	
		t_{ig} (s)	$t_{ig,120s}$ (s)	t_{ig} (s)	$t_{ig,120s}$ (s)	t_{ig} (s)	$t_{ig,120s}$ (s)
1	29.6	84.5	213.5	24.6	36.8	38.7	75.3
2	10.8	--	8667.1	--	--	--	9848.9
3	10.4	--	11018.6	--	--	--	16174.0
4	12.3	--	4093.7	--	--	--	2775.4
5	37.4	38.7	117.1	21.1	16.1	24.6	39.6
6	20.9	--	568.0	52.8	197.8	102.1	223.1
7	36.1	59.8	127.8	14.1	18.0	24.6	43.5
8	43.4	42.2	81.6	21.1	10.1	24.6	27.1
9	12.7	--	3591.6	--	--	--	2287.8
10	43.6	38.7	80.7	10.6	10.0	24.6	26.7
11	23.6	88.0	399.1	28.2	100.5	45.8	149.8
12	6.4	--	--	--	135.1	--	--

4.3.4. Ignition Experiments

Tests 7, 8, and 9 were run on dry fuel samples to validate the model against experimental data, with results show in Table 19. Of the nine tests that were run, ignition was observed in four. Test 7 and 8 caused ignition on both the SYP and the composite decking, while no ignition was observed for any of the tests on nylon. All test where $p_{ig} = 1$ were observed to induce flaming ignition on the fuel. Significant surface melting of the nylon occurred, allowing the firebrands within the pile to become immersed in the molten substrate.

Table 19. Ignition testing results

	Test	Ignition	$t_{ig,obs}$	Piloted			Spontaneous		
				p_{ig}	t_{ig}	$t_{ig,120s}$	p_{ig}	t_{ig}	$t_{ig,120s}$
Nylon	7	No	--	0.97	52.8	90.5	0.93	59.8	127.8
	8	No	--	0.62	38.7	62.1	0.59	42.2	81.6
	9	No	--	0.00	--	829.4	0.00	--	3591.6
SYP Decking	7	Yes	4	1.00	17.6	19.3	1.00	14.1	18.0
	8	Yes	8	0.90	21.1	12.5	0.86	21.1	10.1
	9	No	--	0.07	323.8	394.9	0.00	--	--
Composite Decking	7	Yes	177	1.00	21.1	34.1	1.00	24.6	43.5
	8	Yes	55	0.83	24.6	23.4	0.83	24.6	27.1
	9	No	--	0.21	285.1	311.1	0.00	--	2287.8

4.4. DISCUSSION

The application of this model to the ignition of common materials by firebrand piles gives useful insight into this pressing problem. The model itself was chosen due to its relative simplicity and its ease of use in predicting material ignition from a time-varying heat flux. Given knowledge of representative heat flux and material properties, the model can quickly simulate a great number of ignition scenarios. While this model is applied here for heat fluxes from firebrand piles, there is no reason that it could not be applied to ignition by singular firebrands as well.

The material tests conducted in the cone calorimeter revealed that the nylon was harder to ignite than either the SYP or the composite decking. Although the composite decking had a lower q''_{min} and T_{ig} than the SYP, its higher thermal inertia gave it a lower probability of ignition for most firebrand exposure fluxes.

The experimental data allowed several interesting comparisons to be made. The presence of a pilot in the cone calorimeter testing significantly affected the ignition behavior of the material. While results for both piloted and spontaneous modeling are presented here, the experimental data allows a direct comparison. Figure 36 shows the probability of ignition calculated using piloted and spontaneous ignition properties as well as the true probability of ignition from the physical testing. Tests where ignition was observed were said to have a true $p_{ig} = 1$, while tests that did not ignite were said to have a true $p_{ig} = 0$. Close agreement between the probability of ignition for both the piloted and spontaneous properties can be seen for most tests. The majority of the tests did not ignite, and the spontaneous ignition model has slightly better agreement with the physical results for this reason. Using material properties for spontaneous ignition, the model was 78% accurate in predicting whether the physical tests would ignite. The model was only 55% accurate using piloted ignition properties. For the accuracy assessment, $p_{ig} > 0$ was considered to predict ignition. In all cases, the model error was Type I error, with the model predicting ignition that was not observed in the physical tests. The only major inconsistency between the model and the experimental results occurred on nylon.

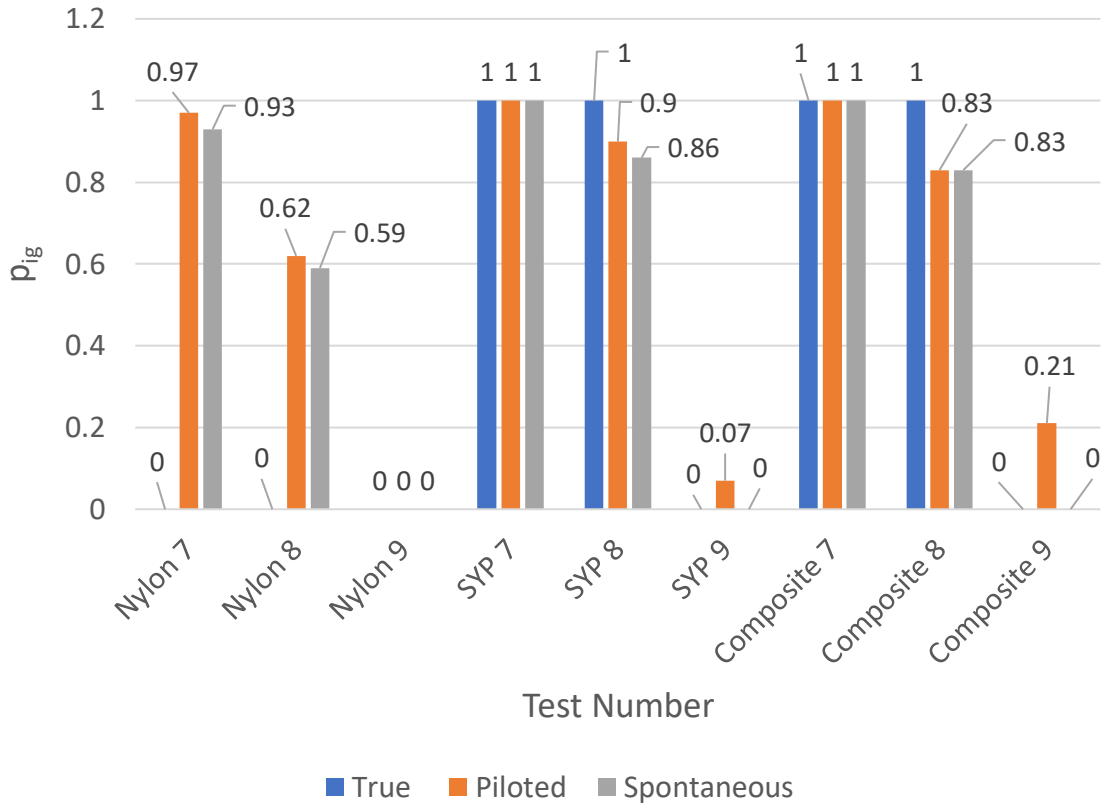

Figure 36. Probability of ignition

A possible reason why the model may have over-predicted ignition for the nylon comes from the interaction between the material and the firebrand pile. The material properties were developed in a radiation-only environment without any direct contact between the heat source and the material. The firebrand piles, on the other hand, rested directly on the combustible surface. As the nylon heated, the top surface melted to some degree allowing the firebrands to become immersed in the molten material effectively quenching the bottom layer of the ignition source.

Finally, the experimental data allows an assessment of q''_{120s} as a metric for quantifying the heat transfer from firebrand piles. q''_{120s} is the 75th percentile, 120 s average grid heat flux and has been used as an important metric in quantifying heat transfer from firebrand piles [51]. Figure 37 shows a comparison of the time to ignition (t_{ig}) for the time-varying heat flux data with the time to ignition ($t_{ig,120s}$) calculated using q''_{120s}. Data is shown for spontaneous ignition properties along with the true time to ignition for cases where ignition was observed. Interestingly, $t_{ig,120s}$ shows a better agreement with the observed time to ignition than t_{ig} for 75% of the cases. This suggests that q''_{120s} is in fact a good metric to use for quantifying heat flux from firebrand piles.

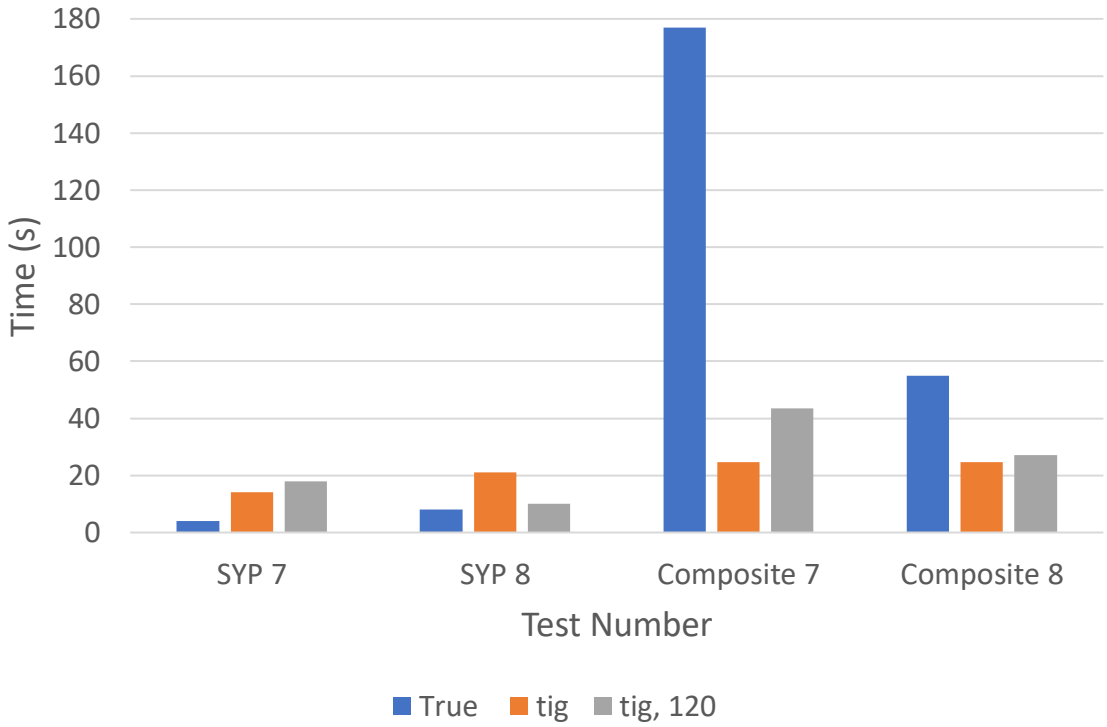

Figure 37. Comparison of time to ignition using experimental data (True), time-varying heat flux data and spontaneous ignition material properties ($\boldsymbol{t_{ig}}$), and q''_{120s} ($\boldsymbol{t_{ig,120s}}$)

4.5. CONCLUSION

In conclusion, a simple engineering model was developed for using time-varying heat fluxes from firebrand piles to predict the ignition of building materials. The model requires known material thermal properties and heat flux values to make its predictions. To assess the model, piloted and spontaneous ignition properties of nylon, pressure-treated southern yellow pine decking, and composite decking were developed through cone calorimeter testing. A series of twelve firebrand pile tests were run to obtained representative heat fluxes. The measured heat fluxes were used in conjunction with the material properties to predict probability of ignition and time to ignition. These predictions were validated through experiments.

The material properties developed through the cone calorimeter testing revealed that nylon was substantially harder to ignite than both southern yellow pine and composite decking. The model was found to have the best agreement with experimental results when spontaneous ignition properties were used. Using these material properties, the model correctly predicted the ignition outcome of 78% of the ignition experiments. The experimental results were also used to assess the utility of the 75th percentile, 120 s average grid flux as a representative value for firebrand pile exposure. This metric was found to out-perform more complex time-varying models in the prediction of time to ignition, indicating that this metric can provide a useful simplification that allows the quantification of heat transfer from firebrand piles.

REFERENCES

[1] S. E. Caton, R. S. P. Hakes, D. J. Gorham, A. Zhou, and M. J. Gollner, "Review of Pathways for Building Fire Spread in the Wildland Urban Interface Part I: Exposure Conditions," *Fire Technol.*, vol. 53, no. 2, pp. 429–473, 2017, doi: 10.1007/s10694-016-0589-z.

[2] R. S. P. Hakes, S. E. Caton, D. J. Gorham, and M. J. Gollner, "A Review of Pathways for Building Fire Spread in the Wildland Urban Interface Part II: Response of Components and Systems and Mitigation Strategies in the United States," *Fire Technol.*, vol. 53, no. 2, pp. 475–515, 2017, doi: 10.1007/s10694-016-0601-7.

[3] E. Koo, P. J. Pagni, D. R. Weise, and J. P. Woycheese, "Firebrands and spotting ignition in large-scale fires," *Int. J. Wildl. Fire*, vol. 19, no. 7, pp. 818–843, 2010, doi: 10.1071/WF07119.

[4] S. L. Manzello, "Enabling the investigation of structure vulnerabilities to wind-Driven firebrand showers in wildland-Urban Interface (WUI) fires," *Fire Saf. Sci. 11*, vol. 11, pp. 83–96, 2014, doi: 10.3801/IAFSS.FSS.11-83.

[5] V. P. Dowling, "Ignition of timber bridges in bushfires," *Fire Saf. J.*, vol. 22, no. 2, pp. 145–168, 1994, doi: 10.1016/0379-7112(94)90070-1.

[6] S. L. Manzello, S. H. Park, and T. G. Cleary, "Investigation on the ability of glowing firebrands deposited within crevices to ignite common building materials," *Fire Saf. J.*, vol. 44, no. 6, pp. 894–900, 2009, doi: 10.1016/j.firesaf.2009.05.001.

[7] R. S. P. Hakes, H. Salehizadeh, M. J. Weston-dawkes, and M. J. Gollner, "Thermal characterization of firebrand piles," *Fire Saf. J.*, vol. 104, no. June 2018, pp. 34–42, 2019, doi: 10.1016/j.firesaf.2018.10.002.

[8] S. L. Manzello and S. Suzuki, "Exposing decking assemblies to continuous wind-driven firebrand showers," *Fire Saf. Sci.*, vol. 11, pp. 1339–1352, 2014, doi: 10.3801/IAFSS.FSS.11-1339.

[9] S. S. Wessies, M. K. Chang, K. C. Marr, and O. A. Ezekoye, "Experimental and Analytical Characterization of Firebrand Ignition of Home Insulation Materials," *Fire Technol.*, vol. 55, no. 3, pp. 1027–1056, 2019, doi: 10.1007/s10694-019-00818-8.

[10] T. J. Ohlemiller, "Smoldering combustion propagation on solid wood," *Fire Saf. Sci. 3*, pp. 565–574, 2006, doi: 10.4324/9780203973493.

[11] P. Ellis, "The Aerodynamic and Combustion Characteristics of Eucalypt Bark - A Firebrand Study," *Disseration, Aust. Natl. Univ. Dep. For.*, p. 205, 2000.

[12] S. L. Manzello, T. G. Cleary, J. R. Shields, A. Maranghides, W. Mell, and J. C. Yang, "Experimental investigation of firebrands: Generation and ignition of fuel beds," *Fire Saf. J.*, vol. 43, no. 3, pp. 226–233, 2008, doi: 10.1016/j.firesaf.2006.06.010.

[13] S. L. Manzello, T. G. Cleary, J. R. Shields, and J. C. Yang, "On the ignition of fuel beds by firebrands," *Fire Mater.*, vol. 30, no. 1, pp. 77–87, 2006, doi: 10.1002/fam.901.

[14] A. Warey, "Influence of thermal contact on heat transfer from glowing firebrands," *Case Stud. Therm. Eng.*, 2018, doi: 10.1016/j.csite.2018.04.018.

[15] A. Filkov *et al.*, “Investigation of firebrand production during prescribed fires conducted in a pine forest,” *Proc. Combust. Inst.*, 2017, doi: 10.1016/j.proci.2016.06.125.

[16] S. L. Manzello, A. Maranghides, J. R. Shields, W. E. Mell, Y. Hayashi, and D. Nii, “Mass and size distribution of firebrands generated from burning Korean pine (Pinus koraiensis) trees,” *Fire Mater.*, 2009, doi: 10.1002/fam.977.

[17] Y. M. Abul-huda, “Development of a Spatially Resolved Optical Technique for Measuring Heat Flux and Thermal Footprint of Firebrand Piles,” *NIST Tech. Note 2052*, p. 28, 2019.

[18] J. Hodges, C. Rippe, S. W. Case, and B. Y. Lattimer, “Predicting the structural response of a compartment fi re using full-field heat transfer measurements,” *Fire Saf. J.*, vol. 91, no. March, pp. 471–479, 2017, doi: 10.1016/j.firesaf.2017.03.011.

[19] C. M. Rippe and B. Y. Lattimer, “Full-field surface heat flux measurement using non-intrusive infrared thermography,” *Fire Saf. J.*, vol. 78, pp. 238–250, 2015, doi: 10.1016/j.firesaf.2015.10.004.

[20] N. Cholewa, P. T. Summers, S. Feih, A. P. Mouritz, B. Y. Lattimer, and S. W. Case, “A Technique for Coupled Thermomechanical Response Measurement Using Infrared Thermography and Digital Image Correlation (TDIC),” *Exp. Mech.*, vol. 56, pp. 145–164, 2016, doi: 10.1007/s11340-015-0086-1.

[21] J. L. Urban, A. C. Fernandez-pello, M. Vicariotto, and D. Dunn-Rankin, “Temperature Measurement of Glowing Embers with Color Pyrometry,” *Fire Technol.*, vol. 55, no. 3, pp. 1013–1026, 2019, doi: 10.1007/s10694-018-0810-3.

[22] R. J. Goldstein, E. M. Sparrow, and D. C. Jones, “Natural convection mass transfer adjacent to horizontal plates,” *Int. J. Heat Mass Transf.*, vol. 16, no. 5, pp. 1025–1035, 1973, doi: 10.1016/0017-9310(73)90041-0.

[23] J. R. Lloyd and W. R. Moran, “Natural convection adjacent to horizontal surface of various planforms,” *J. Heat Transfer*, vol. 96, no. 4, pp. 443–447, 1974, doi: 10.1115/1.3450224.

[24] F. P. Incropera, D. P. DeWitt, T. L. Bergman, and A. S. Lavine, *Fundamentals of Heat and Mass Transfer*, 6th ed. John Wiley & Sons, 2007.

[25] P. Deb *et al.*, “Causes of the Widespread 2019–2020 Australian Bushfire Season,” *Earth’s Futur.*, vol. 8, no. 11, 2020, doi: 10.1029/2020EF001671.

[26] M. Ward *et al.*, “Impact of 2019–2020 mega-fires on Australian fauna habitat,” *Nat. Ecol. Evol.*, vol. 4, no. 10, pp. 1321–1326, 2020, doi: 10.1038/s41559-020-1251-1.

[27] A. I. Filkov, T. Ngo, S. Matthews, S. Telfer, and T. D. Penman, “Impact of Australia’s catastrophic 2019/20 bushfire season on communities and environment. Retrospective analysis and current trends,” *J. Saf. Sci. Resil.*, vol. 1, no. 1, pp. 44–56, 2020, doi: 10.1016/j.jnlssr.2020.06.009.

[28] M. Turco *et al.*, “Climate drivers of the 2017 devastating fires in Portugal,” *Sci. Rep.*, vol. 9, no. 1, pp. 1–8, 2019, doi: 10.1038/s41598-019-50281-2.

[29] K. Lagouvardos, V. Kotroni, T. M. Giannaros, and S. Dafis, “Meteorological conditions

conducive to the rapid spread of the deadly wildfire in eastern attica, Greece," *Bull. Am. Meteorol. Soc.*, vol. 100, no. 11, pp. 2137–2145, 2019, doi: 10.1175/BAMS-D-18-0231.1.

[30] T. Brown, S. Leach, B. Wachter, and B. Gardunio, "THE NORTHERN CALIFORNIA 2018 EXTREME FIRE SEASON," *Bull. Am. Meteorol. Soc.*, vol. 95, no. 9, pp. S1–S96, 2014, doi: 10.1175/1520-0477-95.9.s1.1.

[31] D. M. Theobald and W. H. Romme, "Expansion of the US wildland-urban interface," *Landsc. Urban Plan.*, vol. 83, no. 4, pp. 340–354, 2007, doi: 10.1016/j.landurbplan.2007.06.002.

[32] W. Mell and Alexander Maranghides, "NIST Technical Note 1635: A Case Study of a Community Affected by the Witch and Guejito Fires," 2009.

[33] N. A. McArthur and P. Lutton, "Ignition of exterior building details in bushfires: An experimental study," *Fire Mater.*, vol. 15, no. 2, pp. 59–64, 1991, doi: 10.1002/fam.810150204.

[34] A. Filkov, D. Kasymov, V. Zima, and O. Matvienko, "Experimental investigation of surface litter ignition by bark firebrands," *AIP Conf. Proc.*, vol. 1698, no. January, 2016, doi: 10.1063/1.4937859.

[35] S. Santamaria *et al.*, "Investigation of Structural Wood Ignition By Firebrand Accumulation," *First Int. Conf. Struct. Saf. under Fire Blast*, no. July 2016, pp. 1–13, 2015.

[36] E. D. Bearinger, J. L. Hodges, F. Yang, C. M. Rippe, and B. Y. Lattimer, "Localized heat transfer from firebrands to surfaces," *Fire Saf. J.*, vol. 120, no. April 2020, p. 103037, 2021, doi: 10.1016/j.firesaf.2020.103037.

[37] Z. Tao, B. Bathras, B. Kwon, B. Biallas, M. J. Gollner, and R. Yang, "Effect of firebrand size and geometry on heating from a smoldering pile under wind," *Fire Saf. J.*, no. May, p. 103031, 2020, doi: 10.1016/j.firesaf.2020.103031.

[38] J. R. Lloyd and W. R. Moran, "Natural Convection Adjacent To Horizontal Surface of Various Planforms.," *Am. Soc. Mech. Eng.*, vol. 96, no. 74-WA/HT-66, pp. 443–447, 1974, doi: 10.1115/1.3450224.

[39] T. Conners, "Distinguishing Softwoods from Hardwoods," *Agric. Nat. Resour. Publ.*, p. 105, 2015.

[40] S. X. Li, J. Zhao, P. Lu, and Y. Xie, "Maximum packing densities of basic 3D objects," *Chinese Sci. Bull.*, vol. 55, no. 2, pp. 114–119, 2010, doi: 10.1007/s11434-009-0650-0.

[41] R. P. Zou, X. Y. Lin, A. B. Yu, and P. Wong, "Packing of cylindrical particles with a length distribution," *J. Am. Ceram. Soc.*, vol. 80, no. 3, pp. 646–652, 1997, doi: 10.1111/j.1151-2916.1997.tb02880.x.

[42] D. Thomas, D. Butry, S. Gilbert, D. Webb, and J. Fung, "The Costs and Losses of Wildfires: A Literature Survey (NIST Special Publication 1215)," 2017, [Online]. Available: https://doi.org/10.6028/NIST.SP.1215.

[43] S. Wang, X. Huang, H. Chen, N. Liu, and G. Rein, "Ignition of low-density expandable polystyrene foam by a hot particle," *Combust. Flame*, vol. 162, no. 11, pp. 4112–4118,

2015, doi: 10.1016/j.combustflame.2015.08.017.

[44] R. M. Hadden, S. Scott, C. Lautenberger, and C. C. Fernandez-Pello, “Ignition of Combustible Fuel Beds by Hot Particles: An Experimental and Theoretical Study,” *Fire Technol.*, vol. 47, no. 2, pp. 341–355, 2011, doi: 10.1007/s10694-010-0181-x.

[45] A. Ganteaume *et al.*, “Spot fires: Fuel bed flammability and capability of firebrands to ignite fuel beds,” *Int. J. Wildl. Fire*, vol. 18, no. 8, pp. 951–969, 2009, doi: 10.1071/WF07111.

[46] C. Lautenberger and A. C. Fernandez-Pello, “Spotting ignition of fuel beds by firebrands,” *WIT Trans. Modelling Simul.*, vol. 48, pp. 603–612, 2009, doi: 10.2495/CMEM090541.

[47] H. S. Carslaw and J. C. Jaeger, *Conduction of Heat in Solids*, 2nd ed. London: Oxford University Press, 1959.

[48] J. G. Quintiere, “A simulation model for fire growth on materials subject to a room-corner test,” *Fire Saf. J.*, vol. 20, no. 4, pp. 313–339, 1993, doi: 10.1016/0379-7112(93)90053-S.

[49] SFPE, *Engineering Guide - Piloted Ignition of Solid Materials Under Radiant Exposure*. Society of Fire Protection Engineers, 2002.

[50] A. Tewarson, “Generation of Heat and Chemical Compounds in Fires,” in *The SFPE Handbook of Fire Protection Engineering*, 1995, p. Section 3-Chapter 4.

[51] E. D. Bearinger, B. Y. Lattimer, J. Hodges, C. Rippe, and A. Kapahi, “Statistical Assessment of Parameters Affeting Firebrand Pile Heat Transfer to Surfaces,” *Curr. under Rev. by Front. Mech. Eng.*

5. CONCLUSION

This research focused on understanding the heat transfer from firebrands and firebrand piles to horizontal surfaces and developing a model to predict ignition from firebrand pile exposure. The effects of wind speed, wind direction, and firebrand shape on the heat flux from individual firebrands was investigated using high-resolution infrared thermography. It was found that localized heat flux values were significantly higher than had previously been reported. Additionally, it was found that wind speed, wind direction, and firebrand shape all affect the heat transfer from individual firebrands.

A series of experiments on firebrand piles was used to investigate the role of different pile characteristics and external environmental conditions on the heat transfer to a horizontal surface. Design of experiments and statistical analysis was used to assess which factors had a significant impact on the heat transfer from firebrand piles. It was found that wind speed, firebrand length, and an interaction between firebrand length and diameter were important. The importance of these parameters suggests that allowing oxygen to more freely flow into the firebrand pile will result in higher heat flux levels. Additionally, it was found that there was a difference between the heat transfer from piles made with artificial (dowels) and real firebrands, suggesting that using dowels as surrogate firebrands may produce higher heat transfer levels than real firebrands. Pile mass was found to not have a significant impact the heat flux from firebrand piles.

Lastly an ignition model was developed to predict ignition of common material by heat flux exposure from firebrand piles. The model used material properties developed through experimental testing and time-varying heat fluxes from firebrand piles to predict which pile/fuel combinations were expected to ignite. Ignition predictions were validated with experimental testing and good agreement was observed between the model and experimental results for material which did not melt.

6. FUTURE WORK

There are several important steps that should be taken by future work to expand upon this research and increase its impact in fire safety engineering. All work presented here is for heat transfer from firebrands or firebrand piles to horizontal surfaces. While decks, gutters, and some portions of roofs may be modeled as horizontal surfaces, future work should investigate heat transfer and ignition by firebrands in other geometries. Angled roofs, walls, corners, and decks with gaps all may affect behavior of the firebrands and the subsequent ignition of these building assemblies.

Additionally, experimentation with a greater number of building materials is needed. While the materials tested in this work provide a good foundation, common siding and roofing materials need to be tested to expand the applicability of the ignition model to all vulnerable components of typical structures. Cone calorimeter testing to determine material properties and further firebrand pile ignition experiments are both required to meet this objective.